NAVAL POSTGRADUATE SCHOOL
Monterey, California

THESIS

COMPARATIVE ANALYSIS OF THE SAFARI MODEL WITH NATIVE 1 DATA IN THE VLF REGIME

by

Jerome L. Cleveland Jr.

September, 1991

Thesis Advisors: Alan B. Coppens
James V. Sanders

Approved for public release; distribution is unlimited.

REPORT DOCUMENTATION PAGE

Form Approved
OMB No 0704 0188

1a REPORT SECURITY CLASSIFICATION UNCLASSIFIED	1b RESTRICTIVE MARKINGS
2a SECURITY CLASSIFICATION AUTHORITY	3 DISTRIBUTION AVAILABILITY OF REPORT Approved for public release; distribution unlimited
2b DECLASSIFICATION DOWNGRADING SCHEDULE	
4 PERFORMING ORGANIZATION REPORT NUMBER(S)	5 MONITORING ORGANIZATION REPORT NUMBER(S)
6a NAME OF PERFORMING ORGANIZATION Naval Postgraduate School 6b OFFICE SYMBOL (If applicable) 3A	7a NAME OF MONITORING ORGANIZATION Naval Postgraduate School
6c ADDRESS (City, State, and ZIP Code)	7b ADDRESS (City, State, and ZIP Code)
8a NAME OF FUNDING/SPONSORING ORGANIZATION 8b OFFICE SYMBOL (If applicable)	9 PROCUREMENT INSTRUMENT IDENTIFICATION NUMBER
8c ADDRESS (City, State, and ZIP Code)	10 SOURCE OF FUNDING NUMBERS PROGRAM ELEMENT NO / PROJECT NO / TASK NO / WORK UNIT ACCESSION NO

11 TITLE (Include Security Classification)
Comparative Analysis of the SAFARI Model with NATIVE 1 Data in the VLF Regime

12 PERSONAL AUTHOR(S)
Jerome L. Cleveland Jr.

13a TYPE OF REPORT	13b TIME COVERED	14 DATE OF REPORT (Year, Month, Day)	15 PAGE COUNT
Master's Thesis	FROM _____ TO _____	1991, September 30	120

16 SUPPLEMENTARY NOTATION
The views expressed in this thesis are those of the author and do not reflect the official policy or position of the Department of Defense or the U.S. Government.

17 COSATI CODES			18 SUBJECT TERMS (Continue on reverse if necessary and identify by block number)
FIELD	GROUP	SUB-GROUP	

19 ABSTRACT (Continue on reverse if necessary and identify by block number)

Few underwater acoustic models have been validated in the Very Low Frequency (VLF) regime. The purpose here is to explore one model's abilities and compare it with ocean data once it is ascertained the model has converged to its final solution. A comparative analysis of data recorded in NATIVE 1 (the Noise and Transmission Loss in VLF Environments) Event 1 and results generated using the Seismo-Acoustic Fast field Algorithm for Range-Independent Environments (SAFARI) is the focus of this study, with emphasis on understanding some of the model's features.

20 DISTRIBUTION/AVAILABILITY OF ABSTRACT ☒ UNCLASSIFIED/UNLIMITED ☐ SAME AS RPT ☐ DTIC USERS	21 ABSTRACT SECURITY CLASSIFICATION UNCLASSIFIED
22a NAME OF RESPONSIBLE INDIVIDUAL Coppens, Alan B.	22b TELEPHONE (Include Area Code) 408-646-2941 22c OFFICE SYMBOL 3A

Approved for public release; distribution is unlimited.

COMPARATIVE ANALYSIS OF THE SAFARI MODEL WITH NATIVE 1 DATA IN THE VLF REGIME

by

Jerome L. Cleveland Jr.
Lieutenant Commander, United States Navy
B.S., University of Florida

Submitted in partial fulfillment
of the requirements for the degree of

MASTER OF SCIENCE IN Applied Sciences

from the

NAVAL POSTGRADUATE SCHOOL
September 1991

Author: 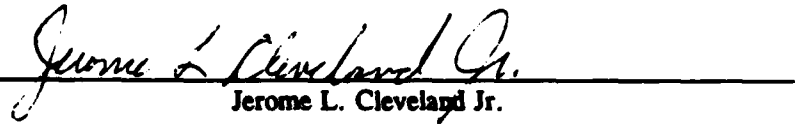
Jerome L. Cleveland Jr.

Approved by: 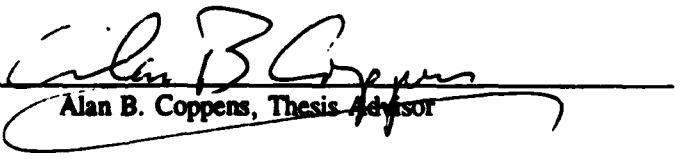
Alan B. Coppens, Thesis Advisor

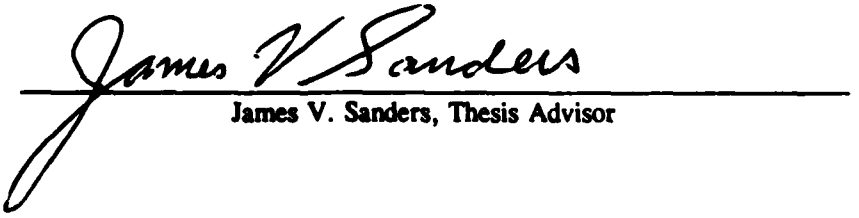
James V. Sanders, Thesis Advisor

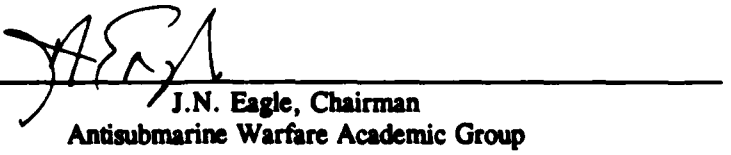
J.N. Eagle, Chairman
Antisubmarine Warfare Academic Group

ABSTRACT

Few underwater acoustic models have been validated in the Very Low Frequency (VLF) regime. The purpose here is to explore one model's abilities and compare it with ocean data once it is ascertained the model has converged to its final solution. A comparative analysis of data recorded in NATIVE 1 (the Noise and Transmission Loss in VLF Environments) Event 1 and results generated using the Seismo-Acoustic Fast field Algorithm for Range-Independent Environments (SAFARI) is the focus of this study, with emphasis on understanding some of the model's features.

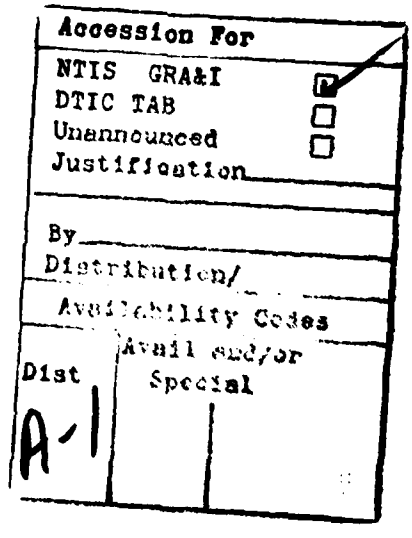

TABLE OF CONTENTS

I. INTRODUCTION

In submarine warfare there is a need for accurate acoustic models both for the prediction of how well a given sensor will work and to support the design of new sensors. These acoustic models need to be verified, in the acoustic regime of interest, against a database of experimentally-measured data representative of the environment.

The verification of an acoustic model requires three primary ingredients. The first is a model that produces results that are testable, the second is a database against which to compare the results of the model, and third is a method of comparison; whether statistical or graphical. One purpose of any acoustic model is to simulate the environment with sufficient accuracy so results can be compared to measurements. Limitations on the model input parameters have direct ramifications on its results. Similarly the precision and accuracy of the equipment used in recording the data as well as any perturbations which may occur during the collection of the data must be taken into account when determining its quality. A model is only as good as its theoretical design and an experiment is only as good as its design and equipment. Once both results are compiled they can be compared. Then a determination can be made as to whether the model matches with the features of the measured data.

The objective of this research is to verify the Seismo Acoustic Fast field Algorithm for Range-Independent environments (SAFARI) in the very-low-frequency (VLF) acoustic regime (from 5 Hz to 20 Hz) by comparison with the data recorded by Marine Physical Laboratory (MPL) in the Noise and Transmission Loss in Very Low Frequency Environment (NATIVE 1) experiment, which they conducted in August of 1990. Chapter II gives a thorough background on the NATIVE 1 experiment, including a description of the site's geoacoustic and bathymetric makeup as well as the types of source and receiver used. Chapter III goes into a description of the theory behind SAFARI. Chapter IV discusses the data sources used in the comparison. Chapter V investigates model aliasing and contour offset features. Chapter VI presents a graphical comparison of model results and data. Chapter VII gives the conclusions reached and proposes areas for further investigation.

II. NATIVE 1

A. BACKGROUND

In August of 1990, the NATIVE 1 experiments were conducted to acquire data to provide insight into VLF-propagation effects. Along with the development of a VLF data base was the effort to design VLF performance prediction models which would support the development of new Antisubmarine Warfare (ASW) acoustic sensors. NATIVE 1 was a multi-laboratory,at-sea exercise conducted on Blakes Plateau, Figure 1 [Ref. 1]. Two sites were used, one in deep water and one in shallow water. Five events, lasting several weeks were conducted using a variety of devices and equipment. Data from the first of these events at the deep water site will be used. Figure 2 [Ref. 2] shows the locations of the initial entry and recovery points of the receivers. Typical Swallow Float deployments consist of forming an equilateral triangle pattern with three floats, at known positions, spaced about 6.5 km between floats. This provides a reference for float localization. A 15-lb anchor on a 3-m tether replaces the ballast. The remaining floats are deployed in the center of the triangle. Figure 3 shows the path of the source over the day and a half comprising the recording time. The event

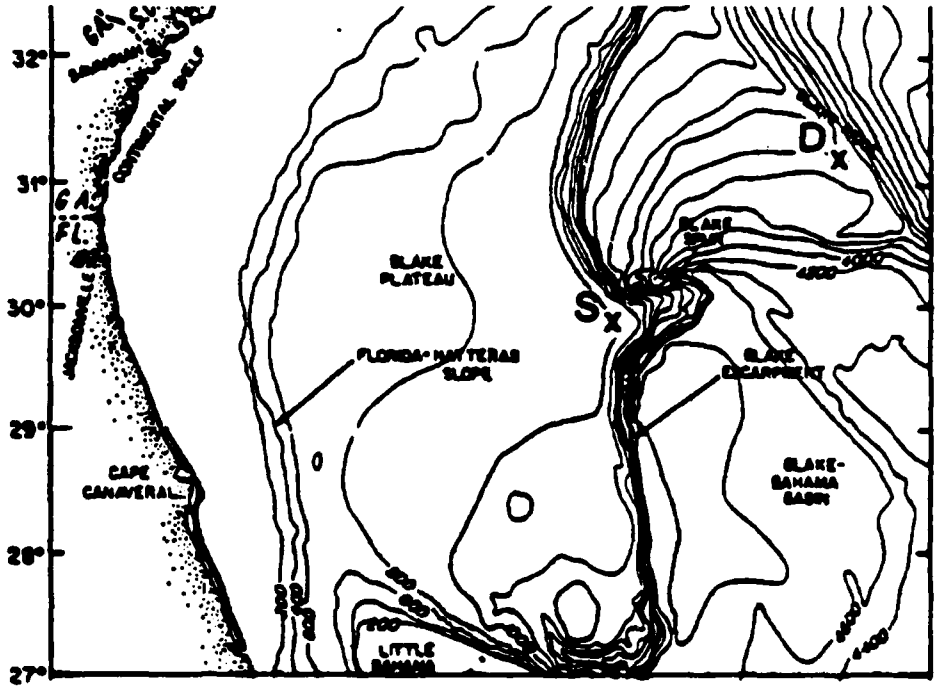

Figure 1 Native 1 Site "D" in 3400 m of water and "S" in 1000 m of water.[Ref. 1:p. 2]

starts with the source well north, approximately 12 km, of the center of the sensor site. It maintains a track of approximately 193 degrees past the receivers and continues south for another 50 km, and then turns around on the reciprocal heading finishing approximately 6 km north of the site.

B. EXTREMELY LOW FREQUENCY SOURCE

In this event a calibrated extremely low frequency (ELF) source projector was towed by the research vessel (R/V) Gyre. A precise positional log (Appendix A) was maintained from

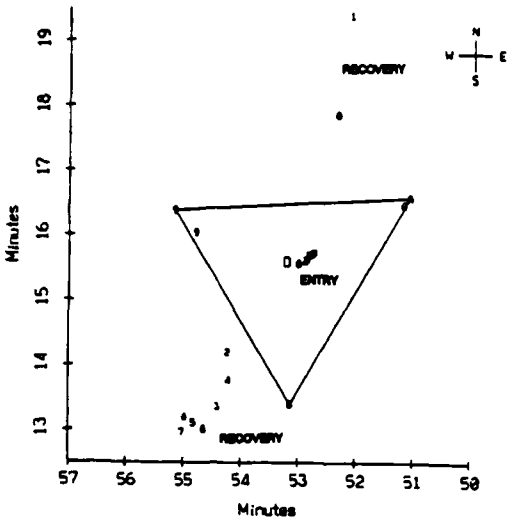

Figure 2 Plan view of entry and recovery positions of Swallow floats. Event 1, NATIVE 1, (34°N, 74°W) [Ref 2:p. 2]

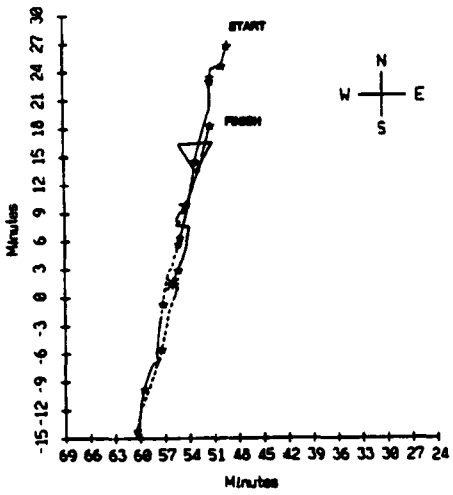

Figure 3 Research vessel Gyre track during Event 1, NATIVE 1 (31°N, 74°W) [Ref. 2:p. 2]

multiple navigational sources. These included Global Positioning Systems (GPS), LORAN, and Transit Satellite Navigation (Transit Sat Nav). Towing speed was 4.0 ± 0.5 knots and the source depth was 122 ± 7 meters. The source projected two continuous wave frequencies simultaneously; 7 Hz

and 10 Hz from 1630 to 2230 on 4 August and 0030 to 0400 on 5 August, and 10 Hz and 16 Hz from 0800 to 1130 on 5 August. At 7 Hz, the average source level was 164 ± 2 dB//μPa, at 10 Hz the average source level was 166 ± 2 dB/μPa, and at 16 Hz the average source level was 161 ± 2 dB/μPa [Ref. 3]. (All estimates were made from visual inspection of the data.) The positional accuracy of the ship was source dependent with the GPS system having the highest degree of accuracy, about ± 60 meters. Transit Sat Nav was next with an accuracy of ± 100 meters and LORAN was accurate to within ± 0.5 nautical miles. The times each of these systems were used on the above dates are highlighted in Appendix A, along with the actual track data.

> "The Transit Sat Nav is dependent on satellite elevation above the horizon, time from satellite fix to position solution and dead reckoning parameters (course and speed) used for updates. Therefore I estimate Transit Sat Nav is only accurate in general, to within 0.5-1.0 nautical miles. LORAN appears to be accurate to within 0.5 nautical miles with better repeatability. For this reason there is a constant offset or position error between GPS and LORAN of -0.021 degrees longitude which should be added to LORAN longitudes. This would move all LORAN positions further to the west. This correction has not been applied to LORAN positions in enclosure(2) (Appendix A) which is taken from the NADC navigation rectification products. It also will not affect ranges along the track from source to receiver due to the north-south orientation of the Event 1 track." [Ref. 4]

C. ENVIRONMENTAL DATA

The exercise area is located off Jacksonville Florida, east of the Gulf Stream in the waters commonly called the Sargasso Sea. At the end of Event 1, 41 bathythermographs and one conductivity, depth, temperature (CDT) cast were made (Figure 4). Sample values of those results [Ref. 1:pp. B1-B23] are in Appendix B, and are typical of the water masses which commonly make up this region. The temperature

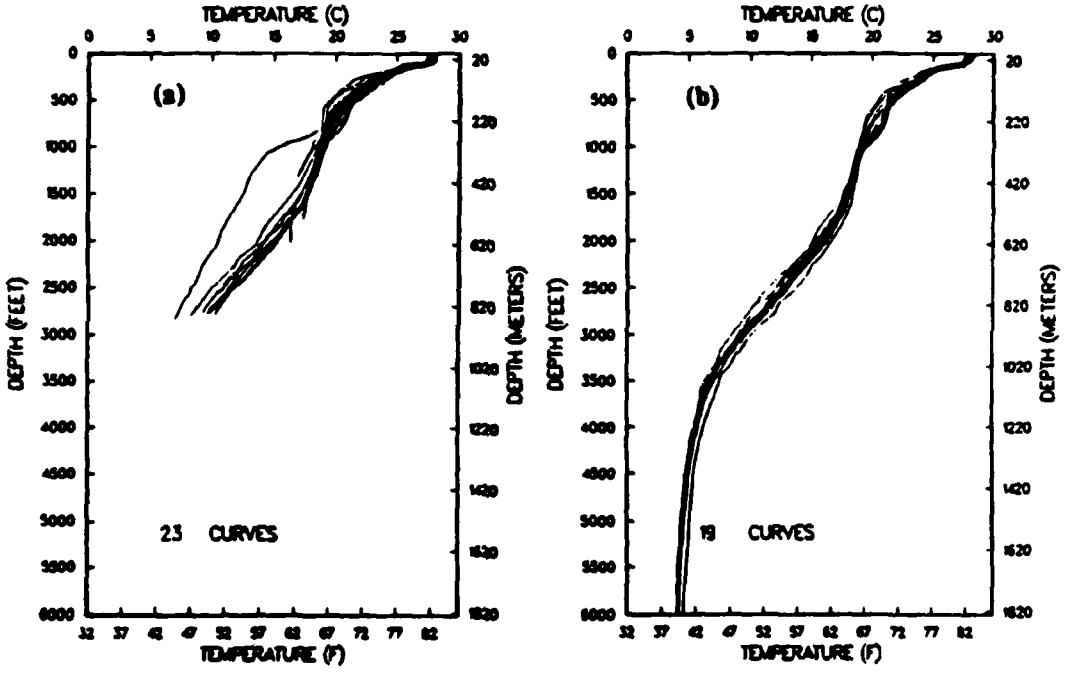

Figure 4 Site "D" temperature profiles for (a)AXBTs, (b)XBTs [Ref. 1:p. 22]

variability was minimal with one exception located in Gulfstream Waters well to the west of the track. Province contours (Figure 5) were generated and representative values of each province are listed in Appendix B. Those profiles

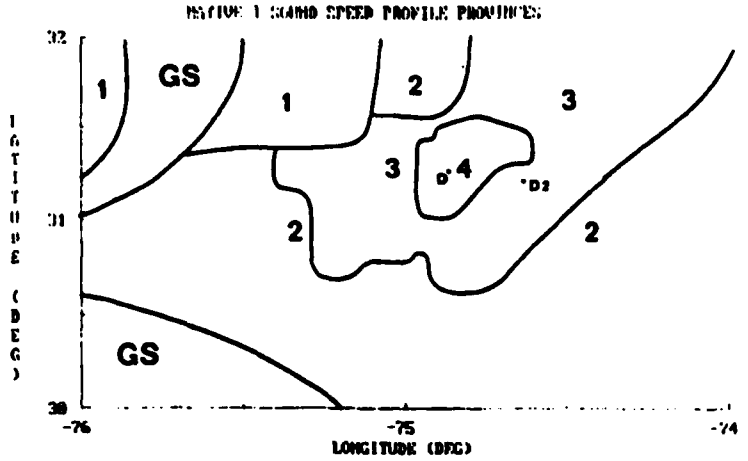

Figure 5 Site "D" sound speed provinces.[Ref. 1:p. 23]

that are generally cooler have lower province numbers. Table I shows the province profile number and range from site "D" along the track of R/V Gyre during Event 1.

Seasonal heating in summertime dominates the surface water while the seasonal thermocline extends to about 100 m. From 100 to 500 m is the regime called '18 degree' water mass where the temperature gradient is small producing an isovelocity water. Below 500 m to any where between 2500 to 3000 m North Atlantic Central Water with a deep sound

Table I RANGE FROM SITE "D" AT WHICH THE SOURCE ENTERED A PROVINCE PROFILE NUMBER ALONG EVENT 1 TRACK.[Ref 1:p.24]

Range (nautical miles)	Province Number
-12.54	4
14.21	3
26.69	2

channel axis at about 1200 meters. Below this is the very stable North Atlantic Deep and Bottom water mass.

D. GEOACOUSTIC BOTTOM

The bathymetric track (Figure 6) was recorded by R/V Gyre

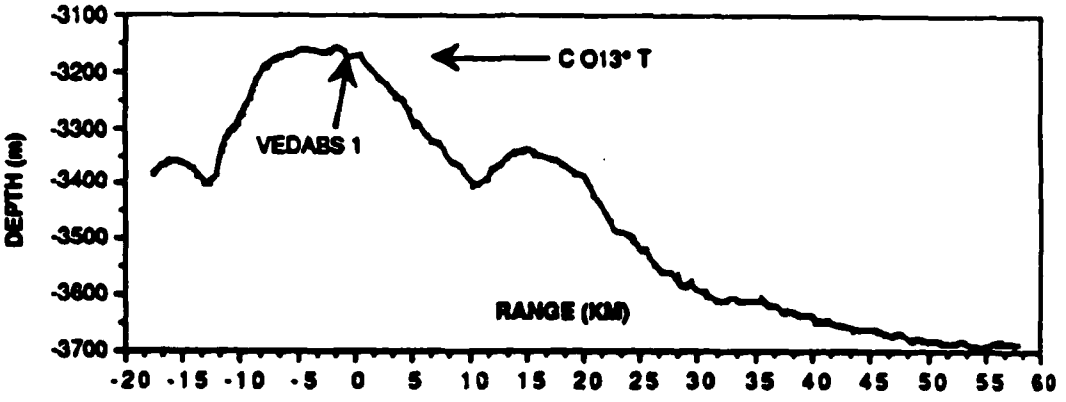

Figure 6 Bathymetric Track from Site "D", Event 1 [Ref. 1:p. 40]

during Event 1. The bottom varied from a minimum of 3159 m near the VEDABS 1 location (center of the site) to a maximum at 3688 m. This yields an approximate slope from 0.002 to 0.001 for the bottom and, as such, is considered horizontal and flat. In Figure 7 representative samples of the geoacoustics of the bottom sediments from [Ref. 5] were generated along the R/V Gyre track using the model found in the front of Appendix C. [Ref 1:p. 45]

E. SWALLOW FLOATS

The following discussion is adapted from D'Spain et.al. [Ref. 6]. A general description of the Swallow Float is followed by a discourse on the data acquisition process, including a discussion of the hydrophone and the electronic

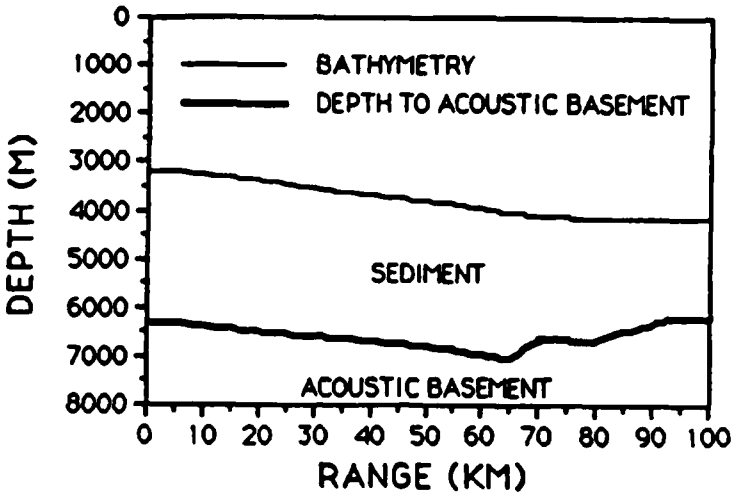

Figure 7 Site "D" Bearing 000°T Water Depth and Depth to Acoustic Basement[Ref. 5:p. B-24]

circuit, and finally a discussion on the hydrophones autospectra.

1. Description

Swallow Floats are independent, freely-drifting, neutrally-buoyant sensors which can be ballasted to float at any desired depth (± 100 m). Figure 8 shows a schematic of a typical Swallow Float. Mounted within the 0.432m diameter Benthos glass shell are three orthogonally mounted geophones, a compass, the electronics with power supply (not shown), and cassette tape recorder (not shown). A polyethylene hard hat covers the glass shell's exterior with an Ocean Applied Research (OAR) xenon flasher attached to one side and an OAR radio beacon on the other. These are used for detection and localization during recovery.

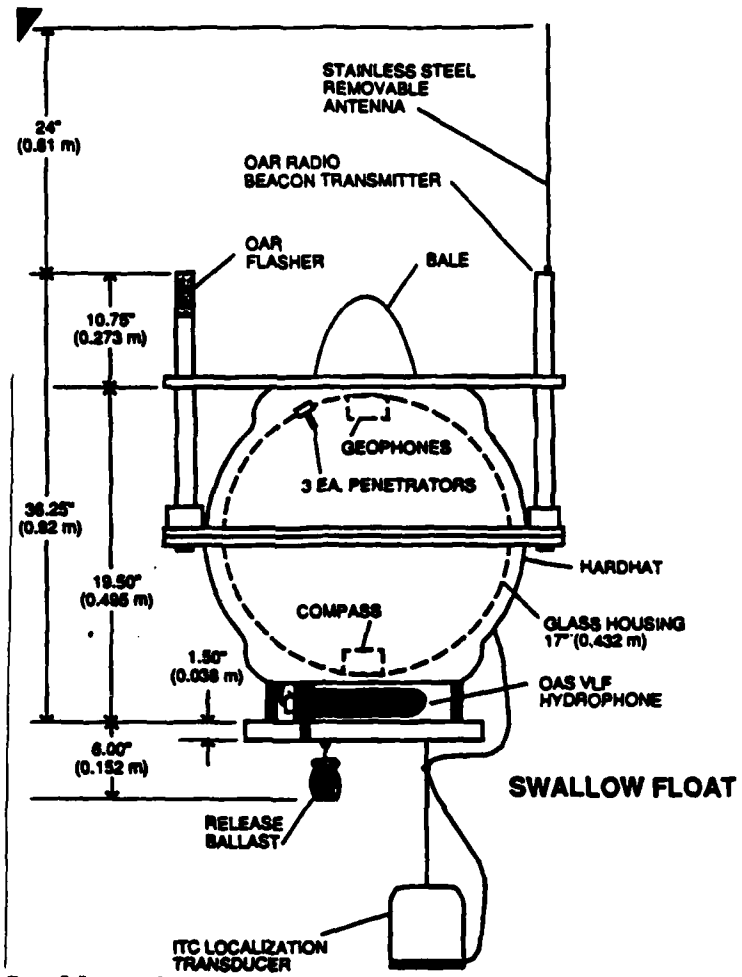

Figure 8 Swallow float [Ref. 6:p. 31]

To prevent distortion of the compass readings, the compass is mounted on the bottom of the shell at its maximum distance from the magnetic fields of the geophones, mounted on the top of the shell. The power supply provides a maximum of 200 hours of data acquisition and 25 days of acoustic-transponder life. Duration of Swallow float deployments is not limited by power supply requirements but by the capacity of the 17-megabyte cassette tape recorder.

An infrasonic hydrophone is mounted outside the glass shell on the base plate just below the compass, approximately 0.5 m below the geophones. Suspended below the base plate is the expendable ballast. The ballast can be acoustically commanded to release and has two independent backup timed release circuits. The ballast weight is accurately determined prior to float deployment to achieve the desired depth of deployment. A change in ballast of 1 gm results in depth changes of 7 to 10 m. The ballast fits snugly against the base plate in order to reduce its rocking motion relative to the float; herein Figure 8 is distorted.

Each float is also equipped with an International Transducer Corporation (ITC) localization hydrophone which is suspended 1.83 m below the glass shell. This hydrophone has a source level of 191 dB//1μPa at 1 m and a receiving sensitivity of -180 dB//1V/μPa at 8 kHz. Under microprocessor control and synchronized prior to deployment, the floats send 8-kHz localization pulses of 10-ms duration. This allows for post deployment determination of depth and location during deployment. This hydrophone and the associated circuitry also allow for two types of acoustic commands, uniquely coded for each float, to be issued. The first is a 50-ms 8-kHz pulse used for ship to float slant range calculation and the second activates the ballast release circuitry and issues a 500-ms 8-kHz pulse and is used at the end of the experiment for float recall.

2. Data Acquisition

The Swallow Float data acquisition system (Figure 9) records the acoustic pressure and particle motion at the sensors. This discussion is restricted to the acoustic

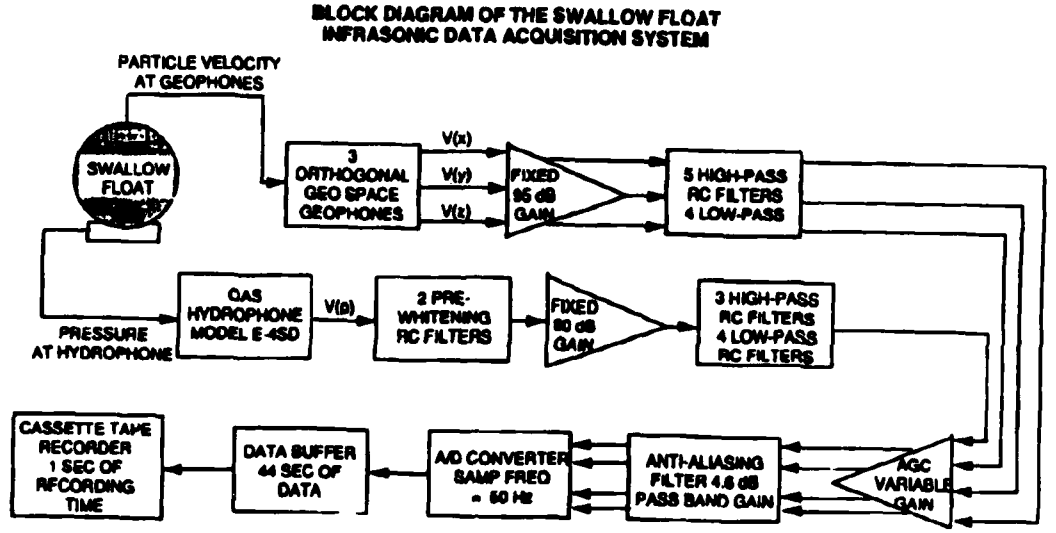

Figure 9 Swallow Float data acquisition system [Ref. 6:p. 31]

pressure only. An OAS model E-4SD hydrophone is the pressure sensor which converts acoustic and nonacoustic pressure fluctuations into voltage signals with a sensitivity of -182 dB// 1 V/μPa. The hydrophone has a frequency response which is flat (± 1 dB) from 0 to 5kHz [Ref 6:p. 8]. The signal then passes in order through:

- two prewhitening RC filters
- fixed 80 dB gain amplifier
- three highpass RC filters and four lowpass RC filters

- automatic gain control (AGC) amplifier
- anti-aliasing filter
- A/D converter
- data buffer with 44 seconds of data
- cassette tape recorder with 1 second of write time for each acoustic record

Each acoustic record is 45 s long (44 seconds of recorded data and 1 second of write time).

3. Pressure Autospectra

From the recorded data, the RMS pressure at each float was calculated. These RMS time series were corrected for AGC gain but were otherwise uncalibrated. The vertical axis of the recorded data is in units of RMS volts at the A/D converter (Figure 9).

> "Each RMS level value results from taking the square root of the average of the squared amplitude levels over a period of five seconds (or 250 points since the data sampling rate is 50 Hz). Since each record is 2250 points (45 seconds) long, then nine RMS power values are calculated for each record. The RMS value for the last five-second period of each record includes one second of zeros. The one second of zeros represents the time during which no data is sampled while data in a temporary buffer is being written to cassette tape." [Ref. 2:p. 21]

> "Spectral estimates with two different frequency resolutions are calculated. Those with a 98 mHz resolution are made by dividing 40.96 seconds in a data record (obtained after skipping the first 3 seconds of data) into seven 10.24-second-long segments, with a 50 percent overlap between segments. The segments are fast Fourier transformed after using a Kaiser-Bessel window of α=2.5 to window the data. The resulting seven spectra within a record are incoherently averaged together. The averaged spectra for four consecutive records (equal to three minutes of data) are then incoherently averaged in

order to further reduce the variance of the spectral estimates. For spectral estimates with a 24 mHz resolution , the segment length which is transformed is quadrupled to 40.96 seconds and the spectra for twenty consecutive records are incoherently averaged."[Ref. 2:p. 26]

The autospectra are calculated in dB // 1(μPa)2/Hz. Records used in the analysis were all three minute averaged data, using four 45 second records for each data point.

III. MATHEMATICAL MODEL

A. BACKGROUND

In the attempt to model the complex environment found in the ocean, there have been a variety of techniques used to determine the solution to the wave equation, each involving its own simplifying assumptions and approximations. One subset of these techniques is the method using separation of variables. Two approaches fall into this general category: the normal mode and the fast field approach. It is the latter that is implemented in SAFARI [Ref. 7]. The following sections provide a summary of the wavefield technique found in Schmidt [Ref 7]. In a horizontally stratified environment, including fluid and solid layers, this technique yields, an exact solution to the linearized wave equation,

$$(\nabla^2 - \frac{1}{c(r,z)^2}\frac{\partial^2}{\partial t^2})\Psi(r,z,t) = F_s(r,z,t) \qquad 3.1$$

The following sections develop the basic mathematical approach, discuss environmental and analytical models, boundary conditions, and numerical techniques including, the global matrix approach, wavenumber integration, aliasing, and contour offsetting.

B. MATHEMATICAL MODEL

As early as 1948 [Ref. 8], the subject of wave propagation in a stratified medium was being studied in planar

two- and three-layer environmental models. The technique applies a series of integral transforms to the linearized Helmholtz wave equation, Eq. 3.1, reducing a partial differential equation in time and three spatial dimensions into a series of ordinary differential equations in the depth coordinate. These ordinary differential equations can be solved analytically in terms of unknown amplitudes by matching boundary conditions at the interfaces. For a cylindrical coordinate system {r,θ,z}, the model solves for an axial symmetric, or planar, wavefield independent of θ. The isotropic media can be expressed in terms of scalar potentials $\Psi(r,z,t)$ which satisfy Equation 3.1, where $c(r,z)$ is the wave speed and $F_s(r,z,t)$ is a forcing term representing the source. The first of two integral transforms is next applied. The forward Fourier transform

$$f(\omega) = \frac{1}{2\pi}\int_{-\infty}^{\infty} F(t)\, e^{-i\omega t} dt \quad (a)$$
$$F(t) = \int_{-\infty}^{\infty} f(\omega)\, e^{i\omega t} dt \quad (b) \qquad 3.2$$

gives the frequency domain wave equation

$$(\nabla^2 + k_m^2(r,z))\,\Psi(r,z,\omega) = f_s(r,z,\omega) \qquad 3.3$$

where ω is the angular frequency and $k_m(r,z)$ is the medium wave number,

$$k_m(r,z) = \omega / c(r,z) \qquad 3.4$$

For stratified range independent environments with a point source present, Equation 3.3 can be simplified to

$$(\nabla^2 + k_m^2(z))\,\Psi(r,z,\omega) = \frac{f_s(z,\omega)\,\delta(r)}{2\pi r} \qquad 3.5$$

In the following, the ω dependence will be suppressed. The Hankel transform pair are utilized

$$\begin{aligned} g(k) &= \int_0^\infty G(r)\,J_0(kr)\,r\,dr \quad (a) \\ G(r) &= \int_0^\infty g(k)\,J_0(kr)\,k\,dk \quad (b) \end{aligned} \qquad 3.6$$

where k is the horizontal wavenumber, and the forward transform, Eq 3.6(a), is applied to obtain the depth-separated wave equation which is an ordinary differential equation in depth only. The solution to this equation is the sum of a particular solution Ψ_p to Eq. 3.5, and any linear combination of the two independent solutions to the homogeneous equation. It is commonly called the depth-dependent Green's function whose coefficients are arbitrary and are determined by the boundary conditions. Once the coefficients are found, the inverse Hankel transform [Eq. 3.6(b)] yields a wavefield at any range r at the angular frequency ω. The inverse Fourier transform yields the time response in the same fashion.

C. BOUNDARY CONDITIONS

1. Environmental Model

In SAFARI, the environment is represented as a horizontally stratified medium, Figure 10, with all interfaces planar and parallel. The properties of the layers are range

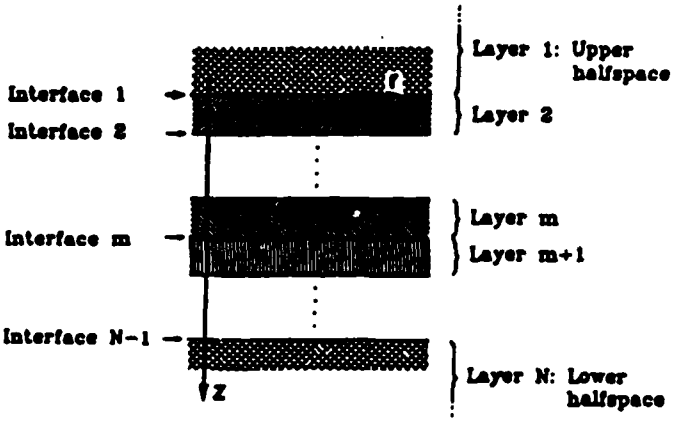

Figure 10 Horizontally stratified environment [Ref. 7:p. 5]

independent. Solid layers are assumed to be homogeneous and isotropic with Lamé constants λ and μ and density ρ. The compressional wave speed is

$$c_c=\sqrt{(\lambda+2\mu)/\rho} \qquad 3.7$$

and the shear speed is

$$c_s=\sqrt{\mu/\rho} \qquad 3.8$$

Physically realistic materials must satisfy the condition

$$c_s<\sqrt{0.75}c_c \qquad 3.9$$

so that the bulk modulus, K= $\lambda+2/3\mu$, be positive, and the solid medium have positive compressibility. The density in fluid layers must be constant while the nonvanishing Lamé constant λ is allowed to vary with depth according to:

$$\frac{1}{\lambda(z)} = az+b \qquad 3.10$$

corresponding to the following depth dependence for the sound speed, Eq 3.7,

$$c_c(z) = \sqrt{1/(\rho(az+b))} \qquad 3.11$$

2. Analytical Models

The analytical field representation for the media included in SAFARI are for a homogeneous fluid, inhomogeneous fluid, and solid representations, and are governed by the equation of motion for each media. The focus of this section is not on the details of each derivation but rather on the fact that the wavefield at each interface has two integral representations one each from the upper and lower layers.

For the homogenous fluid, the solution to the depth-dependent Greens function for the potential is of the form

$$\Phi(r,z) = \int_0^\infty [A^- e^{-\alpha z} + A^+ e^{\alpha z} J_0(kr)\, k\,dk \qquad 3.12$$

where $k_m(z)=h_m$ (a constant), $\alpha(k)=\sqrt{k^2-h_m^2}$, and no source is present. A^- and A^+ are the unknown amplitudes of the downgoing and upgoing waves. If an omnidirectional point source is present the particular solution is added to the homogeneous solution and is of the form

$$\Phi(r,z)=\frac{S_\omega}{4\pi}\int_0^\infty \frac{e^{-\alpha|z-z_s|}}{\alpha}J_0(kr)\,kdk \qquad 3.13$$

where S_ω is the source strength and z_s is the source depth. The associated displacement and stress are

$$w(r,z)=-\frac{S_\omega}{4\pi}\int_0^\infty sign(z-z_s)\,e^{-\alpha|z-z_s|}J_0(kr)\,kdk \qquad 3.14$$

$$\sigma_{zz}(r,z)=-\frac{S_\omega\rho\omega^2}{4\pi}\int_0^\infty \frac{e^{-\alpha|z-z_s|}}{\alpha}J_0(kr)\,kdk \qquad 3.15$$

where

$$sign(z-z_s)=\begin{cases} 1, & z-z_s>0,\\ 0, & z-z_s=0,\\ -1, & z-z_s<0 \end{cases}$$

Since the ocean is not a homogeneous media and the sound velocity varies with depth, a single layer ocean wave guide doesn't properly reflect acoustic propagation. However, if a range independent wave guide is represented by an

number of homogeneous layers, a numerical solution based on their field representation will converge toward the correct solution. It can be shown when modelling a deep water site there must be a velocity profile incorporated, as is the case here, moreover, to ensure a satisfactory convergence the isovelocity layers must be less than one quarter wavelength thick. Once again it can be shown the solution to the depth dependent Greens function, based on c(z), from Eq. 3.11, and not an isovelocity constant, can be obtained by using a variable transformation in which

$$\begin{aligned}\zeta &= c^{-2/3}(cz+d) \\ &= (\rho\omega^2 a)^{-2/3}(k^2-\rho\omega^2(az+b))\end{aligned} \qquad 3.16$$

When substituted into Eq. 3.5 the following is obtained:

$$\left(\frac{d^2}{d\zeta^2}-\zeta\right)\Phi(\zeta)=0 \qquad 3.17$$

This yields the integral form of the potential with a source,

$$\Phi(r,z) = -\frac{S_\omega}{4\pi}\int_0^\infty J_0(kr)\,kdk$$

$$\times\begin{cases}\dfrac{2c^{-1/3}(Ai(\zeta_s)+iBi(\zeta_s))Ai(\zeta)}{Ai'(\zeta_s)(Ai(\zeta_s)+iBi(\zeta_s))-Ai(\zeta_s)(Ai'(\zeta_s)+iBi'(\zeta_s))} \\ \qquad\qquad ,a(z-z_s)\le 0, \\ \dfrac{2c^{-1/3}Ai(\zeta_s)(Ai(\zeta)+iBi(\zeta))}{Ai'(\zeta_s)(Ai(\zeta_s)+iBi(\zeta_s))-Ai(\zeta_s)(Ai'(\zeta_s)+iBi'(\zeta_s))} \\ \qquad\qquad ,a(z-z_s)\ge 0\end{cases} \qquad 3.18$$

By expressing the displacements due to both normal stress and tangential stress forces in terms of scalar potentials the solution to the depth dependent Greens function for a solid are of the form,

$$\Phi(r,z) = \int_0^\infty [A^- e^{-\alpha z} + A^+ e^{\alpha z}] J_0(kr)\, k\,dk \qquad 3.19$$

$$\Psi(r,z) = \int_0^\infty [B^- e^{-\beta z} + B^+ e^{\beta z}] J_0(kr)\, dk \qquad 3.20$$

The normal stress and tangential stress are solved for in the same fashion as in the homogeneous case. Here β is the wavenumber for tangential stress analogous to the normal stress wavenumber α in Eq. 3.12.

3. Matching Boundaries

The boundary conditions are matched at each interface dependent upon the type of interface involved. The following list summarizes the conditions:

- For an interface separating two fluid layers, the vertical displacement w and the normal stress σ_{zz} have to be continuous. If one of the media is a vacuum, the normal stress must vanish.
- For an interface separating a solid and a vacuum, both σ_{zz} and σ_{rz} must vanish, whereas a solid-fluid interface requires that w and σ_{zz} must be continuous and σ_{rz} must vanish.
- For an interface separating two solid media, w,u,σ_{zz}, and σ_{rz} must all be continuous.

"Since the boundary conditions have to be satisfied at all ranges r, it is obvious that they must be satisfied by the kernels in the integral representations as well. The

radiation conditions for $z \to \pm\infty$ together with the conditions to be satisfied at all interfaces simultaneously, lead to a linear system of equations in the unknown kernel coefficients A^-, A^+, B^-, and B^+. In principle, this system has to be solved for all values of the horizontal wavenumber k, and the total field can then be determined by evaluating the inverse transforms. Except for a few trivial cases, however, both the solution of the linear system of equations and the evaluation of the inverse transforms have to be done numerically, requiring truncation and discretization of the horizontal wavenumber axis." [Ref. 7:pp. 17-18]

D. NUMERICAL TECHNIQUES

The global matrix approach and wavenumber integration are now discussed.

1. Global Matrix Approach

The global matrix approach is a more direct and computationally more efficient technique in assembling the local solution to the depth dependent Greens function, for each layer, in terms of its source contribution and unknown scalar potentials, with all other local solutions. The boundary conditions determine a system of equations in the Hankel transforms of the potentials to be satisfied at each interface. In similar fashion to finite element model programs [Ref. 9] these local system of equations are mapped into a global set of equations defining the boundary conditions at all interfaces simultaneously.

"The resulting global coefficient matrix is organized to be block-bidiagonal and diagonally dominant in close analogy to the global stiffness matrix arising from the finite- element method. Unconditionally numerically-stable solutions are determined efficiently by gaussian elimination, yielding the field in all layers simultaneously." [Ref 7:p. 29]

The mechanics of the technique's derivation of the solution is secondary to the understanding that unconditionally stable solutions are obtained, and that the technique is stable for any machine precision. Herein, SAFARI is an excellent choice for depth range contouring of single frequency transmission loss, the focus of this study.

2. Wavenumber Integration

Numerical techniques which evaluate the depth dependent Green's function by the inverse Hankel transform,

$$G(r,z) = \int_0^\infty g(k,z)\, J_m(kr)\, k dk \qquad 3.6(b)$$

derive truncated solutions to the infinite integration interval. Here the subscript m equals 0 except for the shear stress and horizontal displacement where m equals 1. Because the interval on the wavenumber k goes from 0 to ∞ the solution can be done to any degree of accuracy within the computing limits of the machine. In a lossless media, waveguide propagation produces normal modes and interface waves which show up in the wavenumber integration as poles. As the integrand varies over k these plot in the complex plane on the real axis. For lossy media, these poles move out into the complex plane, remaining close to the real axis. In cases where solid layers underlie fluid layers care must be taken to ensure the maximum medium wavenumber truncation point is selected beyond any significant contributions from waves

propagating in those solid layers. Here, evanescent surface, interface or plate modes may exist causing poles to appear in the integration plots. Typically 20% above a maximum medium wavenumber is a good value for truncation of the wavenumber range.

Once the truncation point is selected two factors complicate the remaining solution. The first is the existence of normal modes and interface waves which generate poles in the kernel of the transform. The second is the Bessel function $J_m(kr)$ which may vary rapidly in k, the horizontal wavenumber, for long ranges in r. A very fine sampling interval has to be chosen to avoid aliasing, addressed below.

DiNapoli and Deavenport [Ref. 10] show, for the ranges of this study, the Bessel function,

$$J_m(kr) = \frac{1}{2}\left(H_m^{(1)}(kr) + H_m^{(2)}(kr)\right) \qquad 3.21$$

can be represented by the outgoing Hankel function $H_m^{(2)}$

$$\lim_{kr\to\infty} H_m^{(2)}(kr) = \sqrt{\frac{2}{\pi kr}}\, e^{-i\left(kr-\left(m+\frac{1}{2}\right)\frac{1}{2}\pi\right)} \qquad 3.22$$

(The incoming Hankel function is needed only for evaluation in the near field within a few wavelengths of the source.) This yields an inverse Hankel transform integral

$$G(r,z) = \sqrt{\frac{1}{2\pi r}}\, e^{i\left(m+\frac{1}{2}\right)\frac{1}{2}\pi} \int_0^\infty g(k,z)\sqrt{k}\, e^{-ikr}\, dk. \qquad 3.23$$

The wavenumber space having been truncated is divided equidistantly in SAFARI as follows:

$$k_l = k_{min} + l\Delta k, \quad l = 0, 1 \ldots (M-1) \qquad 3.24$$

where M is the total number of sampling points. The range axis is divided accordingly as

$$r_j = r_{min} + j\Delta r, \quad j = 0, 1 \ldots (M-1) \qquad 3.25$$

where the range step Δr is governed by the relationship

$$\Delta r \Delta k = 2\pi / M \qquad 3.26$$

and M is an integral power of 2. The discrete approximation of Eq 3.23 is finally obtained,

$$G(r_j, z) \approx \frac{\Delta k}{\sqrt{2\pi r_j}} e^{-i(k_{min} r_j - (m+\frac{1}{2})\frac{1}{2}\pi)} \sum_{l=0}^{M-1} [g(k_l, z)\, e^{-i r_{min} l \Delta k} \sqrt{k_l}]\, e^{-i(2\pi lj/M)} \qquad 3.27$$

The summation can be performed by means of a fast Fourier transform (FFT) generating the field at all M ranges, in Eq. 3.25, simultaneously.

3. Aliasing and Contour Offset

Regarding aliasing, the undersampling in one domain causing wrap around in the other domain of a transform, Eq. 3.27 does not yield G(r,z) but a summation from the lower limit to the upper limit of the interval. The range from zero to the lower limit and from the upper limit to infinity will cause some aliasing in the wavenumber. Over the interval $[r_{min}, r_{min} + R]$, where the range window width $R = M\Delta r$, the maximum

useable range is always $R=M\Delta r$, independent of the choice of r_{min}.

For ranges larger than $r_{min}+R$ aliasing can be reduced by choosing the window R so large that the signal is known to dissipate within the window. For a fixed wave number interval this would require a large number of wavenumber samples.

According to Cauchy's theorem the integrals in the complex plane between two points are invariant to a change in the integration contour, that is by moving the integration contour away from the pole, offsetting it, the integrands can be smoothed and aliasing avoided. In SAFARI this is done by replacing k with $\hat{k}=k+i\epsilon$ where ϵ is a vertical offset whose contribution to the total integral is insignificant when compared to that of k ie. $\epsilon \ll k_{max}-k_{min}$. Eq. 3.27 is replaced by

$$G(r,z)=\sqrt{\frac{1}{2\pi r}}e^{i(m+\frac{1}{2})\frac{1}{2}\pi}\int_C g(k,z)\sqrt{k}e^{-ikr}dk \qquad 3.28$$

where C is the contour shown in Figure 11. For ranges larger than r_{min} + R, a factor of $e^{-\epsilon R}$ is introduced to the FFT and the signals will be attenuated. Similarly for ranges smaller than r_{min} signals wrapped around will be amplified by $e^{\epsilon R}$. No change occurs in the maximum range $r_{max}=R$, from the real axis integration. Corresponding to an attenuation of 60 dB of the wrap around signal the value of ϵ is formulated as

$$\epsilon=\frac{3}{R\log e}=\frac{3}{2\pi(M-1)\log e}(k_{max}-k_{min}) \qquad 3.29$$

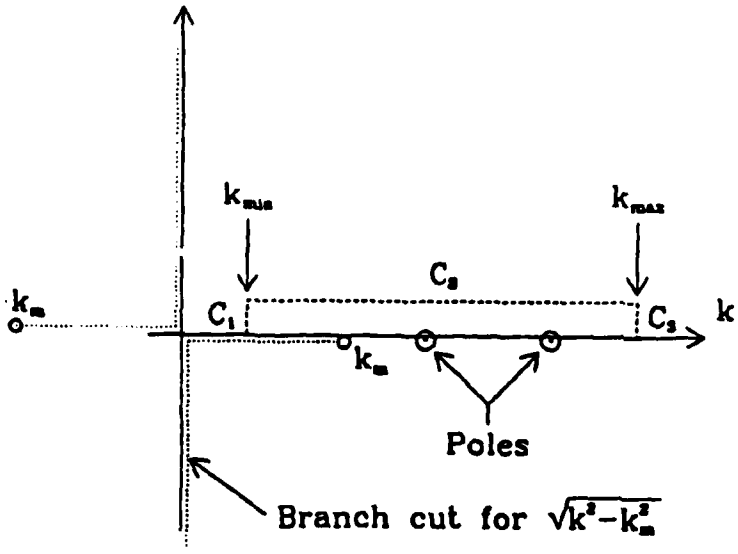

Figure 11 Complex Integration Contour [Ref. 7:p. 33]

which even for a small number of sampling points ensures $\epsilon \ll k_{max}-k_{min}$. Paramount to this numerical integration scheme is that the kernel must vary smoothly between sampling points. If the integration is truncated at a point where the kernels amplitude is significant, the discontinuity will give rise to aliasing. To avoid this, a first order Hermite polynomial is employed and the kernel and its first derivative become continuous at the truncation point.

IV. DATA SOURCES AND ACOUSTIC MODELING INPUTS

The recorded transmission loss data sent by Marine Physical Laboratory (MPL) of Swallow Float 0 is described along with the input files used in running the SAFARI model.

A. SWALLOW FLOAT DATA

The data [Ref. 11] received from MPL were 12 files of Swallow Float 0 data recorded during Event 1 of the NATIVE 1 experiment. It was received via electronic mail and transferred to 5.25" high density floppy disks. The files contained two columns of information. The first column contained the R/V Gyre-to-buoy range in kilometers and the second column contained either the percentage of clipped data points (four files) or the transmission loss (eight files) in units of dB referenced to a source with pressure amplitude of 1 μPa at 1 meter. Reference 11 received from MPL goes into the scheme for defining the data: TL0.[1,2,3,4].[7,10,16] references the Transmission Loss Float 0, the region number and the frequency for the region. The regions are,

Region 1: The Gyre approached the float from the north-northeast near the beginning of Event 1 broadcasting 7 and 10 Hz.

Region 2: The Gyre passed over the float heading south-southwest broadcasting 7 and 10 Hz.

Region 3: After the SUS charge events as the Gyre continued to the south-southwest broadcasting 7 and 10 Hz.

Region 4: The Gyre approached the float from the south-southwest broadcasting 10 and 16 Hz.

With regard to the navigational data and the Gyre-to-float range, the 5 minute log in Appendix A was interpolated every 45 seconds to get a position for each record of data. As of the writing of this paper, there is a question as to whether or not a range offset of approximately 0.5 km occurs in the navigational data.

Unless otherwise annotated, all Swallow Float data presented in the analysis section has less than 5 percent of clipped time series points in the hydrophone channel. Where the percentage of clipped points exceeded 5 percent the record was deleted. This was done using a DOS text editor.

B. SAFARI MODEL AND INPUTS

The SAFARI model was installed at the Fleet Numerical Oceanography Center in Monterey, California in a UNIX environment on an HP workstation. It was supported by DISSPLA graphics, and executed the Fortran code on an F77 Fortran compiler. Upon satisfactory duplication of the results for the test files in Ref. 7, and an independent two-layer split fluid case verified by alternate means, analysis proceeded with the model.

The water column data from province 4 in Appendix B and the geoacoustic model data from Appendix C was used to produce a 43-layer water-sediment input file in the standard SAFARI

FIP format. The FIP module generates single-frequency calculation of the total wavefield for a single point source whose source strength S_ω is normalized to yield a pressure of 1 Pa at 1 meter distance from the source. The graphical results correspond to the standard definition of transmission loss. [Ref 7:p. 67] The table in Figure 12 shows the required input file blocks. The first block contains the title of the run, the second block the options selected. For this study the following options were used at one point:

- N the calculation of normal stress σ_{zz} (equal to negative pressure in a fluid).
- I Hankel transform integrands are plotted versus wavenumber.
- T Transmission loss of the pressure versus range.
- J Complex integration contour.
- Z Plot of the water column velocity profile.

The third block contains the frequency which was either 7 Hz or 10 Hz, and the integration contour offset. If left blank no contour offset was incorporated. A zero input gave the default contour offset which yields 60 dB at the longest range considered in the FFT. The fourth block is the number of layers (NL) including the upper and lower halfspaces, and is followed by each layers upper boundary depth from 1 to NL, the compressional velocity, the shear velocity, the compressional attenuation in dB/λ, the shear attenuation in dB/λ, (both of which are converted from dB/m*kHz to dB/λ by multiplying each

Block		Parameter	Units	Limits
I	TITLE :	title of run	-	$\leq$ 80 char.
II	opt1 opt2 ...:	output options	-	$\leq$ 40 char.
III	FREQ:	source frequency	Hz	> 0
	COFF:	integration contour offset	dB/Λ	COFF $\geq$ 0
IV	NL:	number of layers, incl. halfspaces	-	NL $\geq$ 2
	D:	depth of interface	m	-
	CC:	compressional speed	m/s	CC $\geq$ 0
	CS:	shear speed	m/s	-
	AC:	compressional attenuation	dB/Λ	AC $\geq$ 0
	AS:	shear attenuation	dB/Λ	AS $\geq$ 0
	RO:	density	g/cm^3	RO $\geq$ 0
	RG:	rms value of interface roughness	m	-
	CL:	correlation length of roughness	m	CL > 0
V	SD:	source depth (mean for array)	m	-
	NS:	number of sources in array	-	NS > 0
	DS:	vertical source spacing	m	DS > 0
	AN:	grazing angle of beam	deg	-
	IA:	array type	-	1 $\leq$ IA $\leq$ 5
	FD:	focal depth of beam	m	FD $\neq$ SD
VI	RD1:	depth of first receiver	m	-
	RD2:	depth of last receiver	m	RD2 > RD1
	NR:	number of receivers	-	NR > 0
	IR:	plot output increment	-	IR $\geq$ 0
VII	CMIN:	minimum phase velocity	m/s	CMIN > 0
	CMAX:	maximum phase velocity	m/s	-
VIII	NW:	number of wavenumber samples	-	NW = 2^M
	IC1:	first sampling point	-	IC1 $\geq$ 1
	IC2:	last sampling point	-	IC2 $\leq$ NW

Figure 12 SAFARI Inputs [Ref. 7:p. 68]

by its respective velocity and dividing by 1000), the density in g/cm^3, and the RMS roughness which was left as zero for the study. For this study an average fluid solid interface depth of 3400 m was used in all runs. The next block contains the

source depth which was 122 m for the study. The sixth block contains the receiver depth of the uppermost receiver, the lowermost receiver if more than one, the number of receivers and the interim receiver depths. Here all plots are of just one receiver depth and have the required default place holders of 1 for the number of receivers and interim receiver depths. The seventh block contains the minimum and maximum phase velocity speed. The eighth block contains the number of FFT sampling points, the starting sampling point, and ending sampling point. The ninth through thirteenth blocks deal with the various plotting parameters. Blocks nine, ten, and thirteen are used in generating the output data per the reference guide [Ref 7] and are shown in Figure 13. A representative file sample using contour offset is shown in Figure 14.

Block		Parameter	Units	Limits
IX	RMIN:	minimum range on plots	km	-
	RMAX:	maximum range on plots	km	-
	RLEN:	length of r-axis for all plots	cm	RLEN > 0
	RINC:	distance between tick marks	km	RINC > 0
X[1]	TMIN:	minimum transmission loss	dB	-
	TMAX:	maximum transmission loss	dB	-
	TLEN:	length of vertical TL axes	cm	TLEN > 0
	TINC:	distance between tick marks	dB	TINC > 0
XI[2]	DCUP:	minimum depth for plots	m	-
	DCLO:	maximum depth for plots	m	-
	DCLN:	length of depth axis	cm	DCLN > 0
	DCIN:	distance between tick marks	m	DCIN > 0
XII[3]	ZMIN:	minimum contour level	dB	-
	ZMAX:	maximum contour level	dB	-
	ZINC:	contour level increment	dB	ZINC > 0
XIII[4]	VLEF:	wave speed at left border	m/s	-
	VRIG:	wave speed at right border	m/s	-
	VLEN:	length of wave speed axis	cm	VLEN > 0
	VINC:	wave speed tick mark distance	m/s	VINC > 0
	DVUP:	depth at upper border	m	-
	DVLO:	depth at lower border	m	-
	DVLN:	length of depth axis	cm	DVLN > 0
	DVIN:	depth-axis tick mark interval	m	DVIN > 0

[1] Only for options A, D, I and T. [2] Only for options C and D. [3] Only for option C.
[4] Only for option Z.

Figure 13 SAFARI Plot Parameters [Ref. 7:p. 69]

```
SAFARI FLOAT 0
N T J
7 0
43
0 0 0 0 0 0 0
0 1544.88 -1542.97 0 0 1 0
2.0 1542.97 -1543.93 0 0 1 0
33.4 1543.93 -1542.00 0 0 1 0
36.1 1542.00 -1540.93 0 0 1 0
38.9 1540.93 -1539.59 0 0 1 0
40.2 1539.59 -1538.72 0 0 1 0
42.9 1538.72 -1537.45 0 0 1 0
52.5 1537.45 -1530.84 0 0 1 0
133.8 1530.84 -1530.14 0 0 1 0
170.2 1530.14 -1530.56 0 0 1 0
230.7 1530.56 -1528.08 0 0 1 0
281.6 1528.08 -1527.04 0 0 1 0
321.6 1527.04 -1526.09 0 0 1 0
406.4 1526.09 -1526.05 0 0 1 0
498.6 1526.05 -1523.25 0 0 1 0
599.1 1523.25 -1519.53 0 0 1 0
674.3 1519.53 -1515.17 0 0 1 0
737.4 1515.17 -1511.40 0 0 1 0
811.7 1511.40 -1503.42 0 0 1 0
908.2 1503.42 -1496.45 0 0 1 0
1046.5 1496.45 -1494.06 0 0 1 0
1165.8 1494.06 -1493.51 0 0 1 0
1403.8 1493.51 -1497.37 0 0 1 0
1806.9 1497.37 -1497.44 0 0 1 0
1811.5 1497.44 -1497.85 0 0 1 0
1835.8 1497.85 -1500.13 0 0 1 0
2041.0 1500.13 -1501.43 0 0 1 0
2176.0 1501.43 -1506.97 0 0 1 0
2611.0 1506.97 -1511.75 0 0 1 0
3018.0 1511.75 -1517.13 0 0 1 0
3400.0 1517.13 -1524.38 0 0 1 0
3405.0 1463.56 116.00 0.0771 1.5428 1.46 0
3410.0 1472.09 122.00 0.0792 1.6568 1.47 0
3415.0 1480.61 128.00 0.0814 1.7766 1.48 0
3420.0 1489.11 134.00 0.0837 1.9015 1.49 0
3430.0 1506.05 146.02 0.0881 2.1567 1.51 0
3440.0 1522.92 158.02 0.0926 2.4256 1.53 0
3525.0 1663.28 401.77 0.1341 0 1.69 0
3700.0 1935.24 552.79 0.2349 0 2.00 0
4100.0 2092.86 672.14 0.2354 0 2.18 0
4900.0 2611.13 1074.68 0.1353 0 2.32 0
6350.0 5175.0 2725.0 0.1035 0.19075 2.75 0
122
435.32 435.32 1 1
50 1E8
4096 1 4096
0.0 25 20 10
40 120 12 20
```

Figure 14 SAFARI Input File with standard contour offset selected

V. MODEL INVESTIGATION

In the SAFARI model, two issues must be investigated. The first is whether k_{max} and k_{min} the two endpoints of the sampling regime alias the result by truncating the depth-dependent Greens function at a point where the contribution from the integrand is significant. If the integration is truncated at a point where the kernel's amplitude is significant the discontinuity will give rise to aliasing. The second is the whether a fine enough sampling of the horizontal wavenumber k is taking place, to ensure no aliasing is occurring in the depth-dependent Green's function (the integrand), which oscillates sharply over k_{max}-k_{min}, the span of the horizontal wavenumber. As previously stated, the contour offset is used to smooth the kernel by stepping off the axis. This has the effect of reducing the maximum spatial frequency at which aliasing commences, and therefore in range reduces the distance at which the onset of aliasing occurs.

A. MODEL ALIASING

1. Aliasing Background

A standard definition of aliasing is

> "if a signal contains no frequency components above a frequency f_{max} the signal can be uniquely represented by equally spaced samples if the sampling frequency f_s is greater than twice f_{max}. That is, the sampling frequency must satisfy the inequality $f_s > 2f_{max}$."[Ref. 12]

The inequality is known as the Nyquist rate. Since frequency is analogous to range and time analogous to wavenumber, frequency aliasing occurs when the time domain is undersampled. Similarly, in SAFARI, range aliasing occurs when wavenumber space is undersampled. Since the wavenumber sampling interval $\Delta k=(k_{max}-k_{min})/M$, where M is the total number of sampling points, either increasing M or decreasing the wavenumber span $k_{max}-k_{min}$ will reduce aliasing in range. Just as an impulse function in time domain yields a constant level in the frequency domain, so to will sharp peaks in wavenumber space yield a constant level in the spatial domain. If the Nyquist rate is violated, i.e., the frequency k_s is not greater than twice k_{max} the resulting transmission loss curve will show aliasing.

2. Aliasing Results

In SAFARI, the horizontal wavenumber k, governs the distance at which the aliasing commences. Given the rapidly varying integrand resulting from Eq. 3.27, the wavenumber range must be large enough and the sampling period fine enough to allow for accurate integration. There are five model input parameters governing the wavenumber integration:

- C_{min} the minimum phase velocity
- C_{max} the maximum phase velocity
- NW the number of wavenumber samples, which must be an integer power of 2, i.e. $NW=2^M$.
- IC1 the first sampling point

- IC2 the last sampling point

The relationship between the limits of the horizontal wavenumbers k and phase speeds C is $k_{min}=2\pi f/C_{max}$ and $k_{max}=2\pi f/C_{min}$, where f is the frequency of interest. The wavenumber interval Δk is determined by taking $(k_{max}-k_{min})/M$, where, M is the total number of sampling points. Phrased in another fashion, $k_{max} = k_{min} + (M-1)\Delta k$. Then recalling Eq 3.26 Δr can be determined and the window range $R = M\cdot\Delta r$ can be determined. This is the maximum range at which the integrand can not be aliased due to the truncation. In this study, all graphs start with IC1 equal to 1 and IC2 equal to the last sampling point M. To ensure all compressional and shear speeds were incorporated, C_{min} was chosen well below the minimum speed in the profile. Unless there are computing constraints, a very large value should be chosen for C_{max} to ensure truncation does not occur too soon. The first graphs Figure 15 and Figure 16 show the transmission loss curve and the wavenumber integrand. The transmission loss curve shows the beginning of aliasing just before 30 km, which supports the cutoff of the model at its predicted value of 29000 m. This number was arrived at via Equation 3.26. ,i.e., $M\Delta r=2\pi/\Delta k$, where Δk is $k_{max} - k_{min}$. The wavenumber integrand shows a very confined area over which a very abrupt series of oscillations take place on the axis of integration. Figure 17 and Figure 18 compare the effect of reducing the number of

sampling points by half but keeping Δk the same by reducing k_{max}-k_{min} in half. There are two items to notice. First the onset of aliasing occurs at the predicted range of 29,000 m, the same as the previous result. Second, the graphs are not the same, indicative of a reduction in aliasing in the kernel when the higher value of C_{min} was used, as is expected since the span in k has been reduced.

Inspection of a series a series of these curves allows a C_{max} and C_{min} which will provide the greatest alias-free range for a given number of sampling points. Figure 19 where C_{min}=740 m/s, and C_{max}=1E8 m/s ($1X10^8$), show no aliasing but the picture has converged to a more stable version. In this case, values of phase speed below 740 m/s and above 1E8 m/s do not significantly contribute. The integrand in Figure 20 has been rescaled automatically by SAFARI. There still is a large degree of 'peakness' and this will be investigated later in the contour offset series.

B. CONTOUR OFFSET

As previously described the contour offset is designed to smooth out the peaks in the integrand by moving away from the poles into the complex plane. This is analogous to going along the side of the mountain as opposed to going over its peaks. Since the integrand is composed of many spatial frequencies and the kernel is smoothed by taking an offset contour, this is the same as reducing the maximum range at

which the onset of aliasing will occur. Given the number of sampling points is not changed, nor is the span of k, aliasing should begin at smaller values of r. Figure 21 and Figure 22 show the onset of aliasing as moving to shorter ranges as the contour is moved off the axis. Figures 23 through 29 show the effect of using the contour offset for the 43 layer model with C_{min}=50 m/s and C_{max}=1E8 m/s. Figure 23 has no offset and each following Figure has an increase in the contour offset by a factor of 0.25 times the standard contour offset. With a standard offset and 4096 points, the aliasing begins at about 25 km. Doubling the number of points to 8192 moves the aliasing out beyond the limits of the graph, as seen in Figure 30 and Figure 31.

In Figure 19 and Figure 20, C_{max} was 1E8 and C_{min} was 740 with no contour offset used. With a standard contour offset, Figure 32 shows the change in the nulls. This results in a small change in the transmission loss curve as shown in Figure 33; the nulls are deeper and the overall shape shows a few more peaks. In the next series, the standard contour offset was used, and C_{min} was held constant at 740 m/s, but C_{max} was reduced to 3400 m/s (Figure 34 and Figure 35). This had little effect on the results indicating that phase speeds above 3400 m/s contribute little to the propagation. Figure 35 bears this out as small k shows no significant contribution to propagation. The largest effect was between 5 to 10 km. The

next comparison was in running the same profile with 1024 points vice 4096. Figure 34 shows a transmission loss curve almost identical to the 4096 pt curve in Figure 34, with some very minor changes in the nulls around 8 km. The integrand in Figure 37 has changed dramatically. What were originally spikes in Figure 20, now have some width and continuity, making for an easier evaluation of the integrand and thus less aliasing due to the kernel. Next is the comparison of Figure 36 with the 8192 point graph in Figure 31 both using the contour offset feature, to observe the losses due to the change in parameters. Clearly not much is lost in the overall shape of the transmission loss curve. A few more features are present with deeper nulls and smoother peaks and some resolution of a few peaks around 6 km, but otherwise the shape is the same, with the 1024 point graph taking less time to produce. Finally increasing the number of sampling points to 16384 points (Figure 38) yielded no change in the graph over that of the 8192 point graph (Figure 31) over the range of interest. At this point the model has converged. Note the difference in the integrands between Figure 39 and Figure 37.

Finally, Figure 40 shows the difference between the water column alone and using the water column and sediment combined. Clearly sediment contribution to the final transmission loss is important.

VI. COMPARISON OF SAFARI WITH SWALLOW FLOAT 0 DATA

In this chapter the results of the Swallow Float records are presented graphically for 7 Hz and 10 Hz both without and with range offsets from regions 1 and 2. The results are visually compared and contrasted. Next the data is compared with the model results. In all cases Matlab 386 was used for the graphic presentations. All figures are located in Appendix D.

A. 7 HZ DATA

Figure 41 shows the 7 Hz transmission loss data taken during region 1. Figure 42 shows the 7 Hz transmission loss data taken during region 2. Figure 43 compares region 1 and region 2 data by offsetting region 1 to match predominant features. This offset was 2.4 km.

B. 10 HZ DATA

Figure 44 shows the 10 Hz transmission loss data taken from region 1. Figure 45 shows the 10 Hz transmission loss data taken from region 2. Figure 46 compares region 1 with region 2 by offsetting region 1 to match predominant features. This offset was 2.5 km.

C. SAFARI MODEL VS 7 HZ DATA

Figure 47 shows the SAFARI model at 7 Hz vs 7 Hz transmission loss data taken from region 1. Figure 48 shows the SAFARI model at 7 Hz vs 7 Hz transmission loss data taken

from region 2. Figures 49 and 50 compare the SAFARI model at 7 Hz vs 7 Hz transmission loss data taken from regions 1 and 2 respectively, offset in range to match predominant features. The offset was 2.4 km for region 1 and none for region 2.

D. SAFARI MODEL VS 10 HZ DATA

Figure 51 shows the SAFARI model at 10 Hz vs 10 Hz transmission loss data taken from region 1. Figure 52 shows the SAFARI model at 10 Hz vs 10 Hz transmission loss data taken from region 2. Figures 53 and 54 compare the SAFARI model at 10 Hz vs 10 Hz transmission loss data taken from regions 1 and 2 respectively, offset in range to match predominant features. The offset was 0.5 km for region 1 and -0.75 km for region 2.

VII. CONCLUSIONS AND RECOMMENDATIONS

A. CONCLUSIONS

The initial findings in the Swallow float 0 data show excellent agreement with the SAFARI model; the model produces a result that compares well with ocean data. The model shows that there is a distinct problem with the range used for the data recorded in region 1. No explanation was found as to why the offset found in region 1 at 7 Hz was much larger than the navigation error mentioned in Reference 4. The data at 7 Hz in region 2 and at 10 Hz in both regions 1 and 2 match up reasonably well given errors in the navigation. The slope of the bottom appears to have very little effect on the transmission loss in this case. By comparing results obtained from modelling the velocity profile of the water column alone versus one with sediments included, the impact of the bottom and the importance of modelling the bottom become apparent.

SAFARI is extremely sensitive to aliasing based on its input values of phase speed, number of sampling points, and limits of integration. The contour offset does provide a way to generate less aliasing from poles at the cost of aliasing at long ranges. This can be corrected by increasing the number of sampling points.

B. RECOMMENDATIONS

Two areas which can be addressed in future theses are investigation of data obtained on other floats and investigation of the effect the starting bottom depth has on the model.

APPENDIX A

A. NAVIGATIONAL DATA

The record of the position of the R/V Gyre is enclosed. It is uncorrected with respect to the navigational offset mentioned in Chapter 2. The last page has the time the changes in navigational source occurred.

DATE	TIME (Z)	LAT° (N)	LON°(W)	SPEED	COURSE
8/04/90	16:00:00	31.4644	-74.8247	1.81077	263.6502
8/04/90	16:05:00	31.4667	-74.8244	1.61271	7.24
8/04/90	16:10:00	31.4694	-74.8236	2.08699	16.67036
8/04/90	16:15:00	31.4722	-74.8228	2.08828	16.65955
8/04/90	16:20:00	31.4683	-74.8219	2.86327	167.9302
8/04/90	16:25:00	31.4642	-74.8214	3.02726	172.3882
8/04/90	16:30:00	31.4603	-74.8206	2.86197	167.9244
8/04/90	16:35:00	31.4564	-74.82	2.82866	171.8502
8/04/90	16:40:00	31.4522	-74.8197	3.00751	176.125
8/04/90	16:45:00	31.4364	-74.8236	11.7400	193.8054
8/04/90	16:50:00	31.4417	-74.8222	3.92913	14.7405
8/04/90	16:55:00	31.4369	-74.8242	3.67737	202.3895
8/04/90	17:00:00	31.4322	-74.8261	3.67615	202.3976
8/04/90	17:05:00	31.4269	-74.8272	3.8836	191.9179
8/04/90	17:10:00	31.4219	-74.8283	3.68781	192.4733
8/04/90	17:15:00	31.4164	-74.83	4.17737	196.7371
8/04/90	17:20:00	31.4114	-74.8411	8.77058	245.7706
8/04/90	17:25:00	31.4067	-74.8517	8.32298	245.8878
8/04/90	17:30:00	31.4017	-74.8528	3.68764	192.5612
8/04/90	17:35:00	31.3964	-74.8539	3.88358	191.9179
8/04/90	17:40:00	31.3911	-74.8544	3.82098	186.0241
8/04/90	17:45:00	31.3864	-74.8553	3.45254	189.9869
8/04/90	17:50:00	31.3808	-74.8558	4.02042	185.7242
8/04/90	17:55:00	31.3761	-74.8558	3.3989	180
8/04/90	18:00:00	31.3714	-74.8561	3.406	183.3285
8/04/90	18:05:00	31.3661	-74.8558	3.80503	177.0209
8/04/90	18:10:00	31.3611	-74.8556	3.60648	176.7693
8/04/90	18:15:00	31.3561	-74.8556	3.5994	180
8/04/90	18:20:00	31.3508	-74.8556	3.7999	180
8/04/90	18:25:00	31.3453	-74.8556	4.0004	180
8/04/90	18:30:00	31.3403	-74.8556	3.5994	180
8/04/90	18:35:00	31.3353	-74.8564	3.64989	189.4411
8/04/90	18:40:00	31.3303	-74.8583	3.86049	201.2642
8/04/90	18:45:00	31.3253	-74.86	3.79355	198.4808
8/04/90	18:50:00	31.3203	-74.8617	3.79295	198.3956
8/04/90	19:05:00	31.305	-74.8672	3.60435	199.4836
8/04/90	19:10:00	31.2997	-74.8689	3.9817	197.4919
8/04/90	19:15:00	31.2944	-74.8706	3.98311	197.5672
8/04/90	19:20:00	31.2892	-74.8725	4.04598	200.2354
8/04/90	19:25:00	31.2844	-74.8742	3.60026	199.4085
8/04/90	19:30:00	31.2792	-74.8758	3.98078	197.4919
8/04/90	19:35:00	31.2736	-74.8778	4.23389	199.2979
8/04/90	19:40:00	31.2678	-74.8792	4.31436	193.3908
8/04/90	19:45:00	31.2633	-74.8806	3.34887	197.3512
8/04/90	19:50:00	31.2583	-74.8822	3.79172	198.4743
8/04/90	19:55:00	31.2531	-74.8764	5.62441	132.1214
8/04/90	20:10:00	31.2369	-74.8872	3.68624	192.5566
8/04/90	20:15:00	31.2322	-74.8881	3.4495	189.9908

DATE	TIME (Z)	LAT° (N)	LON°(W)	SPEED	COURSE
8/04/90	20:20:00	31.2272	-74.8892	3.68593	192.5566
8/04/90	20:25:00	31.2219	-74.8903	3.87944	191.8386
8/04/90	20:30:00	31.2167	-74.8911	3.84495	188.9545
8/04/90	20:35:00	31.2114	-74.8922	3.88019	191.9179
8/04/90	20:45:00	31.2039	-74.8944	5.45564	188.3911
8/04/90	20:50:00	31.1961	-74.8956	5.65607	188.1478
8/04/90	20:55:00	31.1908	-74.8967	3.87948	191.9179
8/04/90	21:00:00	31.1856	-74.8978	3.87822	191.8386
8/04/90	21:05:00	31.1803	-74.8994	3.97587	197.5672
8/04/90	21:10:00	31.1747	-74.9011	4.16747	196.7371
8/04/90	21:15:00	31.1694	-74.9014	3.80473	182.9791
8/04/90	21:20:00	31.1639	-74.9019	4.01783	185.7262
8/04/90	21:25:00	31.1586	-74.9036	3.97245	197.4919
8/04/90	21:30:00	31.1536	-74.905	3.72798	195.5173
8/04/90	21:35:00	31.1478	-74.9064	4.30875	193.3908
8/04/90	21:40:00	31.1422	-74.9075	4.07423	191.3364
8/04/90	21:45:00	31.1369	-74.9092	3.97045	197.4919
8/04/90	21:50:00	31.1317	-74.9106	3.92049	194.8179
8/04/90	21:55:00	31.1264	-74.9125	4.02831	200.1625
8/04/90	22:00:00	31.1214	-74.9142	3.77901	198.4808
8/04/90	22:05:00	31.1158	-74.9153	4.07212	191.2608
8/04/90	22:10:00	31.1103	-74.9164	4.07151	191.3402
8/04/90	22:15:00	31.1053	-74.9186	3.90922	203.9382
8/04/90	22:20:00	31.1	-74.9206	4.0264	200.2354
8/04/90	22:25:00	31.0944	-74.9222	4.15861	196.6649
8/04/90	22:30:00	31.0886	-74.9233	4.26764	190.8118
8/04/90	22:35:00	31.0828	-74.9258	4.52963	203.1579
8/04/90	22:40:00	31.0778	-74.9281	3.90579	204.0111
8/04/90	22:45:00	31.0728	-74.9306	3.97705	206.5213
8/04/90	22:50:00	31.0667	-74.9314	4.4365	187.8194
8/04/90	22:55:00	31.0606	-74.9322	4.43705	187.7468
8/04/90	23:00:00	31.0556	-74.9331	3.64274	189.4446
8/04/90	23:05:00	31.0511	-74.9372	4.25651	223.1998
8/04/90	23:10:00	31.0469	-74.9414	4.10235	224.9869
8/04/90	23:15:00	31.0422	-74.9428	3.52536	196.3845
8/04/90	23:20:00	31.0364	-74.9442	4.30097	193.3908
8/04/90	23:25:00	31.0308	-74.9456	4.10629	194.0316
8/04/90	23:30:00	31.0261	-74.9464	3.44372	189.9908
8/04/90	23:35:00	31.02	-74.9475	4.46181	190.33
8/04/90	23:40:00	31.0144	-74.9486	4.06703	191.2608
8/04/90	23:45:00	31.0092	-74.95	3.91044	194.8179
8/04/90	23:50:00	31.0039	-74.9511	3.86935	191.8386
8/04/90	23:55:00	30.9986	-74.9522	3.86903	191.8386
8/04/90	24:00:00	30.9942	-74.9525	3.20514	183.6345
8/05/90	00:05:00	30.9881	-74.9533	3.64156	189.4411
8/05/90	00:10:00	30.9831	-74.9542	3.64156	189.4411
8/05/90	00:15:00	30.9778	-74.955	3.83838	188.9545

DATE	TIME (Z)	LAT° (N)	LON°(W)	SPEED	COURSE
8/05/90	00:35:00	30.9572	-74.9594	5.27599	190.8844
8/05/90	00:40:00	30.9522	-74.9603	3.64037	189.4411
8/05/90	00:45:00	30.9469	-74.9611	3.83861	188.9514
8/05/90	00:50:00	30.9422	-74.9614	3.40508	183.4207
8/05/90	00:55:00	30.9378	-74.9614	3.19977	180
8/05/90	01:00:00	30.9319	-74.9622	4.23283	188.1144
8/05/90	01:05:00	30.9261	-74.9631	4.23263	188.1144
8/05/90	01:10:00	30.9211	-74.9639	3.63912	189.4411
8/05/90	01:15:00	30.9161	-74.9647	3.63825	189.5297
8/05/90	01:20:00	30.9111	-74.9656	3.63871	189.4411
8/05/90	01:25:00	30.9061	-74.9664	3.63714	189.4446
8/05/90	01:30:00	30.9006	-74.9658	4.01558	174.2758
8/05/90	01:35:00	30.8953	-74.9656	3.80377	177.0209
8/05/90	01:40:00	30.8897	-74.965	4.01403	174.2738
8/05/90	01:45:00	30.8842	-74.9644	4.0153	174.2758
8/05/90	01:55:00	30.8803	-74.9747	2.98513	203.2494
8/05/90	02:00:00	30.8747	-74.9769	4.2285	201.7811
8/05/90	02:05:00	30.8694	-74.9794	4.09985	205.3684
8/05/90	02:10:00	30.8644	-74.9817	3.8483	203.9463
8/05/90	02:15:00	30.8594	-74.9836	3.78936	201.1882
8/05/90	02:20:00	30.8544	-74.9858	3.84824	204.0111
8/05/90	02:25:00	30.8489	-74.9867	4.03079	188.5154
8/05/90	02:30:00	30.8439	-74.9881	3.69759	195.5173
8/05/90	02:35:00	30.8389	-74.9908	3.97037	209.0528
8/05/90	02:40:00	30.8347	-74.9928	3.22095	205.0241
8/05/90	02:45:00	30.8294	-74.9942	3.89006	194.7405
8/05/90	02:50:00	30.8253	-74.9947	3.0177	187.6153
8/05/90	02:55:00	30.82	-74.9961	3.88894	194.7405
8/05/90	03:00:00	30.815	-74.9975	3.69532	195.5117
8/05/90	03:05:00	30.8103	-74.9983	3.43436	189.9908
8/05/90	03:10:00	30.8056	-74.9989	3.41611	186.726
8/05/90	03:15:00	30.8011	-74.9997	3.23693	190.5989
8/05/90	03:20:00	30.7961	-75	3.60457	183.2307
8/05/90	03:25:00	30.7914	-75.0006	3.41579	186.726
8/05/90	03:30:00	30.7864	-75.0014	3.63179	189.4446
8/05/90	03:35:00	30.7817	-75.0017	3.404	183.3285
8/05/90	03:40:00	30.7769	-75.0019	3.40281	183.4221
8/05/90	03:45:00	30.7722	-75.0028	3.43383	189.9869
8/05/90	03:50:00	30.7678	-75.0039	3.26302	194.071
8/05/90	03:55:00	30.7633	-75.005	3.26175	193.9784
8/05/90	04:00:00	30.7586	-75.0058	3.43375	190.0766
8/05/90	04:05:00	30.7556	-75.0061	2.20555	185.1364
8/05/90	04:10:00	30.7522	-75.0061	2.40051	180
8/05/90	04:15:00	30.7578	-75.0075	4.07784	345.9684
8/05/90	04:20:00	30.7625	-75.0067	3.43334	9.98686
8/05/90	04:25:00	30.7678	-75.0061	3.81332	6.0241
8/05/90	04:30:00	30.7731	-75.0053	3.83	8.95455
8/05/90	04:35:00	30.7783	-75.0047	3.81353	6.0241
8/05/90	04:40:00	30.7839	-75.0031	4.11513	16.74256

DATE	TIME (Z)	LAT° (N)	LON°(W)	SPEED	COURSE
8/05/90	04:50:00	30.7947	-75	4.08217	14.03162
8/05/90	04:55:00	30.8	-74.9983	3.92472	17.56718
8/05/90	05:00:00	30.8053	-74.9978	3.81407	6.0241
8/05/90	05:05:00	30.8106	-74.9947	4.20758	30.03838
8/05/90	05:10:00	30.8158	-74.9917	4.21236	30.1004
8/05/90	05:15:00	30.8208	-74.9889	3.96448	29.0342
8/05/90	05:20:00	30.8261	-74.9861	4.14734	27.75342
8/05/90	05:25:00	30.8311	-74.9833	3.96485	28.98588
8/05/90	05:30:00	30.8375	-74.9817	4.70951	14.65429
8/05/90	05:35:00	30.8422	-74.98	3.54459	19.40855
8/05/90	05:40:00	30.8467	-74.9783	3.35769	20.59644
8/05/90	05:45:00	30.8519	-74.9764	3.97872	20.24214
8/05/90	05:50:00	30.8572	-74.9742	4.0357	22.80774
8/05/90	05:55:00	30.8625	-74.9722	3.98237	20.23541
8/05/90	06:00:00	30.8689	-74.9697	4.84976	21.3932
8/05/90	06:05:00	30.8733	-74.9678	3.41558	23.55968
8/05/90	06:10:00	30.8736	-74.9658	1.22105	81.88557
8/05/90	06:15:00	30.8814	-74.9639	5.72853	14.04286
8/05/90	06:20:00	30.8894	-74.9617	5.96181	15.40999
8/05/90	06:35:00	30.9064	-74.9567	4.37525	18.44057
8/05/90	06:40:00	30.9119	-74.9553	4.09373	14.03624
8/05/90	06:45:00	30.9178	-74.9539	4.29172	13.38659
8/05/90	06:50:00	30.9233	-74.9528	4.06098	11.3402
8/05/90	06:55:00	30.9292	-74.9517	4.26028	10.8084
8/05/90	07:00:00	30.9353	-74.95	4.525	15.22939
8/05/90	07:05:00	30.9411	-74.9483	4.3338	15.91076
8/05/90	07:10:00	30.9467	-74.9469	4.09857	14.03162
8/05/90	07:15:00	30.9522	-74.9456	4.09911	14.03162
8/05/90	07:20:00	30.9578	-74.9447	4.03628	8.51249
8/05/90	07:25:00	30.9631	-74.9439	3.83785	8.95455
8/05/90	07:30:00	30.9683	-74.9431	3.83874	9.03535
8/05/90	07:35:00	30.9742	-74.9408	4.44119	20.83887
8/05/90	07:40:00	30.98	-74.9389	4.3886	18.44057
8/05/90	07:45:00	30.9858	-74.9369	4.38828	18.44619
8/05/90	07:50:00	30.9914	-74.9339	4.47225	28.78662
8/05/90	07:55:00	30.9972	-74.9314	4.5119	23.21441
8/05/90	08:00:00	31.0033	-74.9292	4.6389	20.02904
8/05/90	08:05:00	31.0092	-74.9272	4.39068	18.37872
8/05/90	08:10:00	31.0153	-74.925	4.6413	20.02904
8/05/90	08:15:00	31.0211	-74.9228	4.4512	20.83887
8/05/90	08:30:00	31.0369	-74.9283	4.59203	25.46043
8/05/90	08:35:00	31.0428	-74.9256	4.59503	25.45316
8/05/90	08:40:00	31.0486	-74.9228	4.59548	25.46043
8/05/90	08:45:00	31.0542	-74.92	4.41593	26.55718

DATE	TIME (Z)	LAT° (N)	LON°(W)	SPEED	COURSE
8/05/90	09:05:00	31.0781	-74.9097	4.4368	7.81942
8/05/90	09:10:00	31.0842	-74.9089	4.43629	7.74921
8/05/90	09:15:00	31.0903	-74.9069	4.59581	17.65898
8/05/90	09:20:00	31.0961	-74.905	4.40502	18.44619
8/05/90	09:25:00	31.1022	-74.9042	4.43673	7.74921
8/05/90	09:30:00	31.1086	-74.9031	4.6636	9.8889
8/05/90	09:35:00	31.1147	-74.9022	4.43702	7.74921
8/05/90	09:40:00	31.1211	-74.9014	4.6347	7.41751
8/05/90	09:45:00	31.1275	-74.9006	4.6362	7.41532
8/05/90	09:50:00	31.1317	-74.9106	7.53516	292.6106
8/05/90	09:55:00	31.1364	-74.9194	7.02376	298.0035
8/05/90	10:00:00	31.1422	-74.9242	5.32476	321.0036
8/05/90	10:05:00	31.145	-74.9197	3.67764	58.00346
8/05/90	10:10:00	31.1481	-74.9153	3.78748	55.46642
8/05/90	10:15:00	31.1508	-74.9106	3.83816	59.50205
8/05/90	10:20:00	31.1547	-74.9092	2.96377	19.74811
8/05/90	10:25:00	31.1583	-74.9078	2.77359	21.03548
8/05/90	10:30:00	31.1622	-74.9064	2.96266	19.64848
8/05/90	10:35:00	31.1661	-74.9047	3.03103	23.15449
8/05/90	10:50:00	31.1942	-74.8933	4.10741	22.81514
8/05/90	10:55:00	31.1994	-74.8914	4.03866	20.23541
8/05/90	11:00:00	31.2047	-74.8892	4.11006	22.80774
8/05/90	11:05:00	31.21	-74.8872	4.03971	20.23541
8/05/90	11:10:00	31.2153	-74.8842	4.3702	30.1004
8/05/90	11:15:00	31.2206	-74.8814	4.27381	27.68852
8/05/90	11:20:00	31.2258	-74.8786	4.27721	27.75342
8/05/90	11:25:00	31.2314	-74.8764	4.29993	21.84887
8/05/90	11:30:00	31.2369	-74.875	4.11826	14.03624
8/05/90	11:35:00	31.2425	-74.8739	4.0766	11.26075
8/05/90	11:40:00	31.2481	-74.8728	4.0778	11.33641
8/05/90	11:45:00	31.2539	-74.8714	4.31387	13.39081
8/05/90	11:50:00	31.2597	-74.8692	4.48658	20.83887
8/05/90	11:55:00	31.2656	-74.8667	4.563	23.21441
8/05/90	12:00:00	31.2711	-74.8647	4.23243	19.30407
8/05/90	12:05:00	31.2769	-74.8631	4.36657	15.98002
8/05/90	12:10:00	31.2825	-74.8614	4.17143	16.67036
8/05/90	12:15:00	31.2881	-74.8597	4.17455	16.73713
8/05/90	12:20:00	31.2939	-74.8581	4.36449	15.9157
8/05/90	12:25:00	31.2994	-74.8567	4.12179	14.03162
8/05/90	12:30:00	31.3053	-74.8553	4.31547	13.39081
8/05/90	12:35:00	31.3111	-74.8547	4.21842	5.45448
8/05/90	12:40:00	31.3169	-74.8539	4.2443	8.10913
8/05/90	12:45:00	31.3228	-74.8531	4.2424	8.1878
8/05/90	12:50:00	31.3289	-74.8522	4.44027	7.74921
8/05/90	12:55:00	31.3347	-74.8514	4.24171	8.11436
8/05/90	13:00:00	31.3406	-74.8506	4.24311	8.11174
8/05/90	13:05:00	31.3464	-74.8497	4.24179	8.11436
8/05/90	13:10:00	31.3522	-74.8492	4.21855	5.45448

DATE	TIME (Z)	LAT° (N)	LON°(W)	SPEED	COURSE
8/05/90	13:20:00	31.3647	-74.8483	4.80102	360
8/05/90	13:35:00	31.3814	-74.8486	3.82097	6.0241
8/05/90	13:40:00	31.3875	-74.8478	4.44054	7.74921
8/05/90	13:50:00	31.3986	-74.8644	4.20444	2.77082
8/05/90	13:55:00	31.4047	-74.8636	4.44057	7.74921
8/05/90	14:00:00	31.4106	-74.8628	4.24199	8.11436
8/05/90	14:15:00	31.4261	-74.8586	2.60806	32.48508

8/04/90.....	..1615-1720	LORAN
8/04-05/90	.1725-0725	GPS
8/05/90.....	..0730-1025	SAT NAV
8/05/90.....	..1030-1320	LORAN
8/05/90.....	..1325-1415	GPS

APPENDIX B

A. SOUND VELOCITY PROFILES

Representative samples of the sound velocity profile of the water column used in the SAFARI model are presented in this appendix. A full listing of all the samples made is available in Reference 1.

SITE "D" PROVINCE PROFILES:

SITE "D" PROVINCE ONE

31.4833 -75.2644 90 8 3850 40 1

DEPTH (M)	TEMP DEG C	SALIN PPT	SOUND SPD M/SEC
.0	27.64	36.61	1542.56
26.5	27.52	36.84	1542.99
29.1	26.96	36.84	1541.80
43.6	26.16	37.44	1540.91
51.7	25.32	37.43	1539.12
54.1	24.94	37.42	1538.28
54.7	24.69	37.39	1537.68
59.8	24.35	37.16	1536.68
67.6	24.12	36.90	1535.97
80.9	23.24	36.78	1533.94
95.9	22.45	36.75	1532.17
99.7	22.42	36.76	1532.16
104.2	22.01	36.76	1531.21
114.6	21.73	36.74	1530.64
118.3	21.40	36.74	1529.83
134.3	21.10	36.71	1529.28
162.3	19.97	36.71	1526.71
206.3	19.26	36.70	1525.50
267.5	19.00	36.61	1525.66
428.0	17.07	36.46	1522.55
561.8	14.35	36.22	1516.06
622.0	13.57	36.02	1514.26
668.1	12.18	35.86	1510.16
691.3	11.86	35.78	1509.35
763.8	9.99	35.60	1503.68
868.0	8.02	35.29	1497.69
900.0	7.75	35.23	1497.10
913.0	7.41	35.19	1495.98
989.0	6.50	35.10	1493.54
1090.0	6.04	35.08	1493.37
1160.0	5.64	35.07	1492.93
1290.0	5.02	35.04	1492.54
1416.0	4.60	35.01	1492.88
1628.0	4.19	34.99	1494.70
2041.0	3.81	34.98	1500.13
2176.0	3.58	34.96	1501.43
2611.0	3.13	34.95	1506.97
3018.0	2.62	34.92	1511.75
3400.0	2.33	34.90	1517.13
3850.0	2.18	34.88	1524.38

SITE "D" PROVINCE TWO

31.5592 -74.9573 90 8 3850 32 2

DEPTH (M)	TEMP DEG C	SALIN PPT	SOUND SPD M/SEC
.0	27.08	36.61	1541.34
2.0	28.00	36.63	1543.40
15.7	28.00	36.77	1543.78
32.1	27.30	37.44	1543.26
34.8	26.90	37.44	1542.42
37.5	26.00	37.44	1540.46
57.9	23.90	37.24	1535.67
81.0	22.90	36.78	1533.09
87.8	22.30	36.75	1531.66
108.1	21.80	36.75	1530.72
128.4	20.90	36.72	1528.67
205.2	19.50	36.70	1526.13
418.3	18.00	36.47	1525.13
480.2	17.30	36.41	1524.04
562.7	15.70	36.22	1520.33
630.3	14.80	35.98	1518.33
685.9	13.60	35.80	1515.14
709.1	12.80	35.73	1512.78
789.9	10.80	35.53	1506.95
812.9	10.40	35.45	1505.79
965.0	7.60	35.12	1497.47
1091.4	6.00	35.08	1493.23
1238.4	5.20	35.05	1492.42
1478.4	4.50	35.01	1493.51
1789.5	4.20	34.98	1497.49
1835.8	4.00	34.98	1497.44
2041.0	3.81	34.98	1500.13
2176.0	3.58	34.96	1501.43
2611.0	3.13	34.95	1506.97
3018.0	2.62	34.92	1511.75
3400.0	2.33	34.90	1517.13
3850.0	2.18	34.88	1524.38

SITE "D" PROVINCE THREE

30.7625 -75.0077 90 8 3850 32 3

DEPTH (M)	TEMP DEG C	SALIN PPT	SOUND SPD M/SEC
.0	27.18	36.61	1541.57
2.0	27.80	36.63	1542.97
19.8	27.90	36.81	1543.68
32.1	27.40	37.44	1543.48
36.1	27.00	37.44	1542.67
38.9	26.40	37.44	1541.38
47.0	25.30	37.44	1539.02
67.4	24.30	36.90	1536.41
127.0	22.20	36.72	1532.02
217.3	20.00	36.69	1527.68
254.8	19.40	36.63	1526.58
407.8	18.40	36.47	1526.11
547.0	17.00	36.27	1524.08
649.7	15.20	35.92	1519.84
667.8	14.50	35.86	1517.84
706.5	13.50	35.75	1515.08
786.1	11.90	35.54	1510.75
839.7	11.20	35.35	1508.95
951.2	8.80	35.14	1501.82
988.9	7.80	35.10	1498.61
1037.8	7.10	35.09	1496.70
1136.1	6.00	35.07	1493.97
1299.5	5.10	35.04	1493.02
1498.7	4.50	35.00	1493.85
1783.7	4.10	34.98	1496.97
1835.8	4.10	34.98	1497.85
2041.0	3.81	34.98	1500.13
2176.0	3.58	34.96	1501.43
2611.0	3.13	34.95	1506.97
3018.0	2.62	34.92	1511.75
3400.0	2.33	34.90	1517.13
3850.0	2.18	34.88	1524.38

SITE "D" PROVINCE FOUR

31.1660 -74.9048 90 8 3850 32 4

DEPTH (M)	TEMP DEG C	SALIN PPT	SOUND SPD M/SEC
.0	28.72	36.61	1544.88
2.0	27.80	36.63	1542.97
33.4	27.60	37.44	1543.93
36.1	26.70	37.44	1542.00
38.9	26.20	37.44	1540.93
40.2	25.60	37.44	1539.59
42.9	25.20	37.44	1538.72
52.5	24.60	37.42	1537.45
133.8	21.70	36.71	1530.84
170.2	21.20	36.71	1530.14
230.7	21.00	36.67	1530.56
281.6	19.80	36.59	1528.08
321.6	19.20	36.55	1527.04
406.4	18.40	36.48	1526.09
498.6	17.90	36.37	1526.05
599.1	16.50	36.11	1523.25
674.3	15.00	35.85	1519.53
737.4	13.40	35.67	1515.17
811.7	12.00	35.45	1511.40
908.2	9.40	35.21	1503.42
1046.5	7.00	35.09	1496.45
1165.8	5.90	35.07	1494.06
1403.8	4.80	35.02	1493.51
1806.9	4.10	34.98	1497.37
1811.5	4.10	34.98	1497.44
1835.8	4.10	34.98	1497.85
2041.0	3.81	34.98	1500.13
2176.0	3.58	34.96	1501.43
2611.0	3.13	34.95	1506.97
3018.0	2.62	34.92	1511.75
3400.0	2.33	34.90	1517.13
3850.0	2.18	34.88	1524.38

PROVINCE ONE PROFILE
SITE "D"

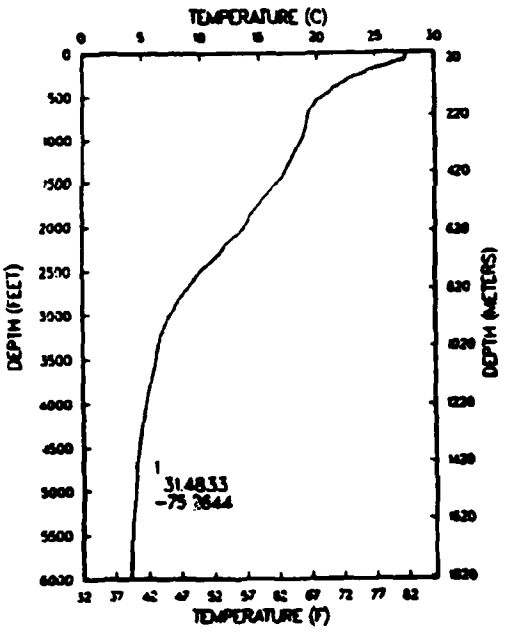

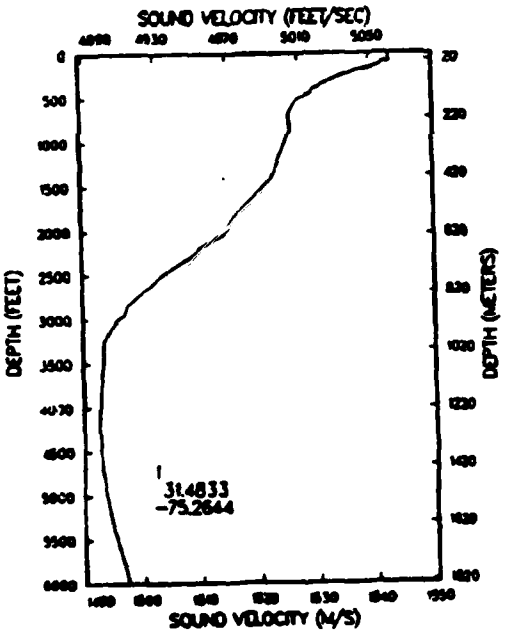

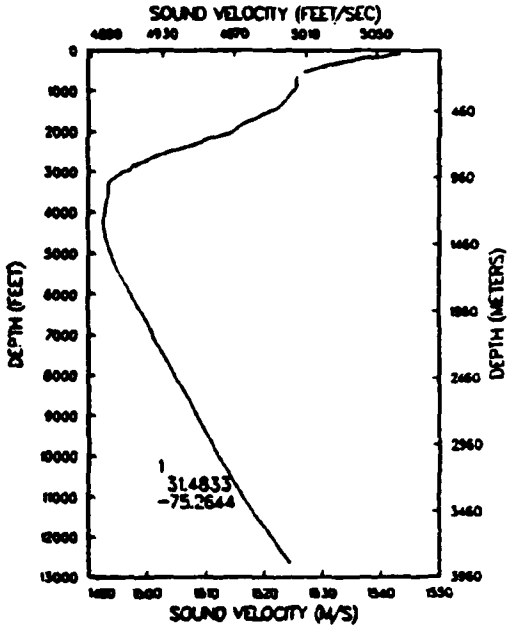

PROVINCE TWO PROFILE
SITE "D"

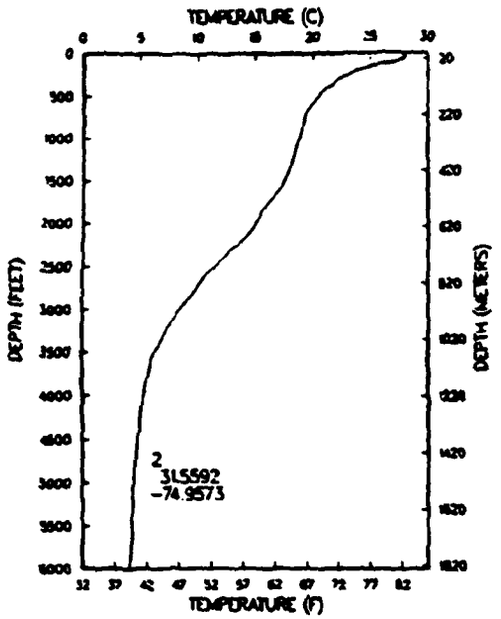

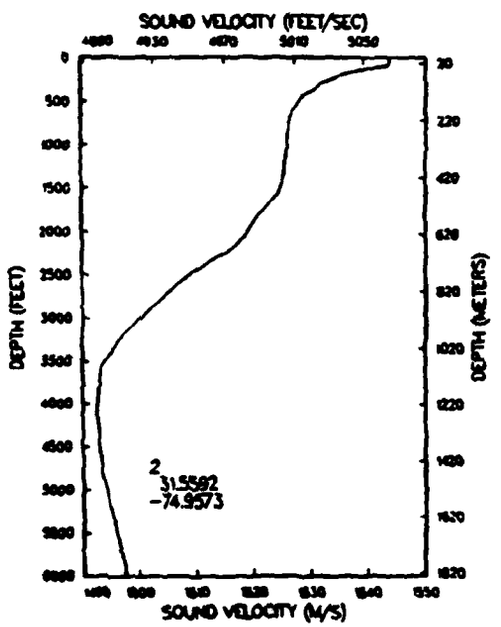

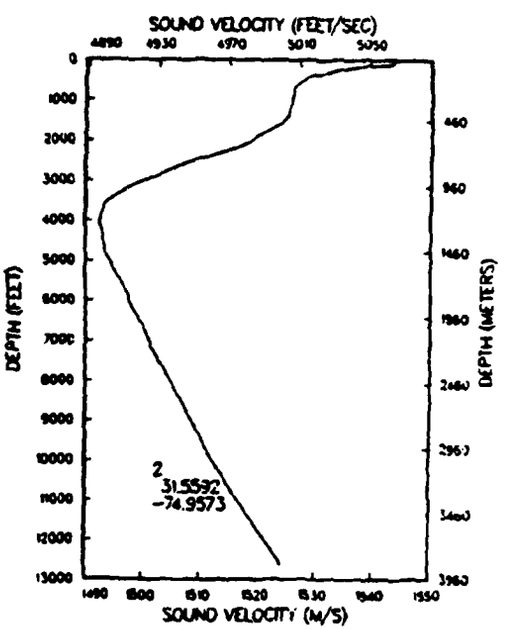

PROVINCE THREE PROFILE
SITE "D"

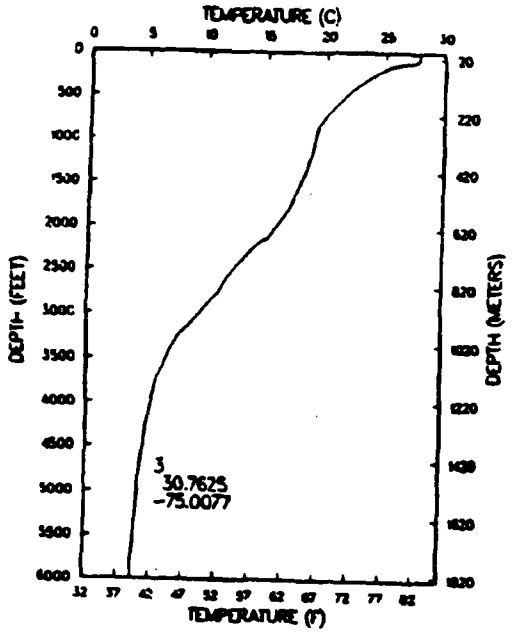

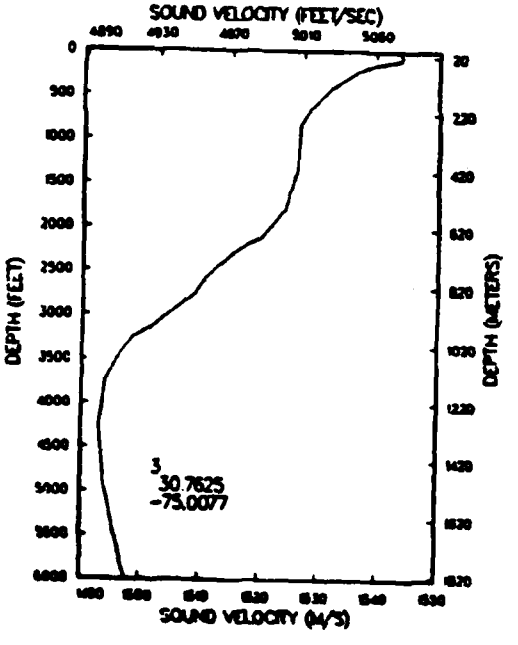

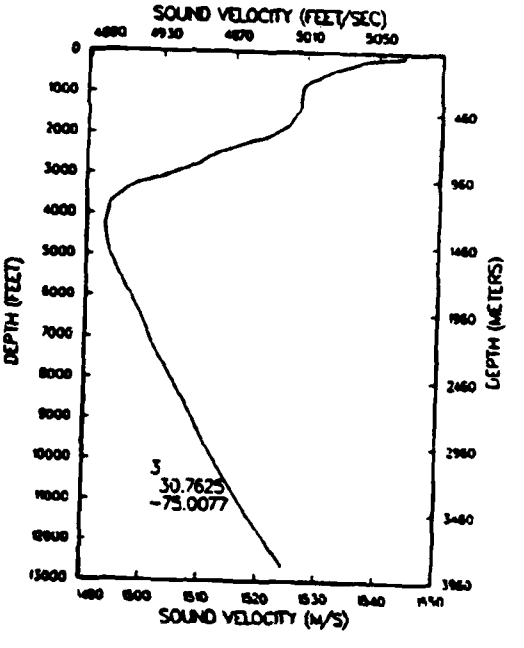

PROVINCE FOUR PROFILE
SITE "D"

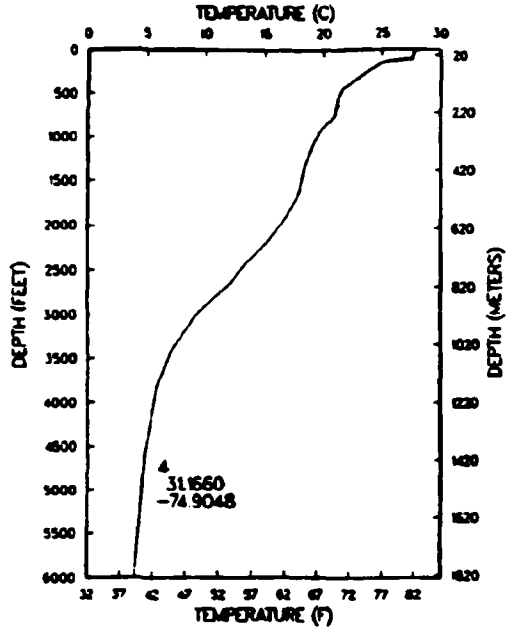

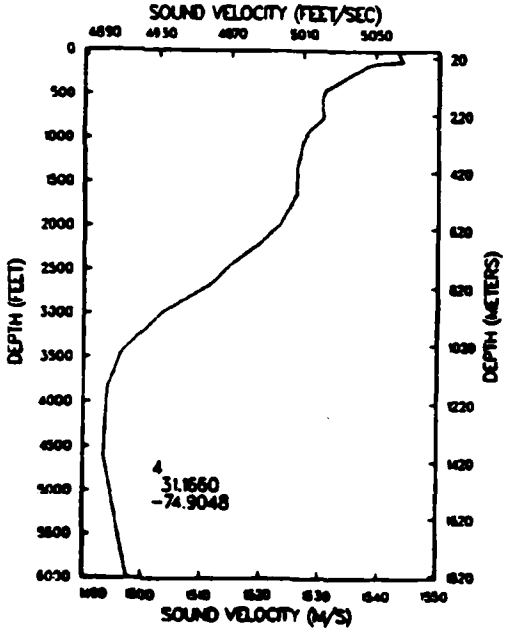

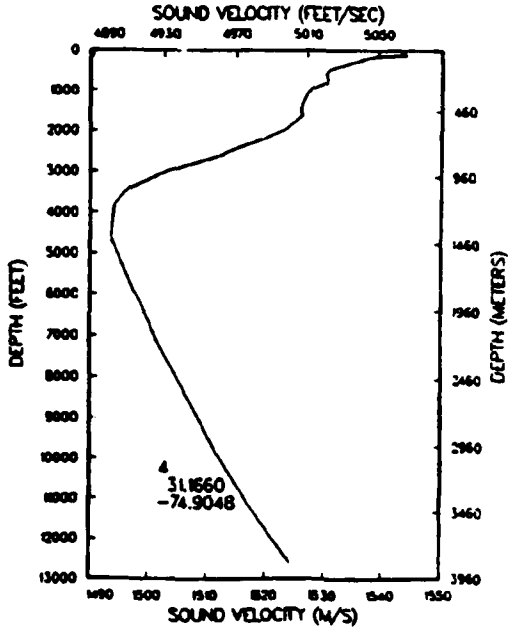

APPENDIX C

A. GEOACOUSTIC BOTTOM

The geoacoustic bottom model and its results are presented in this appendix and are taken from Reference 1. The conversion of the compressional and shear attenuation coefficients from dB/(m*kHz) to dB/Δ, needed as an input in SAFARI, is as follows:

$$A_s = A_m * C_x / 1000$$

where A_s is the attenuation coefficient of the respective compressional wave or shear wave in the SAFARI model, A_m is the attenuation coefficient of the geoacoustic model C_x is the velocity of the x wave, where x is compressional or shear, and 1000 is a scaling factor from kHz to Hz.

Unconsolidated layer - Calcareous Sediment, (DSDP Well 533)

$Vp = 1.455 + 1.713(D) - 0.374(D)^2$ (Hamilton, 1980)

$Vs = 110.0 + 1.2005(D)$ (for $Vp < 1.512$) (Hamilton, 1976)
$Vs = (3.884 \times Vp) - 5.757$ (for Vp 1.512-1.555 km/s) (Hamilton, 1980)
$Vs = 0.991 - (1.136 \times Vp) + 0.47(Vp)^2$ (for Vp 1.65-2.15 km/s)
$Vs = (0.78 \times Vp) - 0.962$ (for $Vp > 2.15$ km/s)

Kp: Estimated from Hamilton, 1980
Ks: Estimated from Hamilton, 1980

$\rho = 1.1379\ (Vp) - 0.20484$ (Hamilton, 1978)

Gas layer beneath BSR (m/s)-
$Vp = 1090.4 + 1.2892(D) - [(2.8628 \times 10^{-4}) \times (D)^2]$

$Vs = Vp/1.9$ (Hamilton, 1980; Pandit and King, 1982)

Kp: Estimated from Hamilton, 1980
Ks: Estimated from Hamilton, 1980

$\rho = 0.112\ (Vp) + 2.088$ (Hamilton, 1978)

BWSS = Bottom Water Sound Speed
D = Depth
Vp = Compressional Velocity
Vs = Shear Velocity
ρ = Density
Kp = Compressional Attenuation
Ks = Shear Attenuation

Geoacoustic models for Site "D"
Event 1Leg 1 Start 31°26'13" N, 74°49'27" W
Bearing 193° Range 0 nm

D (m)	Vp (m/s)	Vs (m/s)	Kp (dB/m*kHz)	Ks (dB/m*kHz)	ρ g/cc
0.0	1455.00	110.00	0.0515	13.00	1.45
5.0	1463.56	116.00	0.0527	13.30	1.46
10.0	1472.09	122.00	0.0538	13.58	1.47
15.0	1480.61	128.00	0.0550	13.88	1.48
20.0	1489.11	134.00	0.0562	14.19	1.49
30.0	1506.05	146.02.	0.0585	14.77	1.51
40.0	1522.92	158.02	0.0608	15.35	1.53
50.0	1539.72	223.27	0.0632	15.95	1.55
75.0	1581.37	313.02	0.0690	17.42	1.59
100.0	1622.56	359.85	0.0748	18.88	1.64
125.0	1663.28	401.77	0.0806	20.00	1.69
150.0	1703.54	419.74	0.0865	20.00	1.73
200.0	1782.64	459.49	0.0981	20.00	1.82
250.0	1859.88	503.98	0.1098	20.00	1.91
300.0	1935.24	552.79	0.1214	20.00	2.00
400.0	2080.36	661.82	0.1575	20.00	2.10
500.0	2218.00	768.04	0.1425	20.00	2.17
600.0	2348.16	869.56	0.1275	20.00	2.21
650.0	1807.41	458.71	0.2400	30.00	1.67
675.0	1951.94	566.07	0.1762	25.00	1.92
700.0	2092.86	672.14	0.1125	20.00	2.18
800.0	2155.54	719.32	0.0975	20.00	2.25
900.0	2215.74	766.28	0.0825	20.00	2.26
1000.0	2275.00	812.50	0.0675	17.04	2.27
1500.0	2611.13	1074.68	0.0518	13.08	2.32
2000.0	3155.00	1498.90	0.0361	9.11	2.37
2450.0	3836.13	2030.18	0.0220	5.55	2.42
2500.0	3861.13	2049.68	0.0205	5.17	2.43
2675.0	3948.63	2117.93	0.0150	3.79	2.44
2700.0	3961.13	2127.68	0.0142	3.58	2.45
2800.0	4011.13	2166.68	0.0111	2.80	2.46

Basement:
Vp: 5175 m/s
Vs: 2725 m/s
Ks: 0.07 dB/m*kHz
ρ: 2.75 g/cc

Appendix G. Event 1Leg 1Start 31°26 '13" N, 74°49 '27" W
Bearing 193° Range 10.45 nm

D (m)	Vp (m/s)	Vs (m/s)	Kp (dB/m*kHz)	Ks (dB/m*kHz)	ρ g/cc
0.0	1455.00	110.00	0.0515	13.00	1.45
5.0	1463.56	116.00	0.0527	13.30	1.46
10.0	1472.09	122.00	0.0538	13.58	1.47
15.0	1480.61	128.00	0.0550	13.88	1.48
20.0	1489.11	134.00	0.0562	14.19	1.49
30.0	1506.05	146.02.	0.0585	14.77	1.51
40.0	1522.92	158.02	0.0608	15.35	1.53
50.0	1539.72	223.27	0.0632	15.95	1.55
75.0	1581.37	313.02	0.0690	17.42	1.59
100.0	1622.56	359.85	0.0748	18.88	1.64
125.0	1663.28	401.77	0.0806	20.00	1.69
150.0	1703.54	419.74	0.0865	20.00	1.73
200.0	1782.64	459.49	0.0981	20.00	1.82
250.0	1859.88	503.98	0.1098	20.00	1.91
300.0	1935.24	552.79	0.1214	20.00	2.00
400.0	2080.36	661.82	0.1575	20.00	2.10
500.0	2218.00	768.04	0.1425	20.00	2.17
600.0	1761.12	434.78	0.2550	30.00	1.66
625.0	1910.65	440.69	0.1875	25.00	1.90
650.0	2060.11	645.42	0.1200	20.00	2.14
700.0	2092.86	672.14	0.1125	20.00	2.18
800.0	2155.54	719.32	0.0975	20.00	2.25
900.0	2215.74	766.28	0.0825	20.00	2.26
1000.0	2275.00	812.50	0.0675	17.04	2.27
1500.0	2611.13	1074.68	0.05181	3.08	2.32
2000.0	3155.00	1498.90	0.0361	9.11	2.37
2450.0	3836.13	2030.18	0.0220	5.55	2.42

Basement:
Vp: 5175 m/s
Vs: 2725 m/s
Kp: 0.02 dB/m*kHz
Ks: 0.07 dB/m*kHz
ρ: 2.75 g/cc

Appendix G. Event 1Leg 1Start 31°26'13" N, 74°49'27" W
Bearing 193° Range 14.21 nm

D (m)	Vp (m/s)	Vs (m/s)	Kp (dB/m*kHz)	Ks (dB/m*kHz)	ρ g/cc
0.0	1455.00	110.00	0.0515	13.00	1.45
5.0	1463.56	116.00	0.0527	13.30	1.46
10.0	1472.09	122.00	0.0538	13.58	1.47
15.0	1480.61	128.00	0.0550	13.88	1.48
20.0	1489.11	134.00	0.0562	14.19	1.49
30.0	1506.05	146.02.	0.0585	14.77	1.51
40.0	1522.92	158.02	0.0608	15.35	1.53
50.0	1539.72	223.27	0.0632	15.95	1.55
75.0	1581.37	313.02	0.0690	17.42	1.59
100.0	1622.56	359.85	0.0748	18.88	1.64
125.0	1663.28	401.77	0.0806	20.00	1.69
150.0	1703.54	419.74	0.0865	20.00	1.73
200.0	1782.64	459.49	0.0981	20.00	1.82
250.0	1859.88	503.98	0.1098	20.00	1.91
300.0	1935.24	552.79	0.1214	20.00	2.00
400.0	1560.27	330.91	0.3150	30.00	1.58
425.0	1659.06	389.67	0.2120	25.00	1.69
500.0	1953.88	565.68	0.1425	20.00	2.02
580.0	2012.19	608.14	0.1305	20.00	2.08
600.0	2026.15	618.78	0.1275	20.00	2.10
650.0	2060.11	645.42	0.1200	20.00	2.14
700.0	2092.86	672.14	0.1125	20.00	2.18
800.0	2155.54	719.32	0.0975	20.00	2.25
900.0	2215.74	766.28	0.0825	20.00	2.26
1000.0	2275.00	812.50	0.0675	17.04	2.27
1500.0	2611.13	1074.68	0.0518	13.08	2.32
2000.0	3155.00	1498.90	0.0361	9.11	2.37
2450.0	3836.13	2030.18	0.0220	5.55	2.42

Basement:
Vp: 5175 m/s
Vs: 2725 m/s
Kp: 0.02 dB/m*kHz
Ks: 0.07 dB/m*kHz
ρ: 2.75 g/cc

Appendix G. Event 1Leg 1Start 31°26'13" N, 74°49'27" W
Bearing 193° Range 28.63 nm

D (m)	Vp (m/s)	Vs (m/s)	Kp (dB/m*kHz)	Ks (dB/m*kHz)	ρ g/cc
0.0	1455.00	110.00	0.0515	13.00	1.45
5.0	1463.56	116.00	0.0527	13.30	1.46
10.0	1472.09	122.00	0.0538	13.58	1.47
15.0	1480.61	128.00	0.0550	13.88	1.48
20.0	1489.11	134.00	0.0562	14.19	1.49
30.0	1506.05	146.02.	0.0585	14.77	1.51
40.0	1522.92	158.02	0.0608	15.35	1.53
50.0	1539.72	223.27	0.0632	15.95	1.55
75.0	1581.37	313.02	0.0690	17.42	1.59
100.0	1622.56	359.85	0.0748	18.88	1.64
125.0	1663.28	401.77	0.0806	20.00	1.69
150.0	1703.54	419.74	0.0865	20.00	1.73
200.0	1782.64	459.49	0.0981	20.00	1.82
250.0	1859.88	503.98	0.1098	20.00	1.91
300.0	1935.24	552.79	0.1214	20.00	2.00
400.0	2080.36	661.82	0.1575	20.00	2.10
500.0	2218.00	768.04	0.1425	20.00	2.17
600.0	2348.16	869.56	0.1275	20.00	2.21
700.0	2470.84	965.26	0.1125	20.00	2.24
800.0	2586.04	1055.11	0.0975	20.00	2.26
900.0	2693.76	1139.13	0.0825	20.00	2.28
1000.0	2794.00	1217.32	0.0675	17.04	2.29
1500.0	3183.00	1520.74	0.0518	13.08	2.34
2000.0	3385.00	1678.30	0.0361	9.11	2.36
2500.0	3955.00	2122.90	0.020	5.15	2.42
2930.0	4385.00	2458.30	0.0070	1.77	2.47

Basement:
Vp: 5175 m/s
Vs: 2725 m/s
Kp: 0.02 dB/m*kHz
Ks: 0.07 dB/m*kHz
ρ: 2.75 g/cc

Appendix G. Event 1Leg 1Start 31°26 '13" N, 74°49 '27" W
Bearing 193°Range 40.13 nm

D (m)	Vp (m/s)	Vs (m/s)	Kp (dB/m*kHz)	Ks (dB/m*kHz)	ρ g/cc
0.0	1455.00	110.00	0.0515	13.00	1.45
5.0	1463.56	116.00	0.0527	13.30	1.46
10.0	1472.09	122.00	0.0538	13.58	1.47
15.0	1480.61	128.00	0.0550	13.88	1.48
20.0	1489.11	134.00	0.0562	14.19	1.49
30.0	1506.05	146.02.	0.0585	14.77	1.51
40.0	1522.92	158.02	0.0608	15.35	1.53
50.0	1539.72	223.27	0.0632	15.95	1.55
75.0	1581.37	313.02	0.0690	17.42	1.59
100.0	1622.56	359.85	0.0748	18.88	1.64
125.0	1663.28	401.77	0.0806	20.00	1.69
150.0	1703.54	419.74	0.0865	20.00	1.73
200.0	1782.64	459.49	0.0981	20.00	1.82
250.0	1859.88	503.98	0.1098	20.00	1.91
300.0	1935.24	552.79	0.1214	20.00	2.00
400.0	2080.36	661.82	0.1575	20.00	2.10
500.0	2218.00	768.04	0.1425	20.00	2.17
580.0	1741.57	424.64	0.2610	30.00	1.65
605.0	1952.21	503.44	0.2110	25.00	1.82
650.0	2060.11	645.42	0.1200	20.00	2.14
700.0	2092.86	672.14	0.1125	20.00	2.18
800.0	2155.54	719.32	0.0975	20.00	2.25
900.0	2215.74	766.28	0.0825	20.00	2.26
1000.0	2275.00	812.50	0.0675	17.04	2.27
1500.0	2611.13	1074.68	0.0518	13.08	2.32
2000.0	3155.00	1498.90	0.0361	9.11	2.37
2450.0	3836.13	2030.18	0.0220	5.55	2.42
2500.0	3861.13	2049.68	0.0205	5.17	2.43
2675.0	3948.63	2117.93	0.0150	3.79	2.44
2700.0	3961.13	2127.68	0.0142	3.58	2.45
2800.0	4011.13	2166.68	0.0111	2.80	2.46
3000.0	4111.13	2244.68	0.0048	1.21	2.48

Basement:
Vp: 5175 m/s
Vs: 2725 m/s
Kp: 0.02 dB/m*kHz
Ks: 0.07 dB/m*kHz
ρ: 2.75 g/cc

Appendix G. Event 1Leg 1Start 31°26 '13" N, 74°49 '27" W
Bearing 193° Range 42 nm

D (m)	Vp (m/s)	Vs (m/s)	Kp (dB/m*kHz)	Ks (dB/m*kHz)	ρ g/cc
0.0	1455.00	110.00	0.0515	13.00	1.45
5.0	1463.56	116.00	0.0527	13.30	1.46
10.0	1472.09	122.00	0.0538	13.58	1.47
15.0	1480.61	128.00	0.0550	13.88	1.48
20.0	1489.11	134.00	0.0562	14.19	1.49
30.0	1506.05	146.02.	0.0585	14.77	1.51
40.0	1522.92	158.02	0.0608	15.35	1.53
50.0	1539.72	223.27	0.0632	15.95	1.55
75.0	1581.37	313.02	0.0690	17.42	1.59
100.0	1622.56	359.85	0.0748	18.88	1.64
125.0	1663.28	401.77	0.0806	20.00	1.69
150.0	1703.54	419.74	0.0865	20.00	1.73
200.0	1782.64	459.49	0.0981	20.00	1.82
250.0	1859.88	503.98	0.1098	20.00	1.91
300.0	1935.24	552.79	0.1214	20.00	2.00
400.0	2080.36	661.82	0.1575	20.00	2.10
500.0	1663.50	384.02	0.2850	30.00	1.63
525.0	1754.48	442.78	0.2456	25.00	1.75
600.0	2026.15	618.78	0.1275	20.00	2.10
700.0	2092.86	672.14	0.1125	20.00	2.18
800.0	2155.54	719.32	0.0975	20.00	2.25
900.0	2215.74	766.28	0.0825	20.00	2.26
1000.0	2275.00	812.50	0.0675	17.04	2.27
1500.0	2611.13	1074.68	0.0518	13.08	2.32
2000.0	3155.00	1498.90	0.0361	9.11	2.37
2500.0	3861.13	2049.68	0.0205	5.17	2.43
2675.0	3948.63	2117.93	0.0150	3.79	2.44

Basement:
Vp: 5175 m/s
Vs: 2725 m/s
Kp: 0.02 dB/m*kHz
Ks: 0.07 dB/m*kHz
ρ: 2.75 g/cc

APPENDIX D

A. MODEL RESULTS

Figures 15 through 40 show the results of the SAFARI model run at a frequency of 7 Hz. OASTL STLRAN and OASTL SINTGR stand for Ocean Acoustic and Seismic Exploration Synthesis Transmission Loss, Single frequency Transmission Loss versus Range, and Ocean Acoustic and Seismic Exploration Synthesis Transmission Loss, Single frequency Integrand. They are located on the top right part of the graphs.

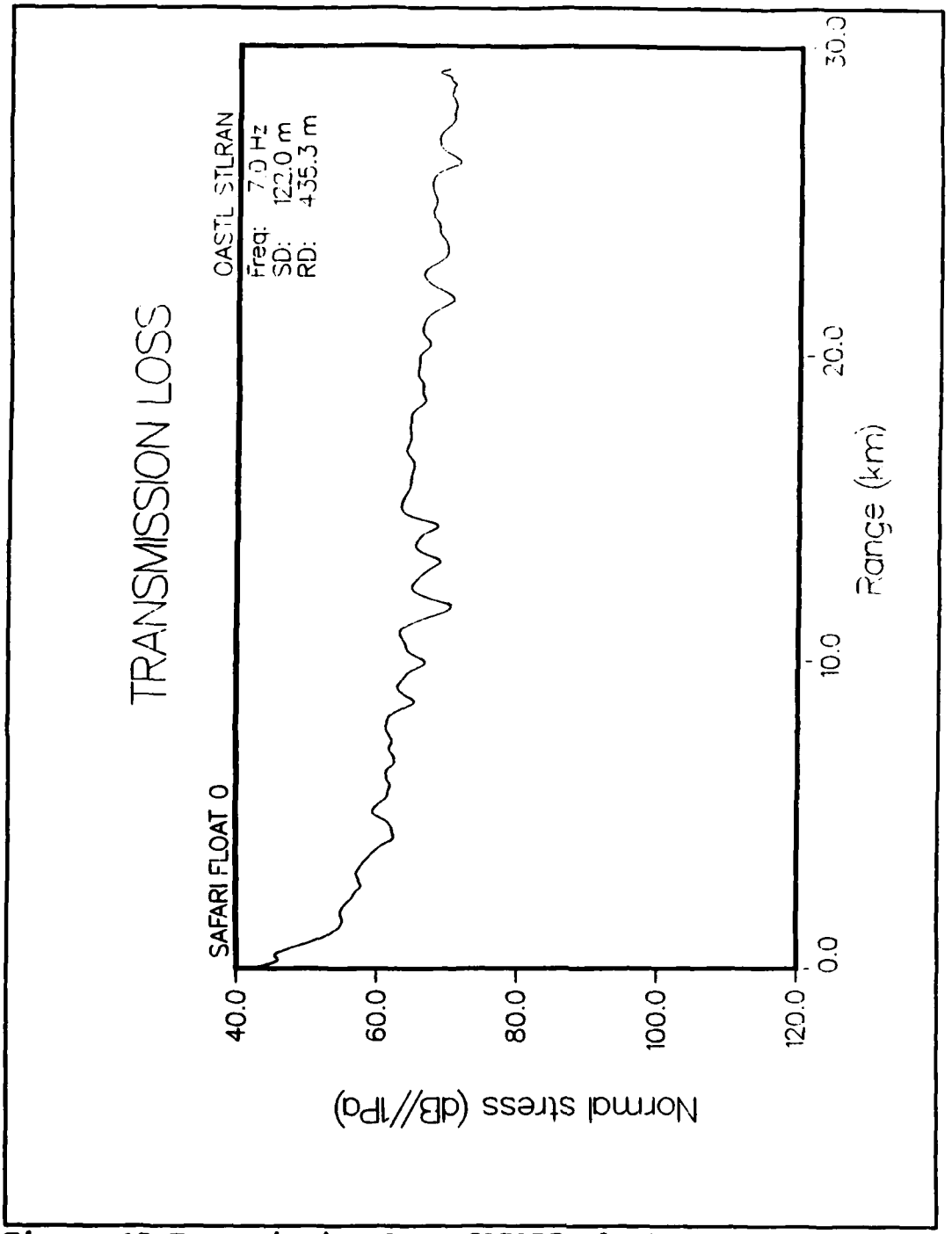

Figure 15 Transmission Loss SAFARI Float 0
Cmin=50 m/s, Cmax=1E8 m/s, 4096 points, Δr=7.141 m,
Max FFT range=29.250 km

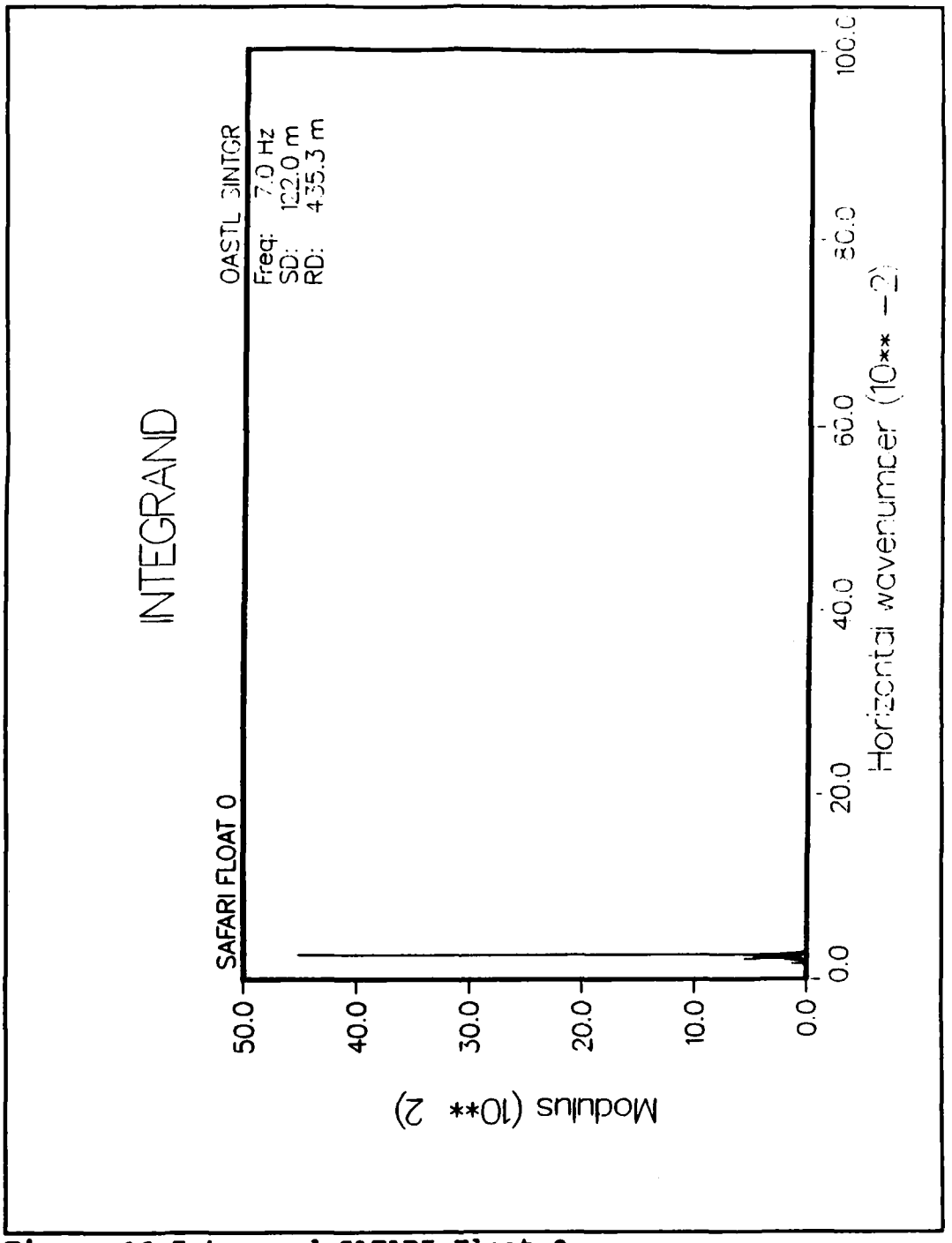

Figure 16 Integrand SAFARI Float 0
Cmin=50 m/s, Cmax=1E8 m/s, 4096 points, Δr=7.141 m, Max FFT range= 29.250 km

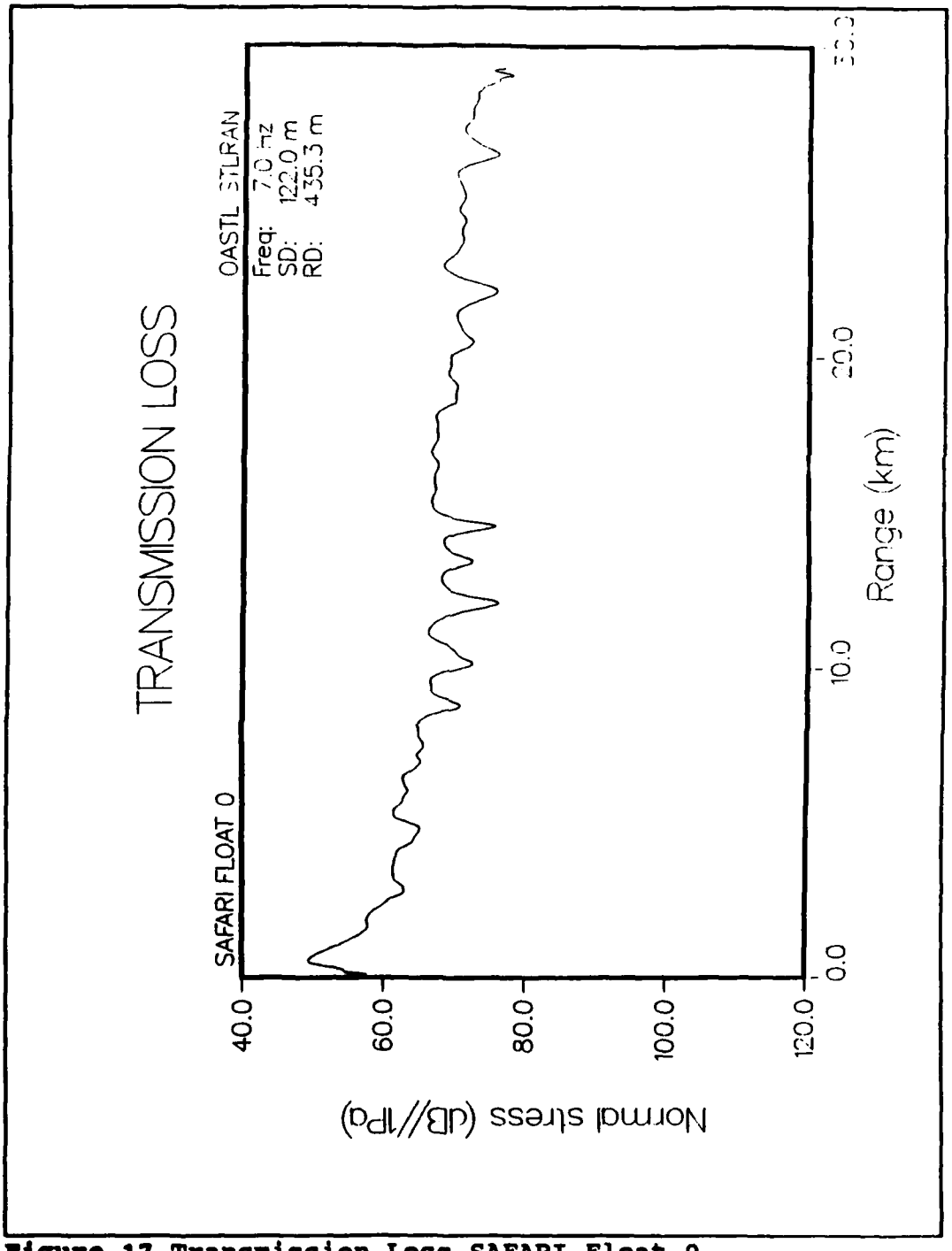

Figure 17 Transmission Loss SAFARI Float 0
Cmin=100 m/s, Cmax=2E8 m/s, 2048 points, Δr=14.279 m, Max FFT range=29.243 km

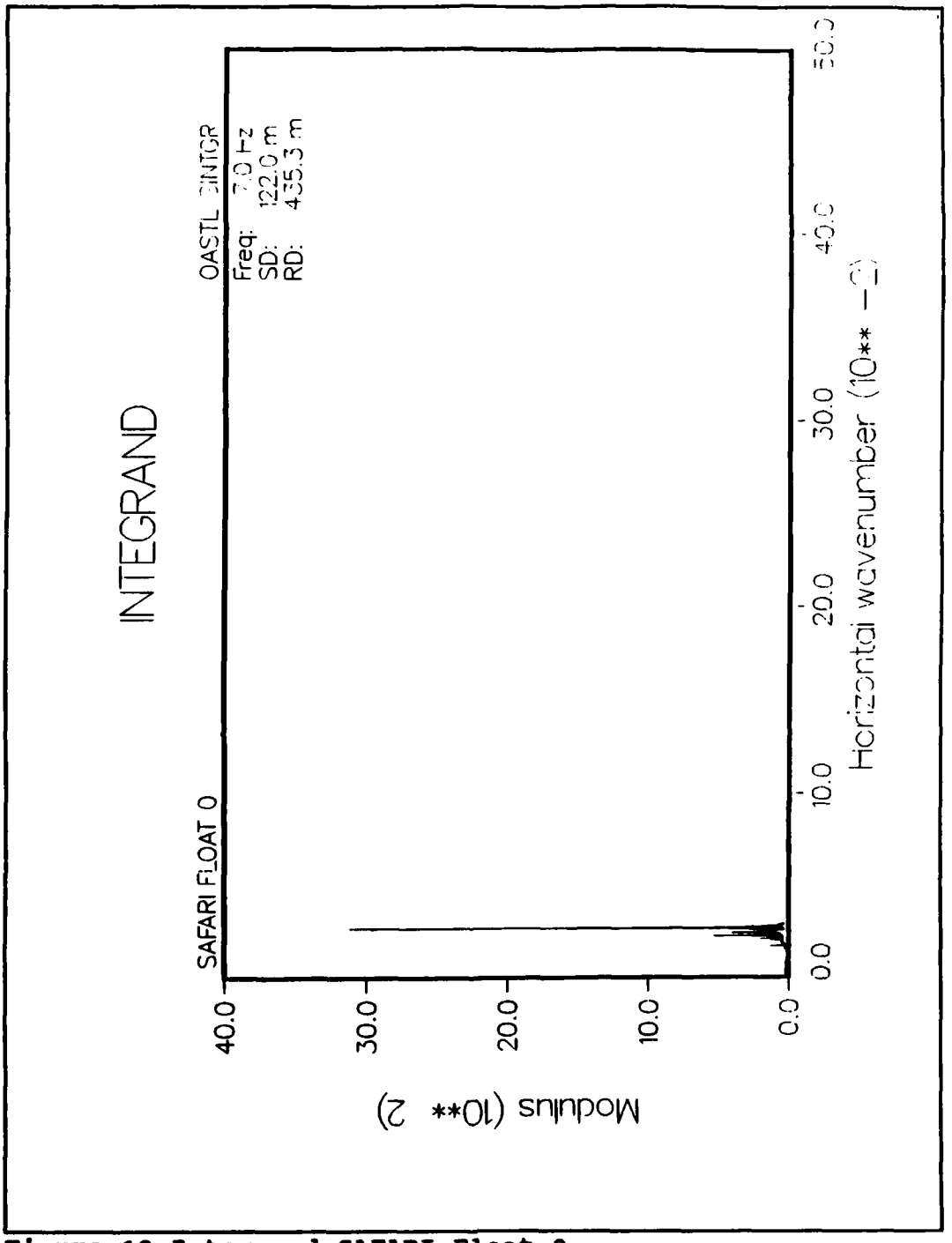

Figure 18 Integrand SAFARI Float 0
Cmin=100 m/s, Cmax=2E8, 2048 points, Δr=14.279 m,
Max FFT range=29.243 km

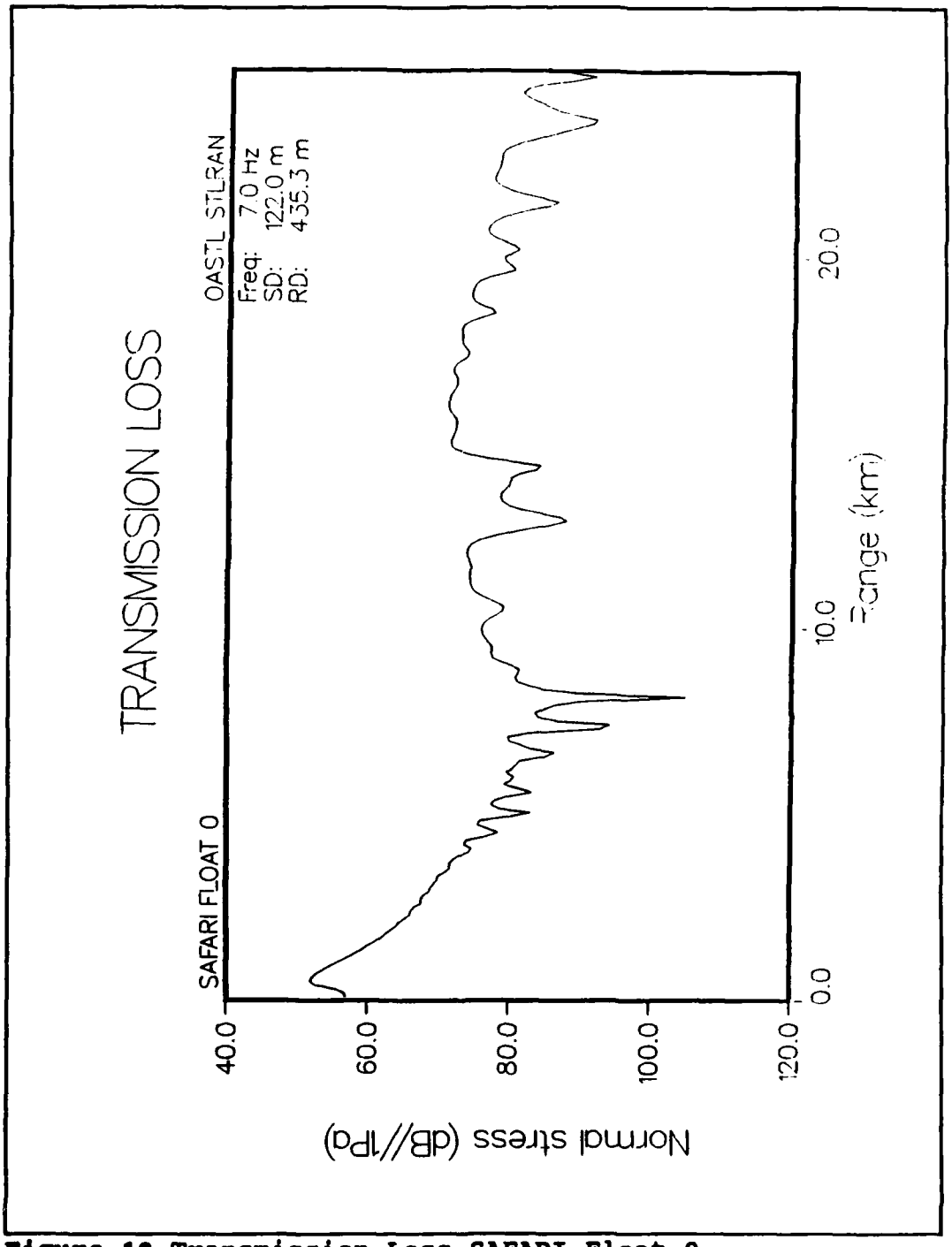

Figure 19 Transmission Loss SAFARI Float 0
Cmin=740 m/s, Cmax=1E8 m/s, 4096 points, Δr=105.7 m,
Max FFT range=432.903 km

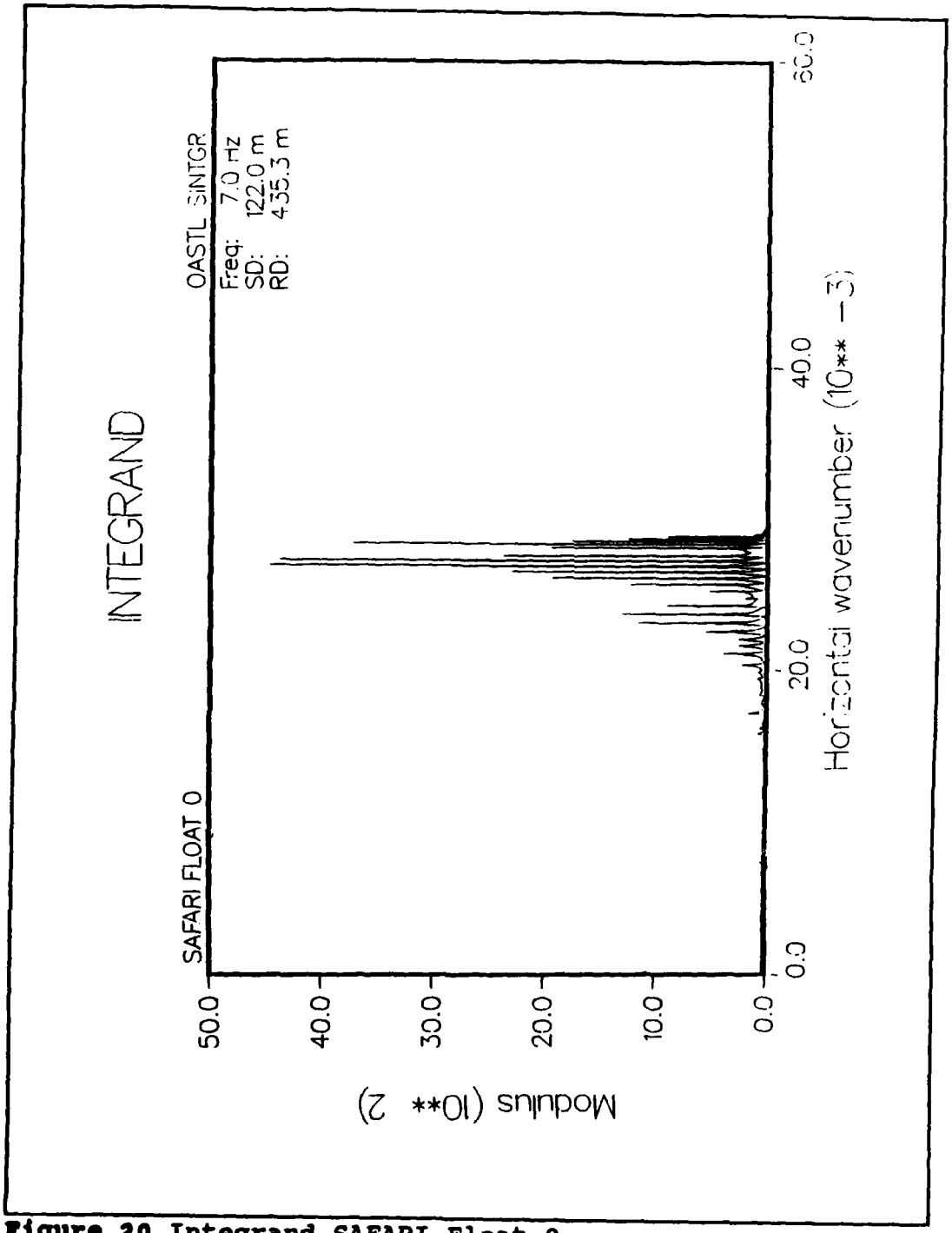

Figure 20 Integrand SAFARI Float 0
Cmin=740 m/s, Cmax=1E8 m/s, 4096 points, Δr=105.7 m, Max FFT range=432.903 km

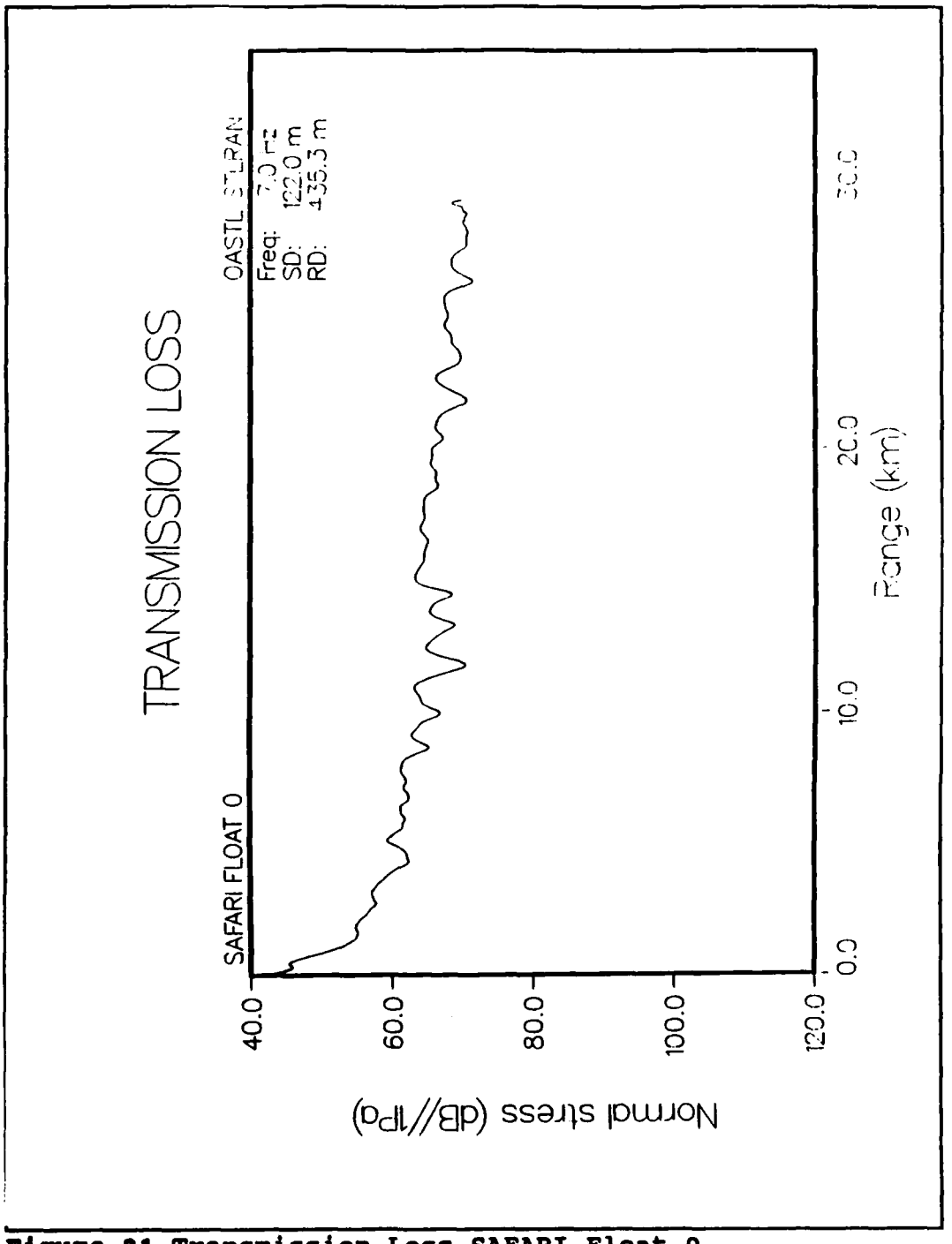

Figure 21 Transmission Loss SAFARI Float 0
No Contour Offset
Cmin=50 m/s, Cmax=1E8 m/s, 4096 points, Δr=7.141 m,
Max FFT range=29.250 km

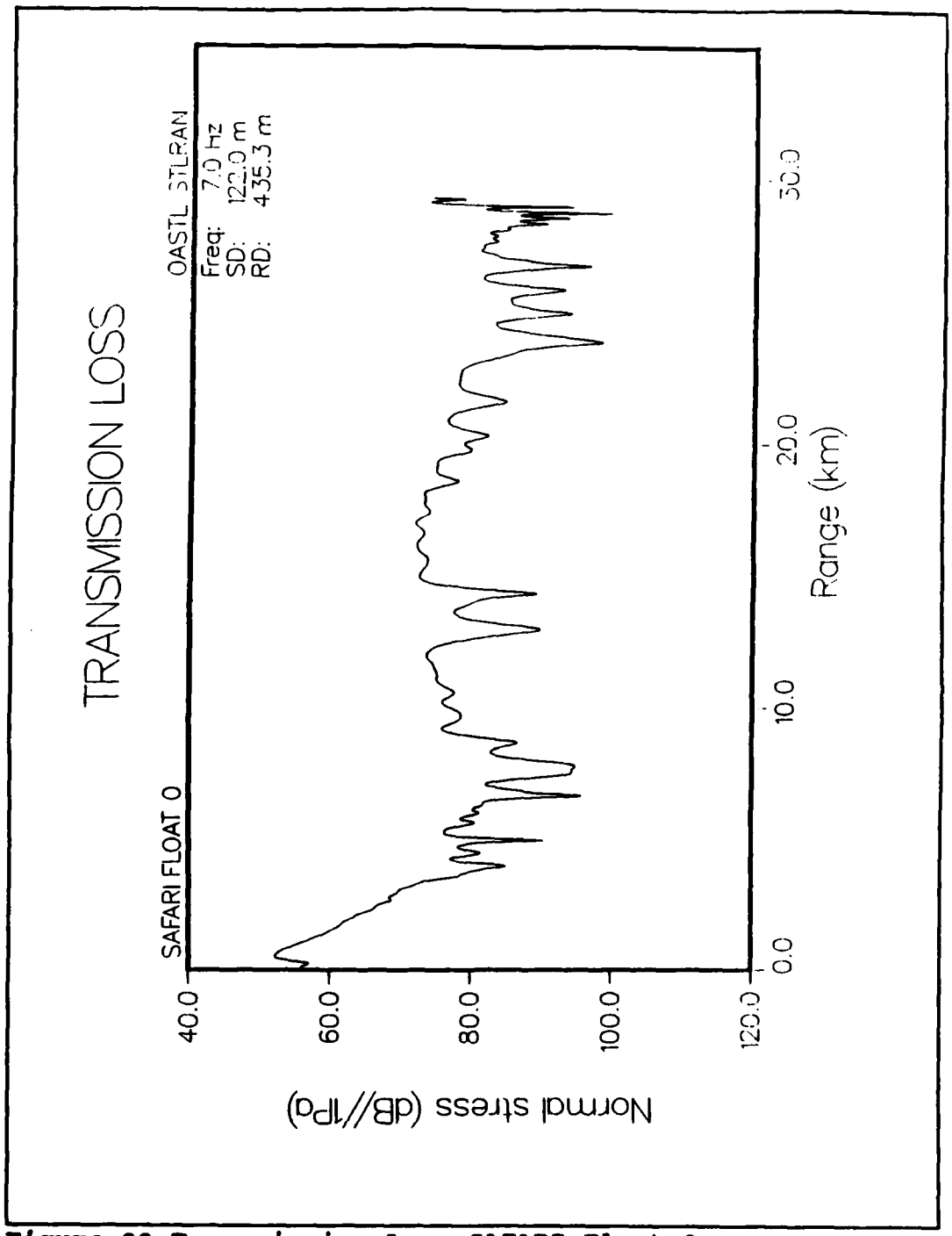

Figure 22 Transmission Loss SAFARI Float 0
0.25 Contour Offset
Cmin=50 m/s, Cmax=1E8 m/s, 4096 points, Δr=7.141 m,
Max FFT range=29.250 km

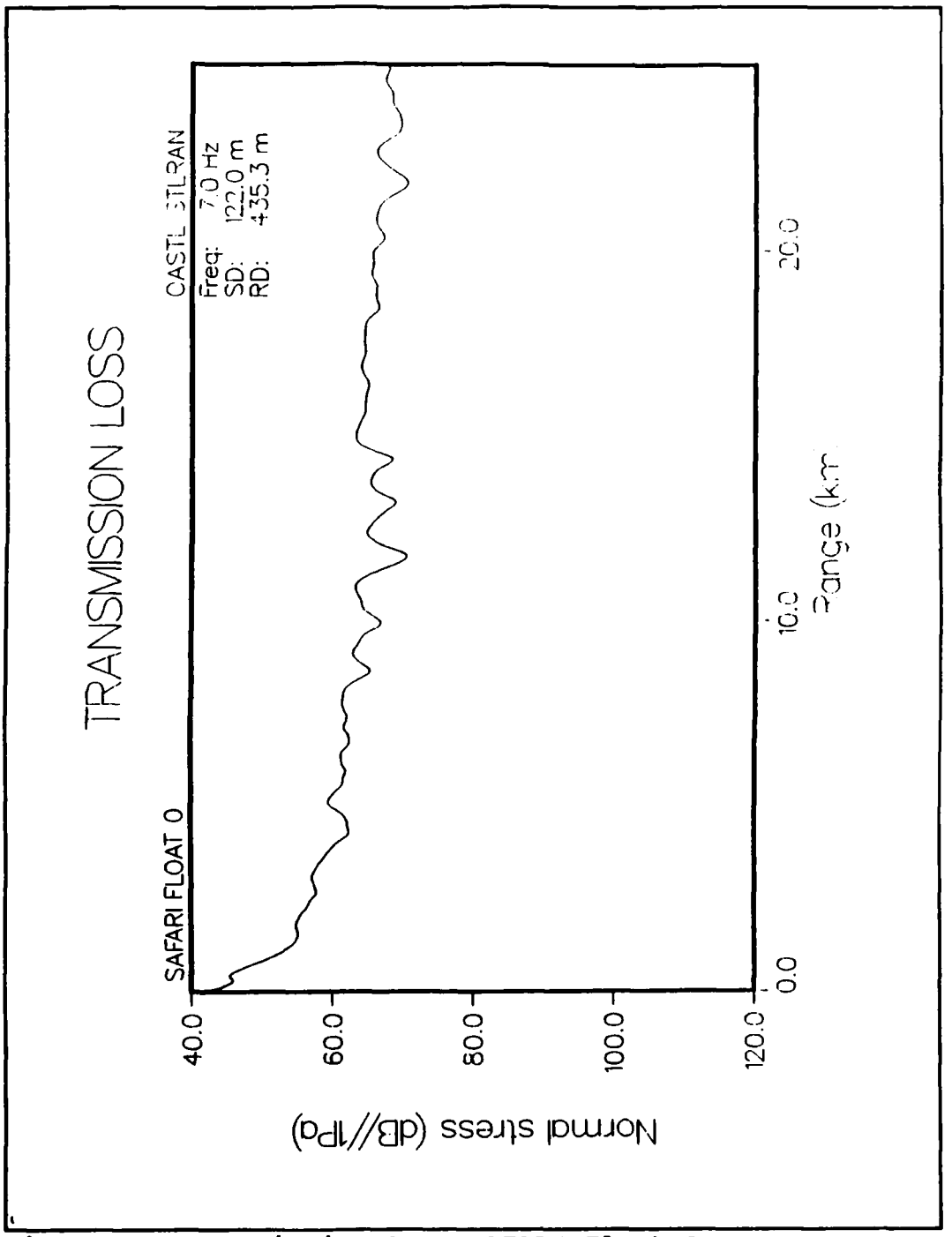

Figure 23 Transmission Loss SAFARI Float 0
No Contour Offset
Cmin=50 m/s, Cmax=1E8 m/s, 4096 points, Δr=7.141 m,
Max FFT range=29.250 km

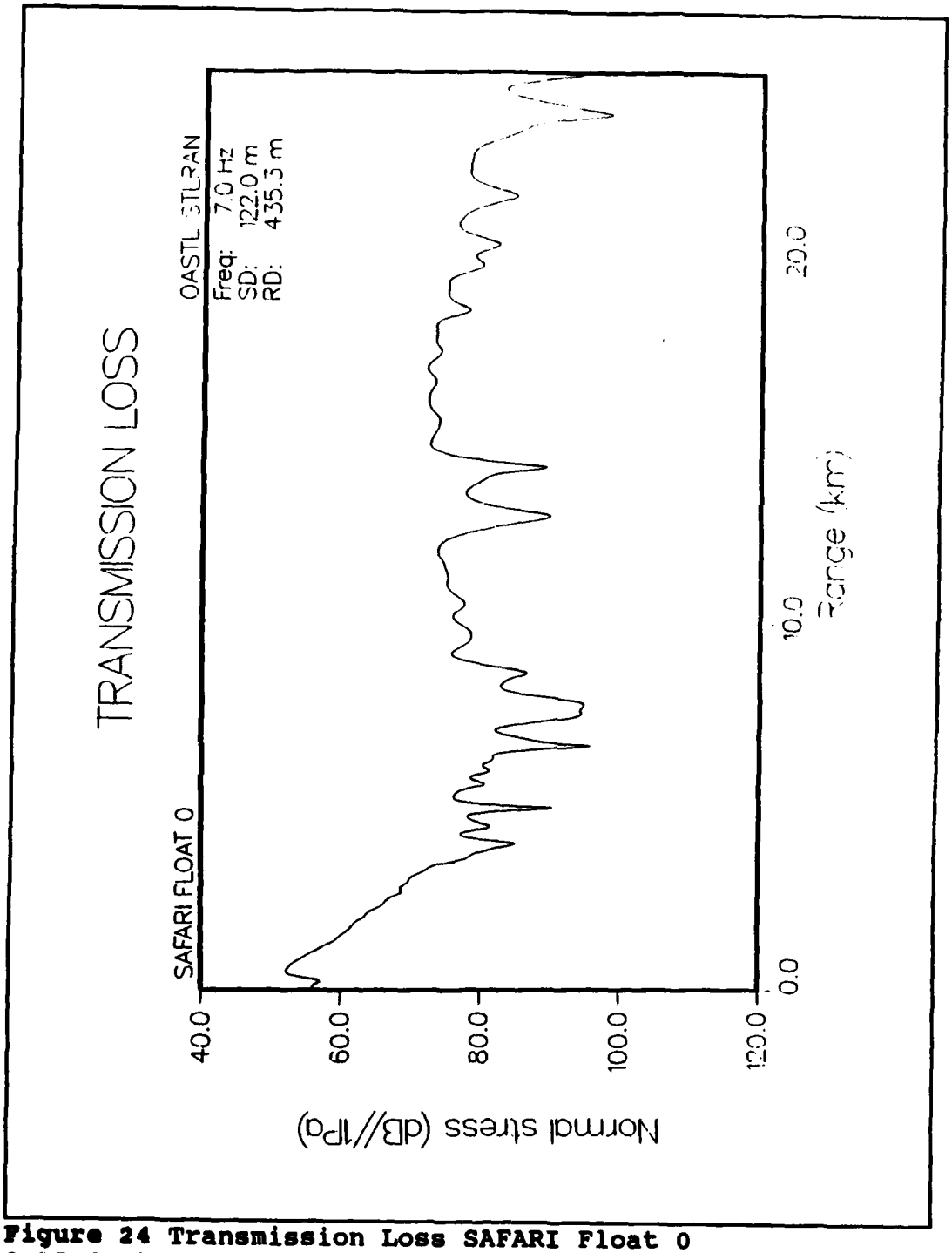

Figure 24 Transmission Loss SAFARI Float 0
0.25 Contour Offset
Cmin=50 m/s, Cmax=1E8 m/s, 4096 points, Δr=7.141 m,
Max FFT range=29.250 km

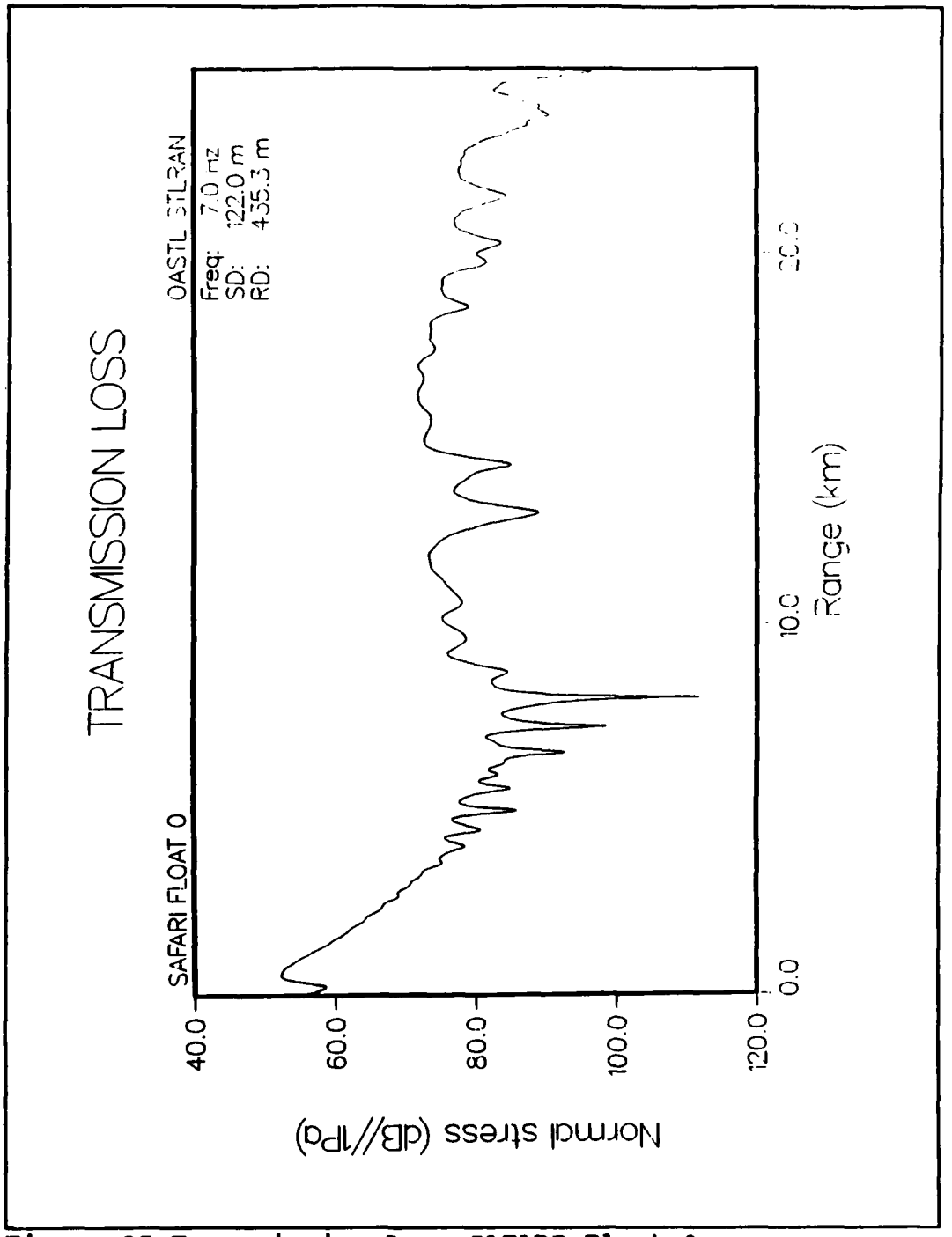

Figure 25 Transmission Loss SAFARI Float 0
0.5 Contour Offset
Cmin=50 m/s, Cmax=1E8 m/s, 4096 points, Δr=7.141 m,
Max FFT range=29.250 km

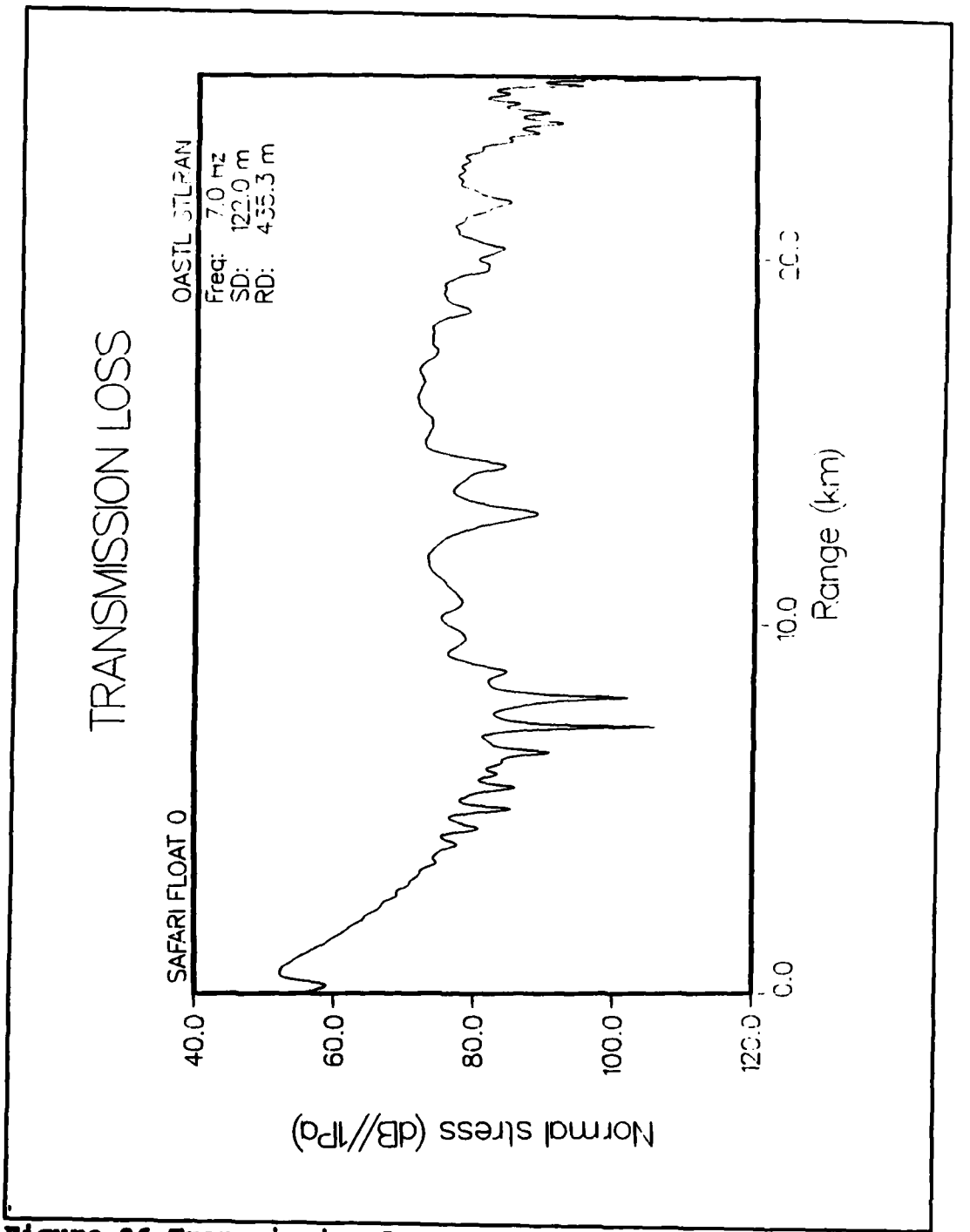

Figure 26 Transmission Loss SAFARI Float 0
0.75 Contour Offset
Cmin=50 m/s, Cmax=1E8 m/s, 4096 points, Δr=7.141 m,
Max FFT range=29.250 km

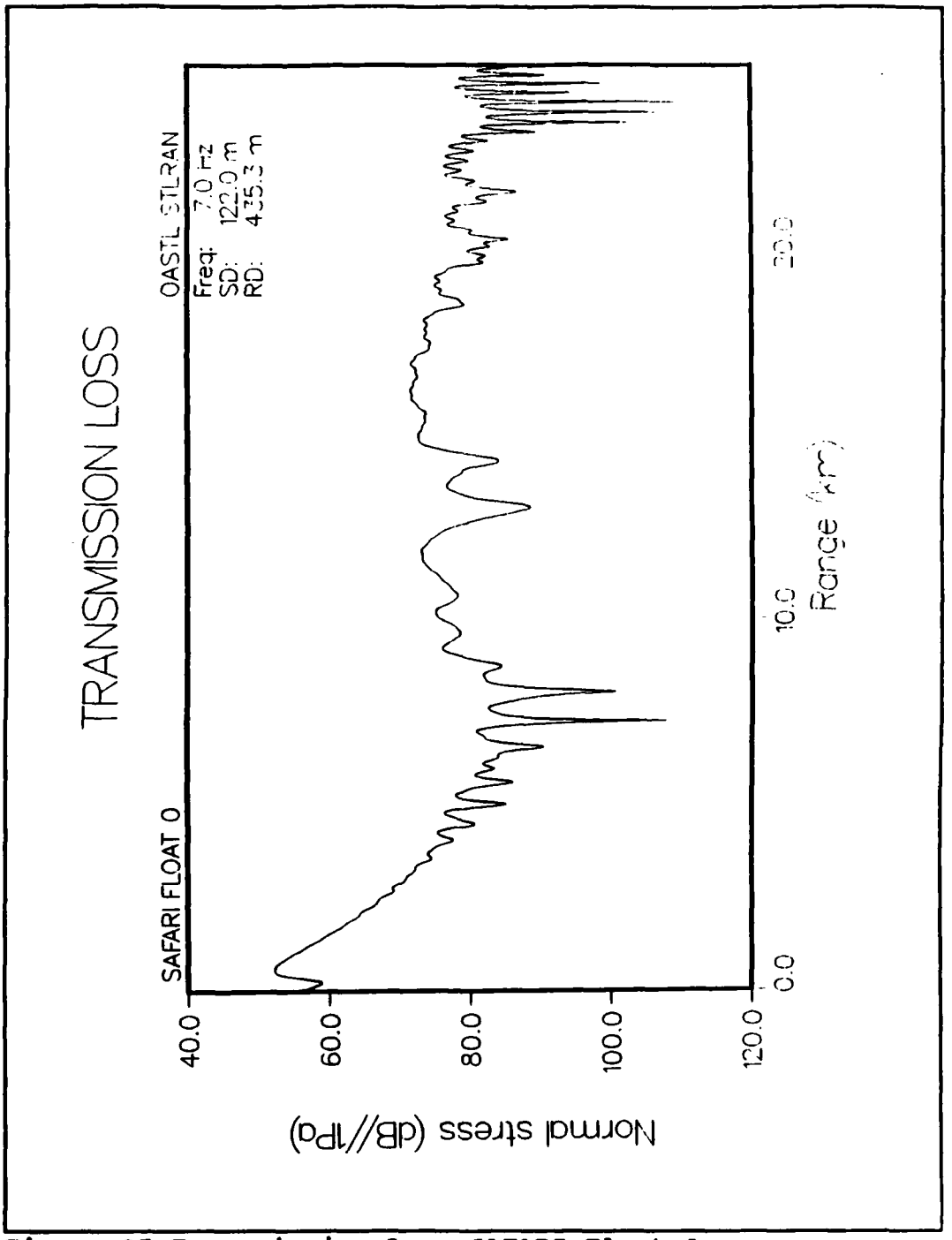

Figure 27 Transmission Loss SAFARI Float 0
1.0 Contour Offset
Cmin=50 m/s, Cmax=1E8 m/s, 4096 points, Δr=7.141 m,
Max FFT range=29.250 km

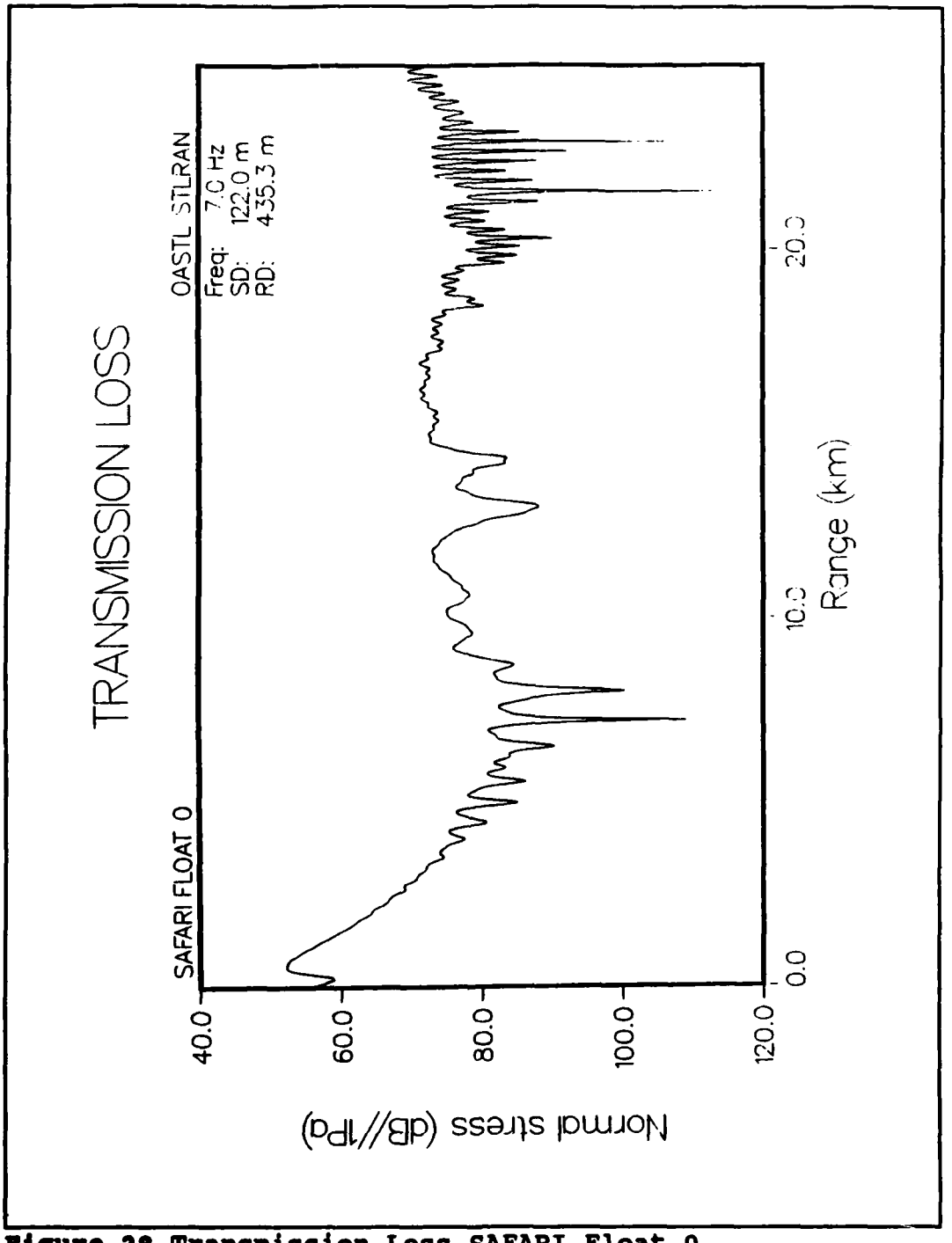

Figure 28 Transmission Loss SAFARI Float 0
1.25 Contour Offset
Cmin=50 m/s, Cmax=1E8 m/s, 4096 points, Δr=7.141 m,
Max FFT range=29.250 km

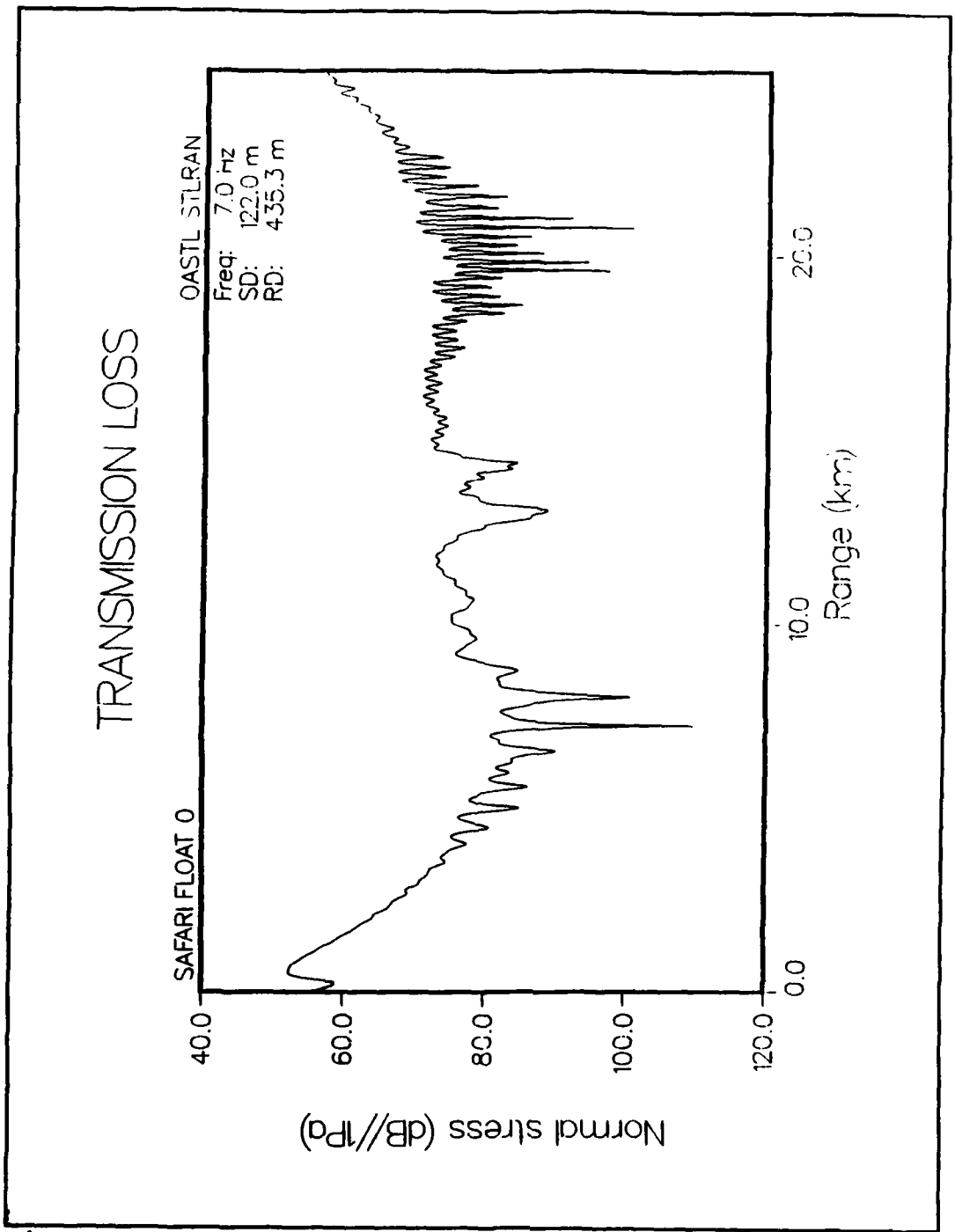

Figure 29 Transmission Loss SAFARI Float 0
1.50 Contour Offset
Cmin=50 m/s, Cmax=1E8 m/s, 4096 points, Δr=7.141 m,
Max FFT range=29.250 km

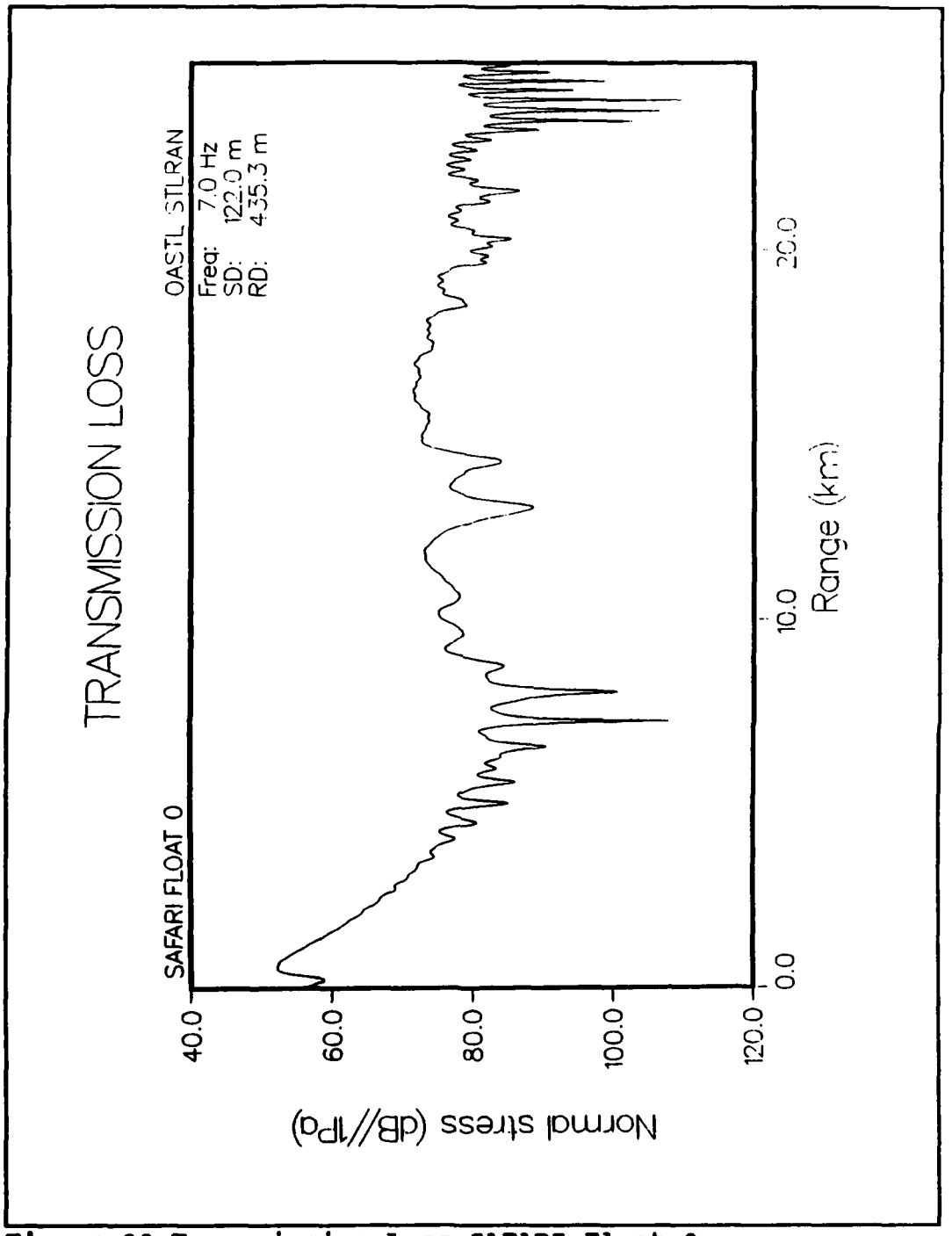

Figure 30 Transmission Loss SAFARI Float 0
Standard Contour Offset
Cmin=50 m/s, Cmax=1E8 m/s, 4096 points, Δr=7.141 m,
Max FFT range=29.250 km

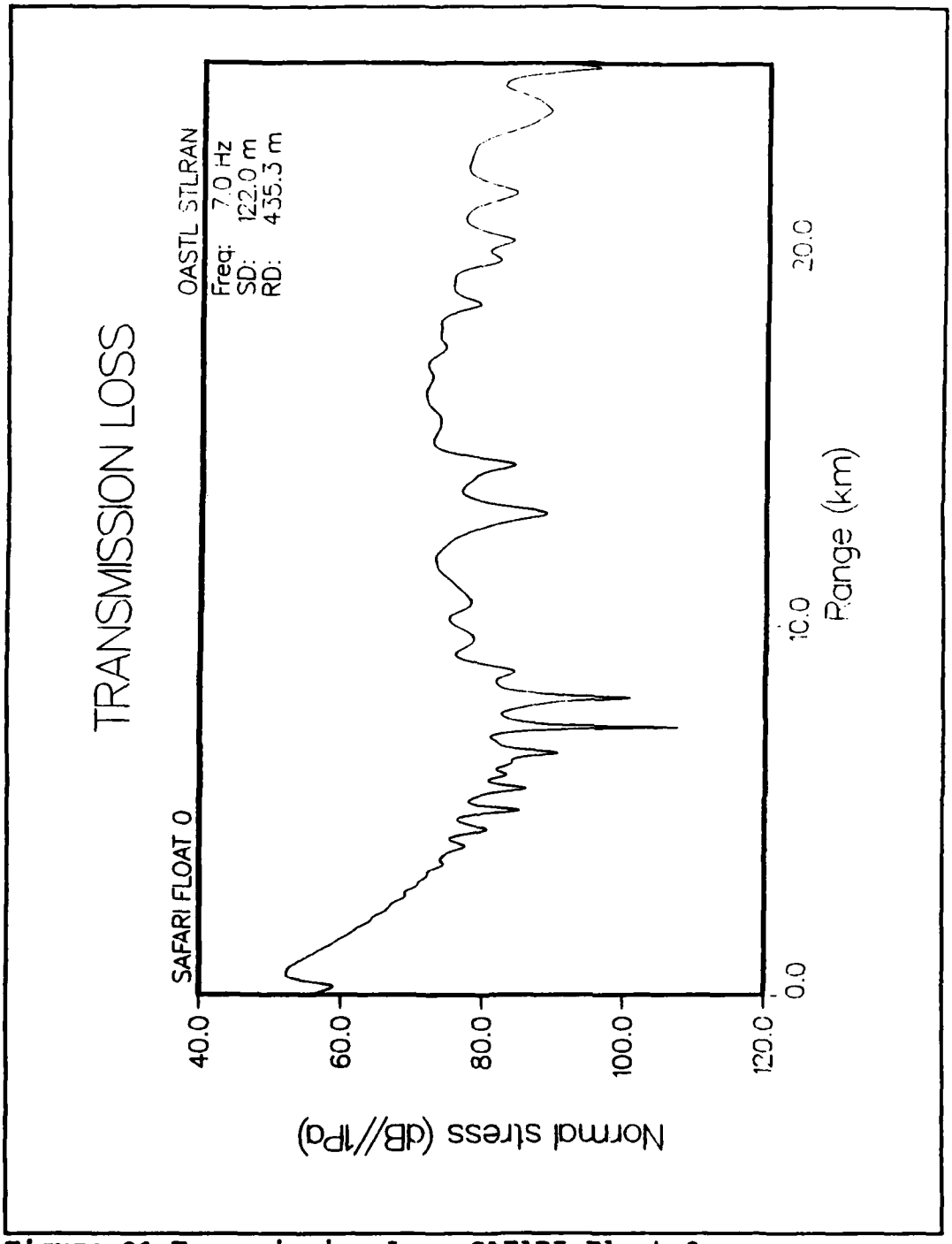

Figure 31 Transmission Loss SAFARI Float 0
Standard Contour Offset
Cmin=50 m/s, Cmax=1E8 m/s, 8192 points, Δr=7.141 m,
Max FFT range=58.500 km

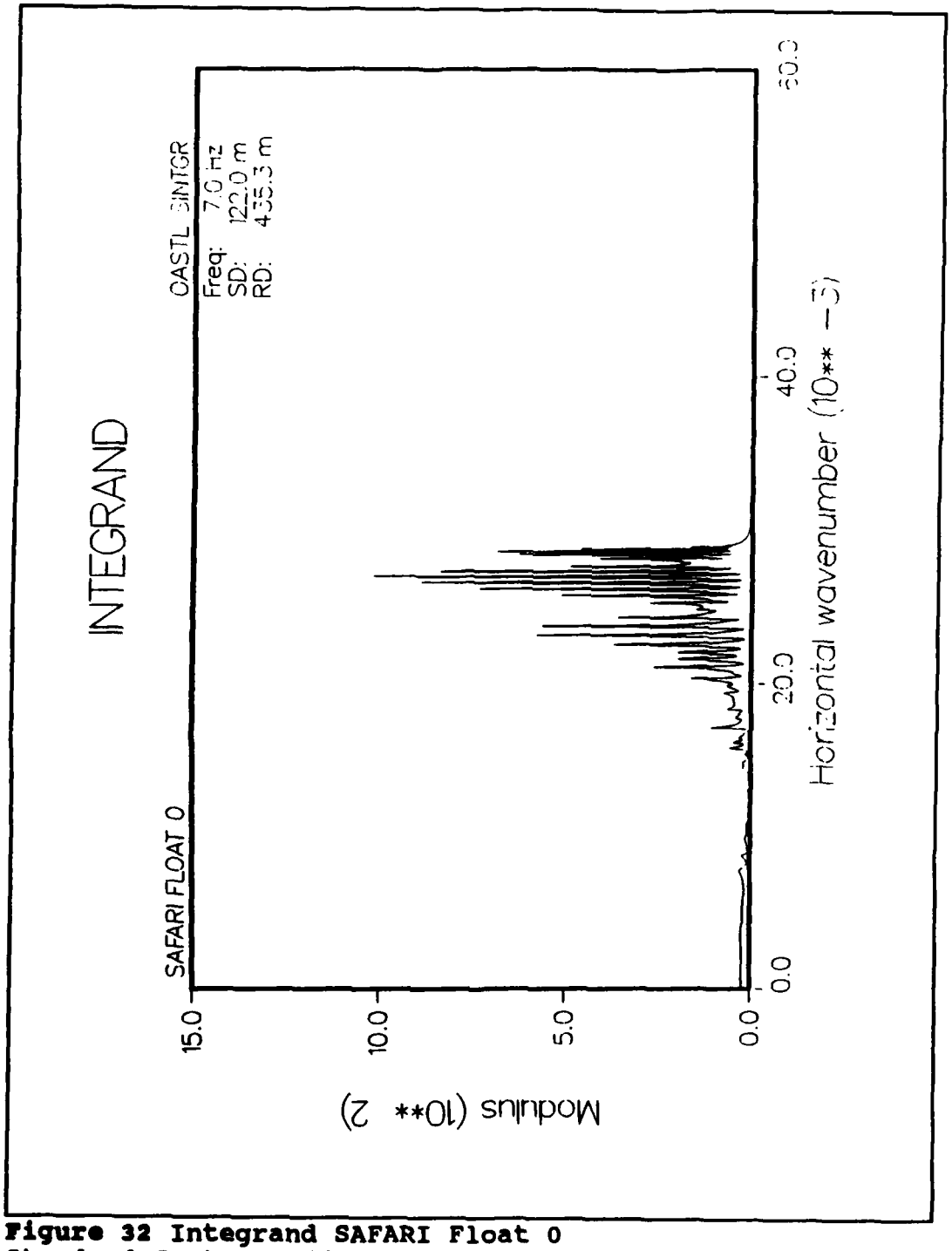

Figure 32 Integrand SAFARI Float 0
Standard Contour Offset
Cmin=740 m/s, Cmax=1E8 m/s, 4096 points, Δr=105.7 m,
Max FFT range=432.903 km

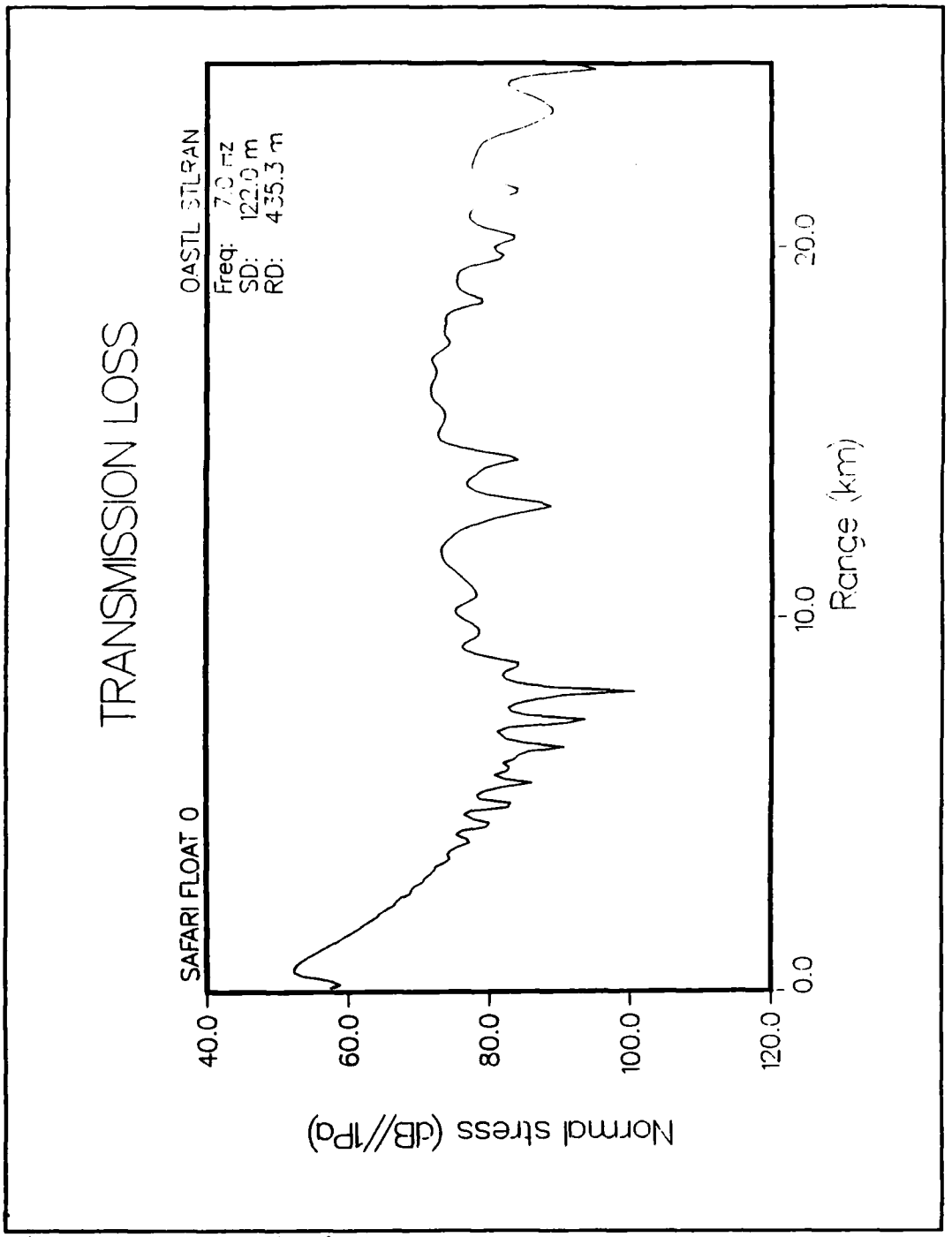

Figure 33 Transmission Loss SAFARI Float 0
Standard Contour Offset
Cmin=740 m/s, Cmax=1E8 m/s, 4096 points, Δr=105.7 m,
Max FFT range=432.903 km

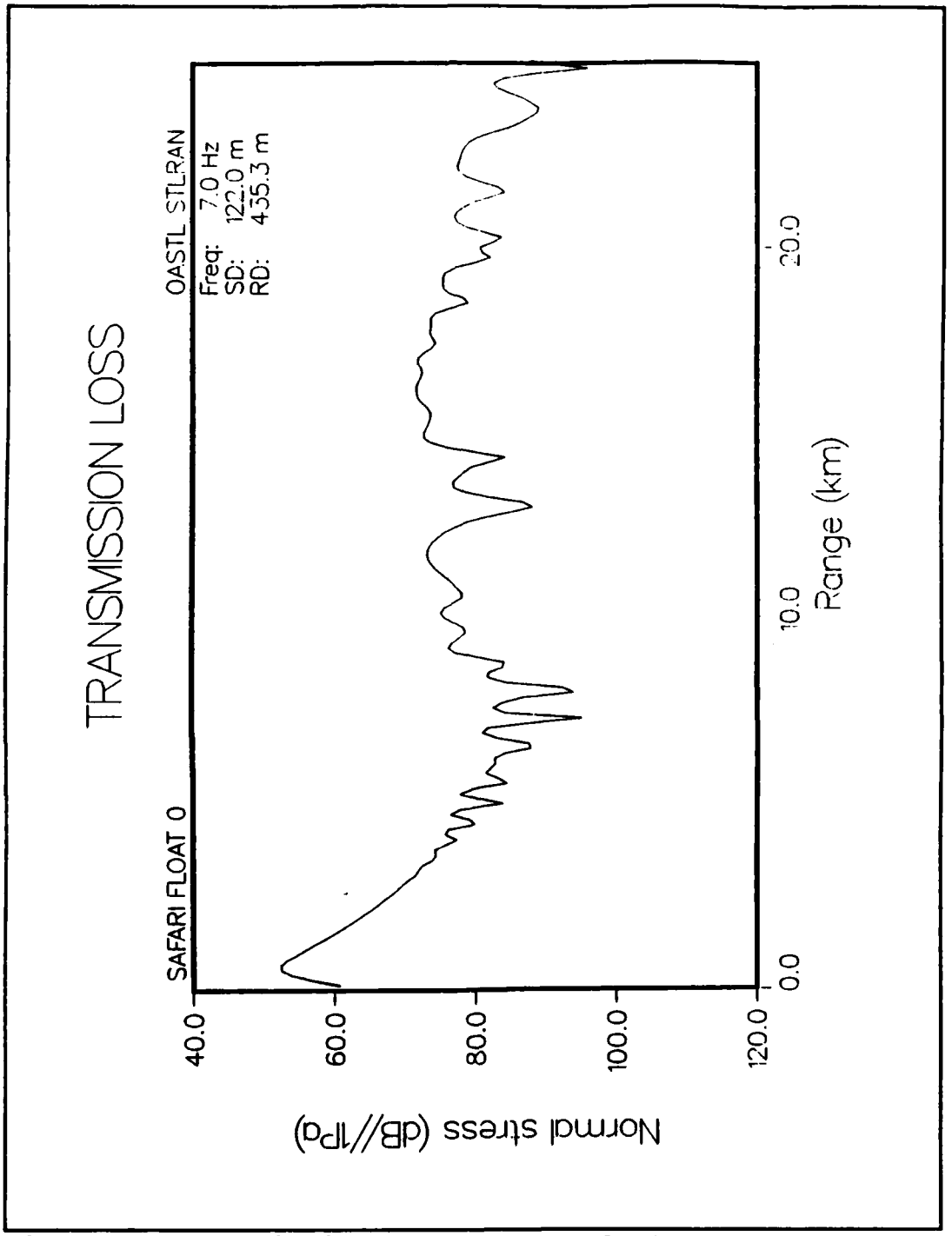

Figure 34 Transmission Loss SAFARI Float 0
Standard Contour Offset
Cmin=740 m/s, Cmax=3400 m/s, 4096 points, Δr=105.7 m,
Max FFT range=432.903 km

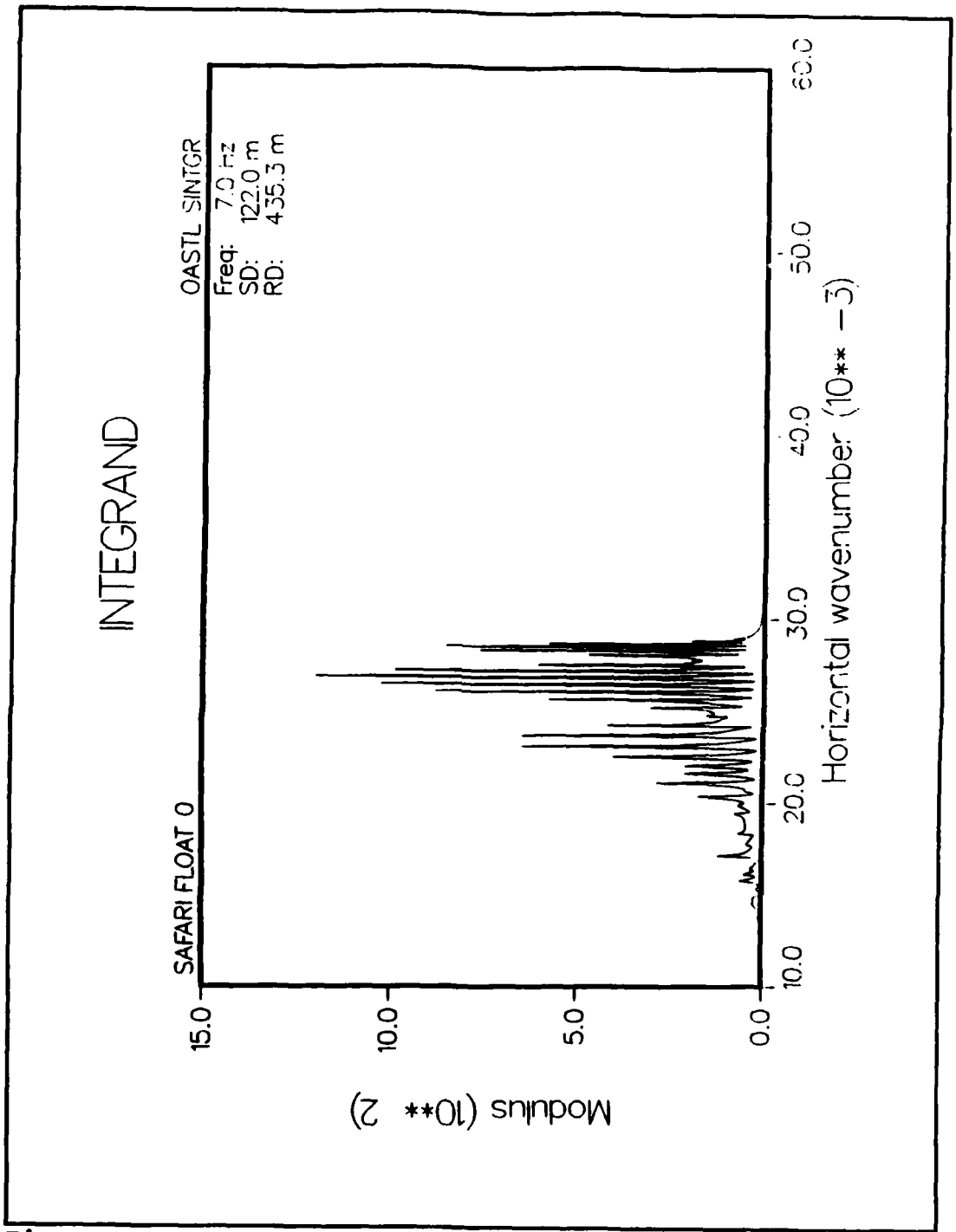

Figure 35 Integrand SAFARI Float 0
Standard Contour Offset
Cmin=740 m/s, Cmax=3400 m/s, 4096 points, Δr=105.7 m,
Max FFT range=432.903 km

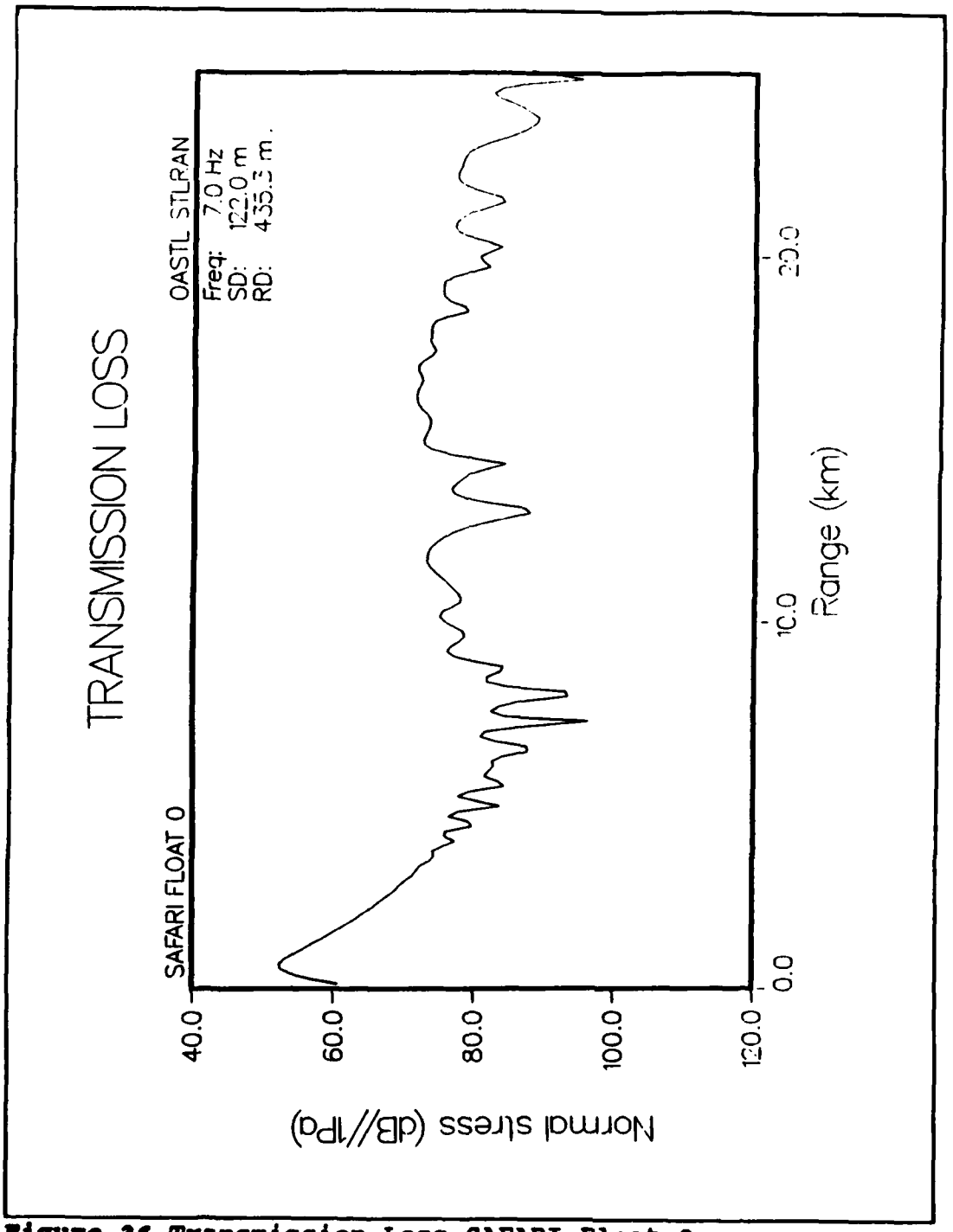

Figure 36 Transmission Loss SAFARI Float 0
Standard Contour Offset
Cmin=740 m/s, Cmax=3400 m/s, 1024 points, Δr=105.7 m,
Max FFT range=432.903 km

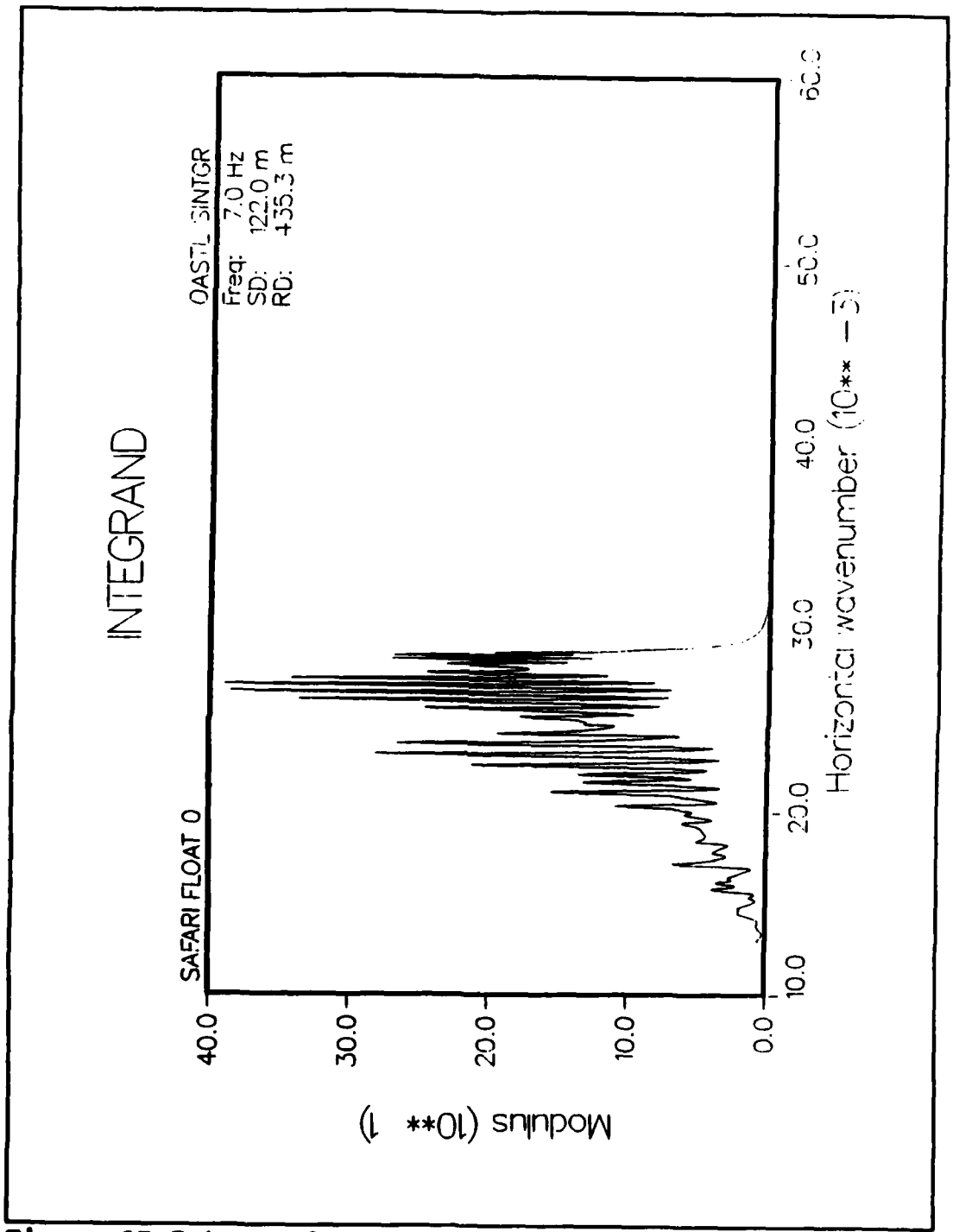

Figure 37 Integrand SAFARI Float 0
Standard Contour Offset
Cmin=740 m/s, Cmax=3400 m/s, 1024 points, Δr=105.7 m,
Max FFT range=432.903 km

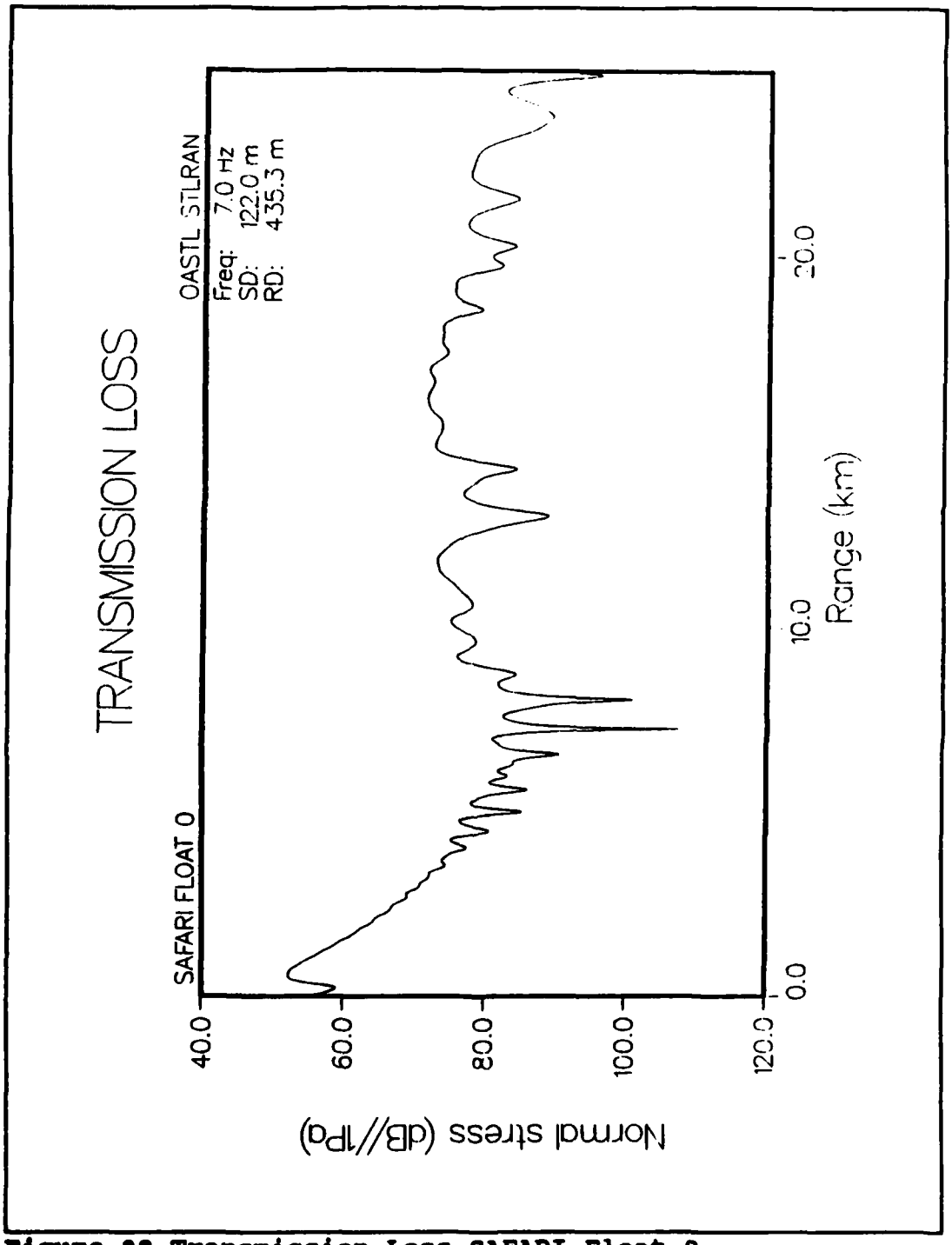

Figure 38 Transmission Loss SAFARI Float 0
Standard Contour Offset
Cmin=50 m/s, Cmax=1E8 m/s, 16384 points, Δr=7.141 m,
Max FFT range=117.000 km

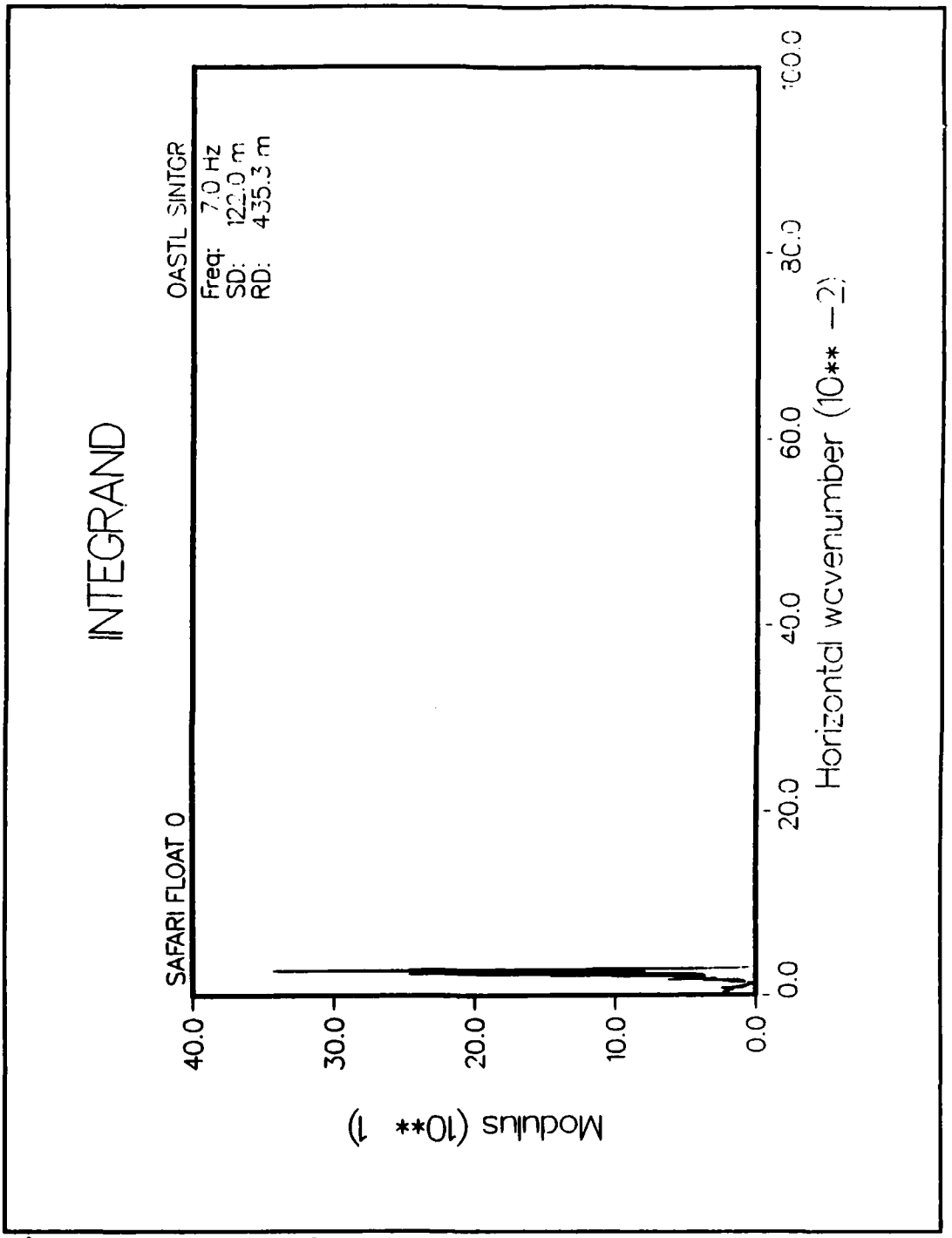

Figure 39 Integrand SAFARI Float 0
Standard Contour Offset
Cmin=50 m/s, Cmax=1E8 m/s, 16384 points, Δr=7.141 m,
Max FFT range=117.000 km

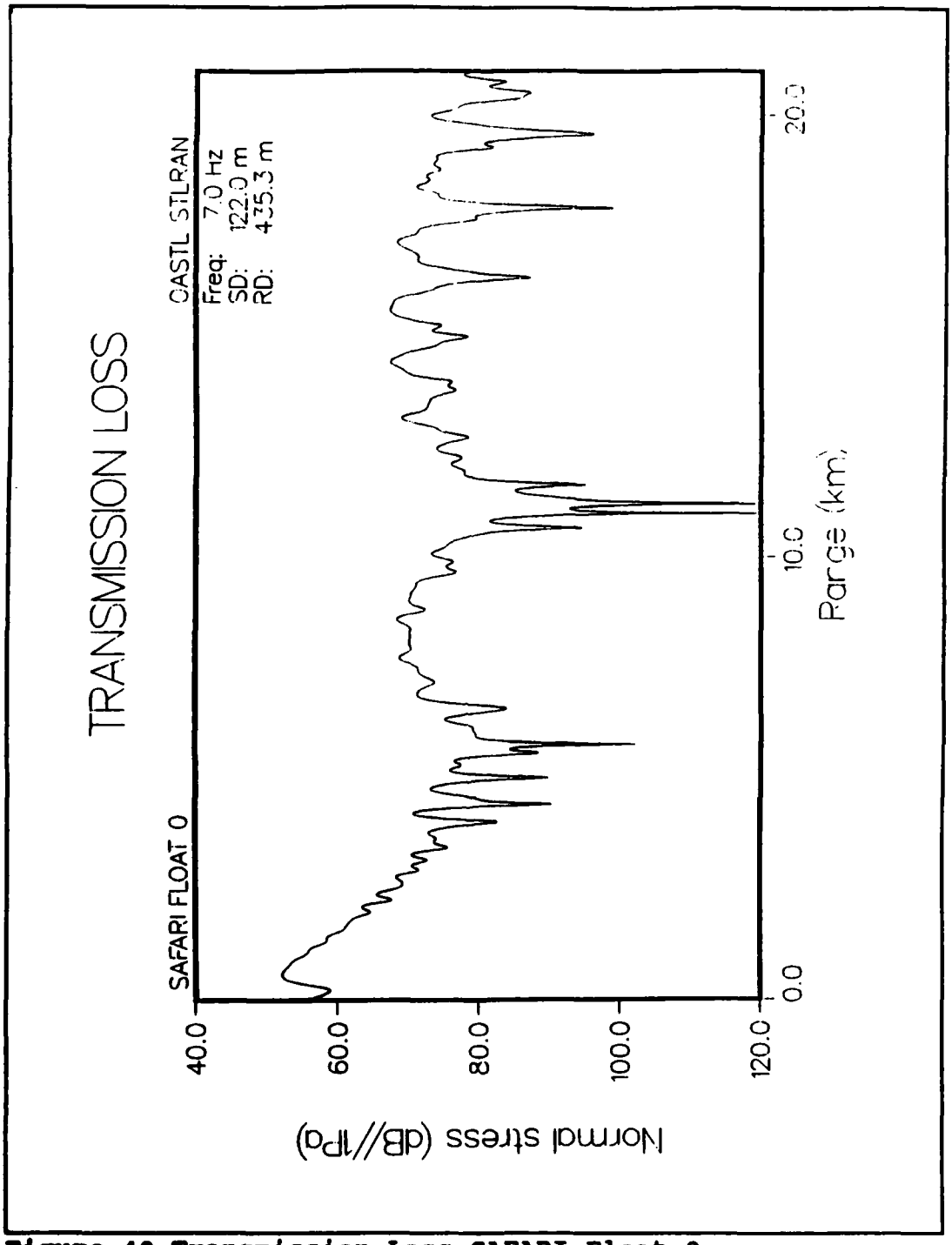

Figure 40 Transmission Loss SAFARI Float 0
Water Column Only
Cmin=50 m/s, Cmax=1E8 m/s, 4096 points, Δr=7.141 m,
Max FFT range=29.250 km

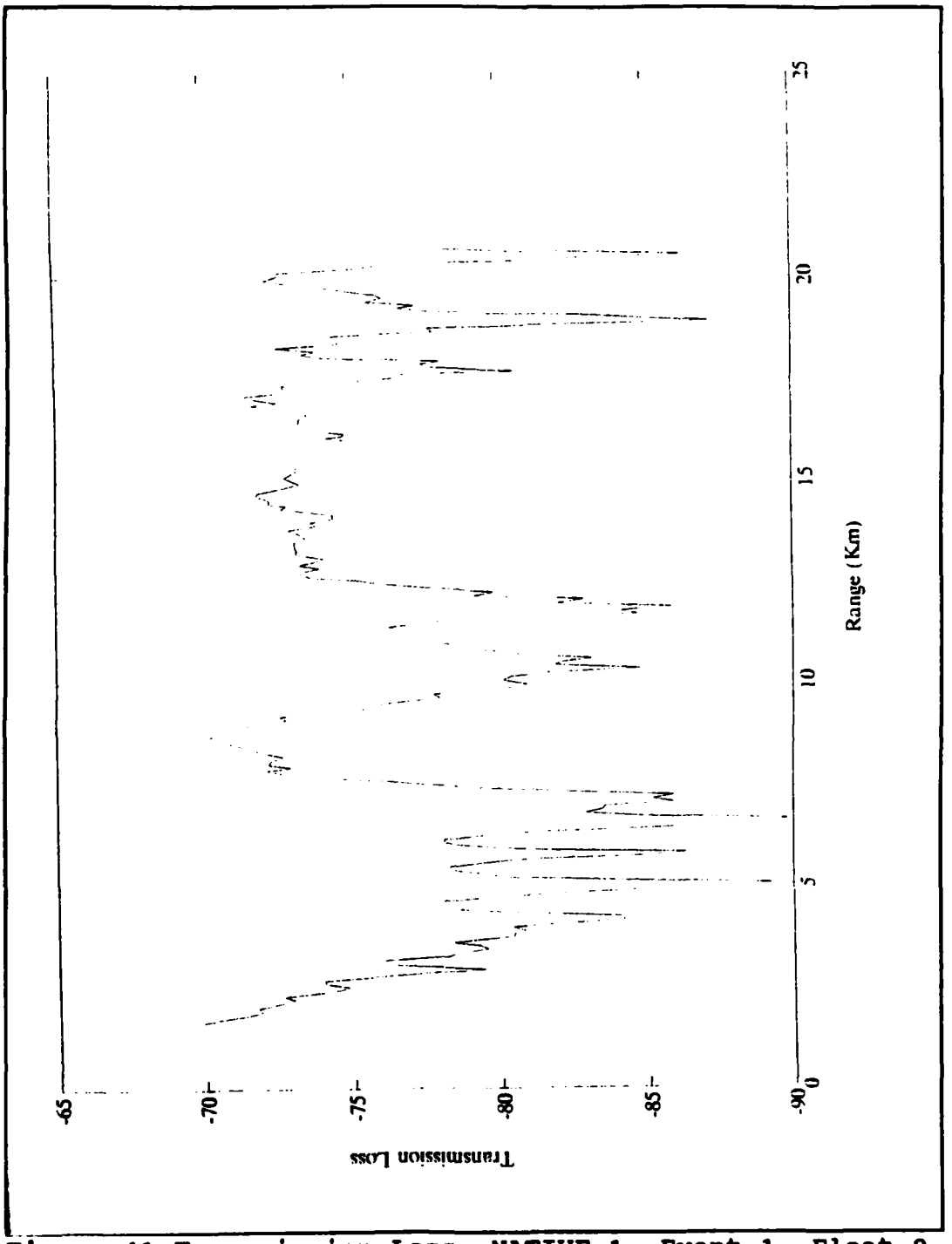

Figure 41 Transmission Loss, NATIVE 1, Event 1, Float 0, 7 Hz, Region 1

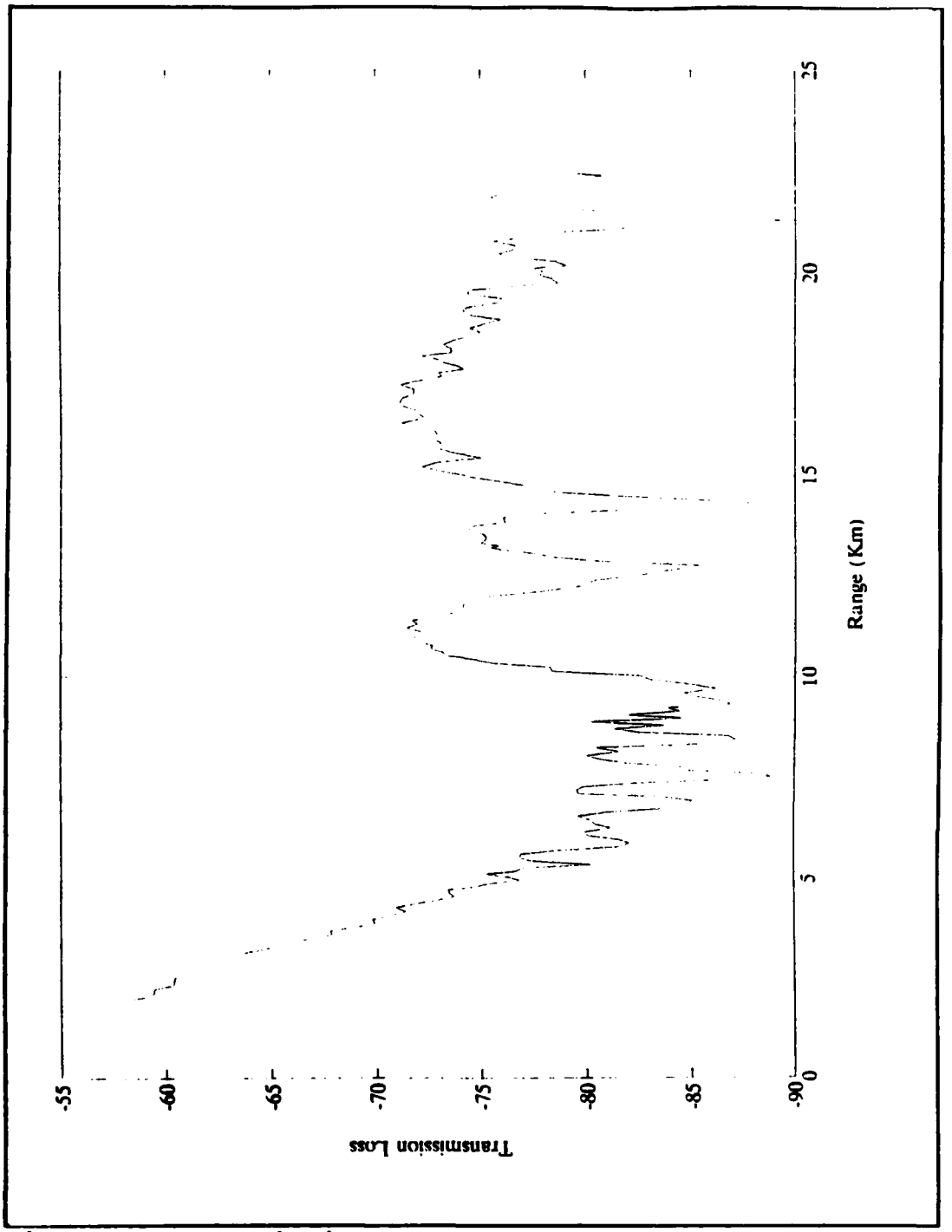

Figure 42 Transmission Loss, NATIVE 1, Event 1, Float 0, 7 Hz, Region 2

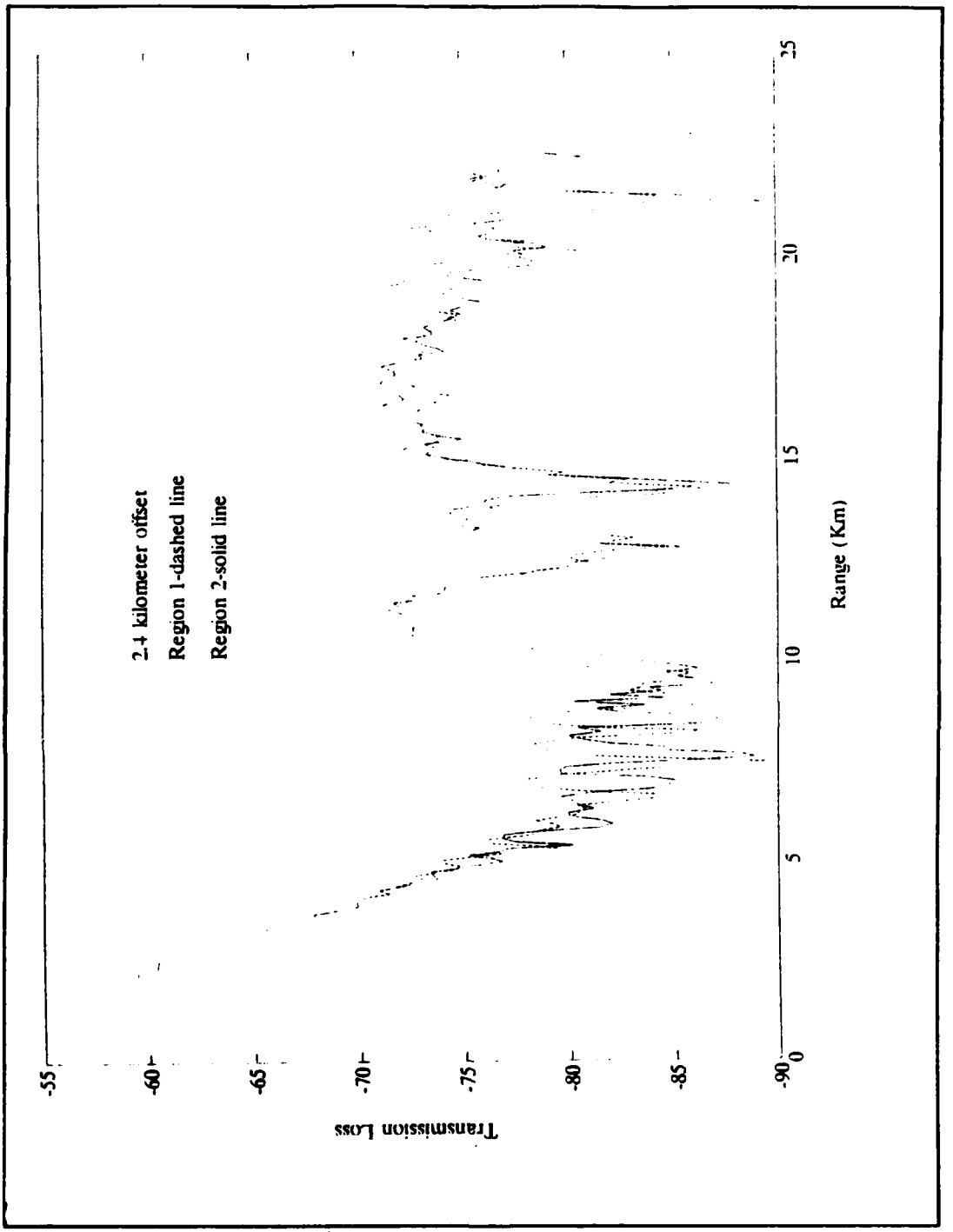

Figure 43 Transmission Loss, NATIVE 1, Event 1, Float 0, 7 Hz, Region 1 vs Region 2

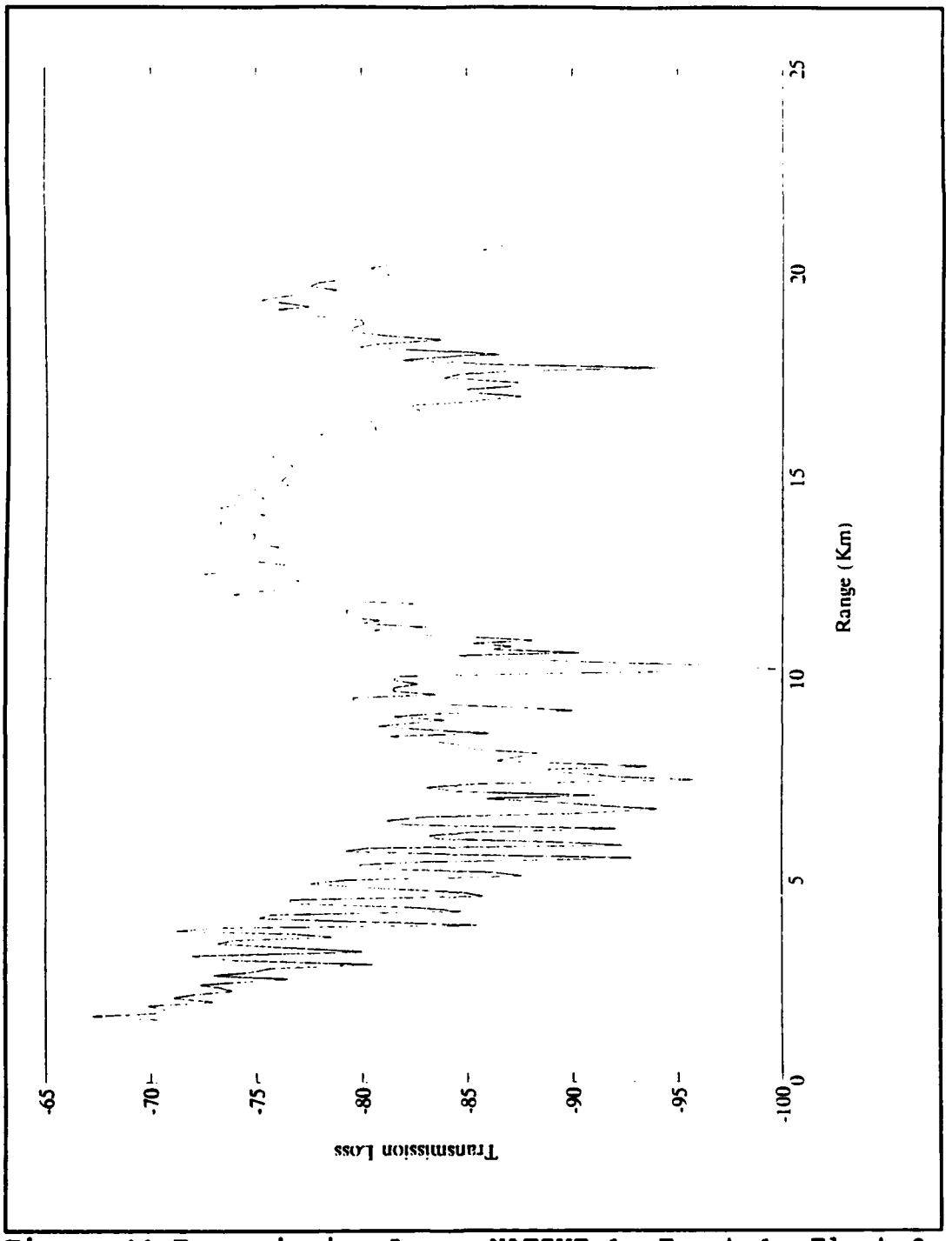

Figure 44 Transmission Loss, NATIVE 1, Event 1, Float 0, 10 Hz, Region 1

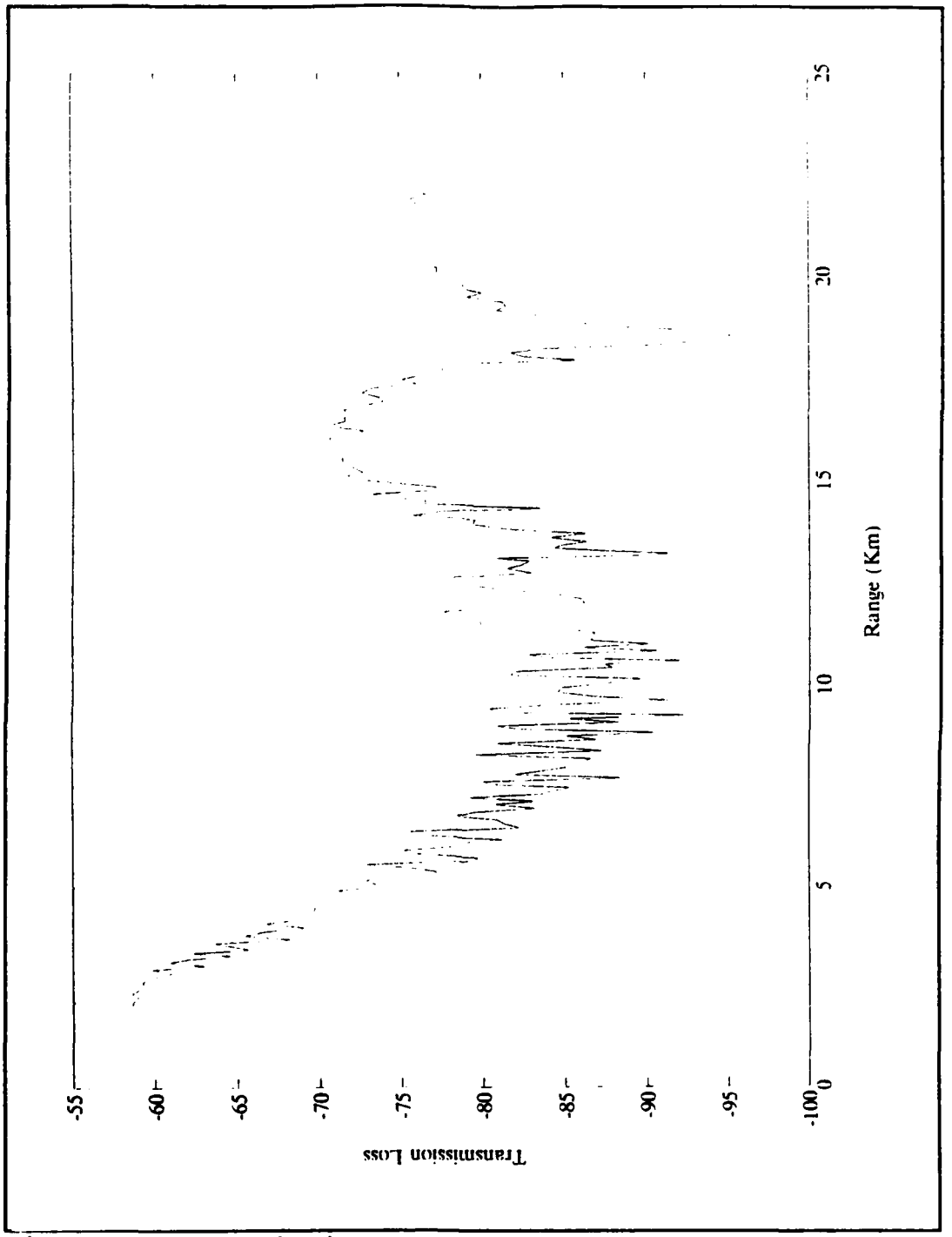

Figure 45 Transmission Loss, NATIVE 1, Event 1, Float 0, 10 Hz, Region 2

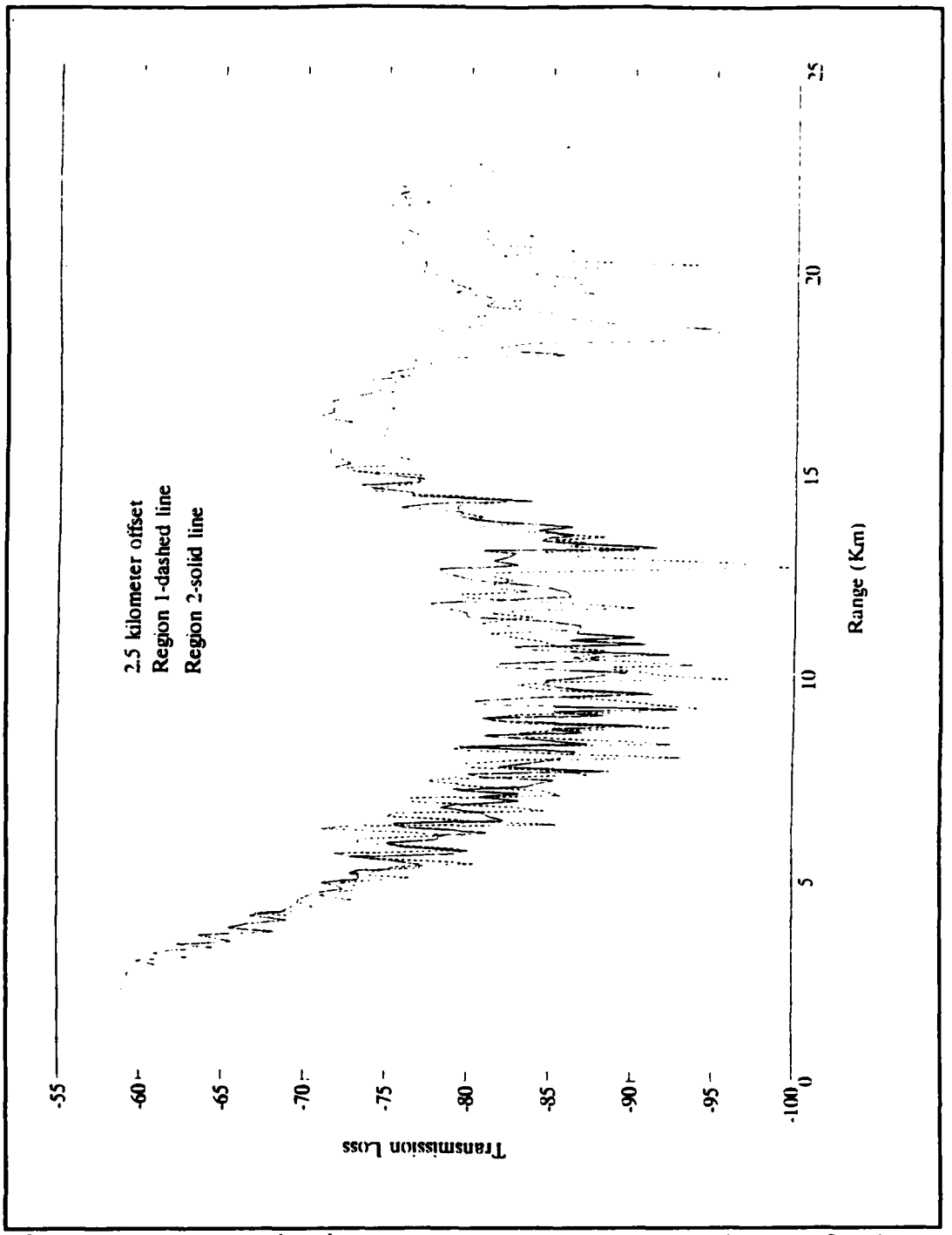

Figure 46 Transmission Loss, NATIVE 1, Event 1, Float 0, 10 Hz, Region 1 vs Region 2

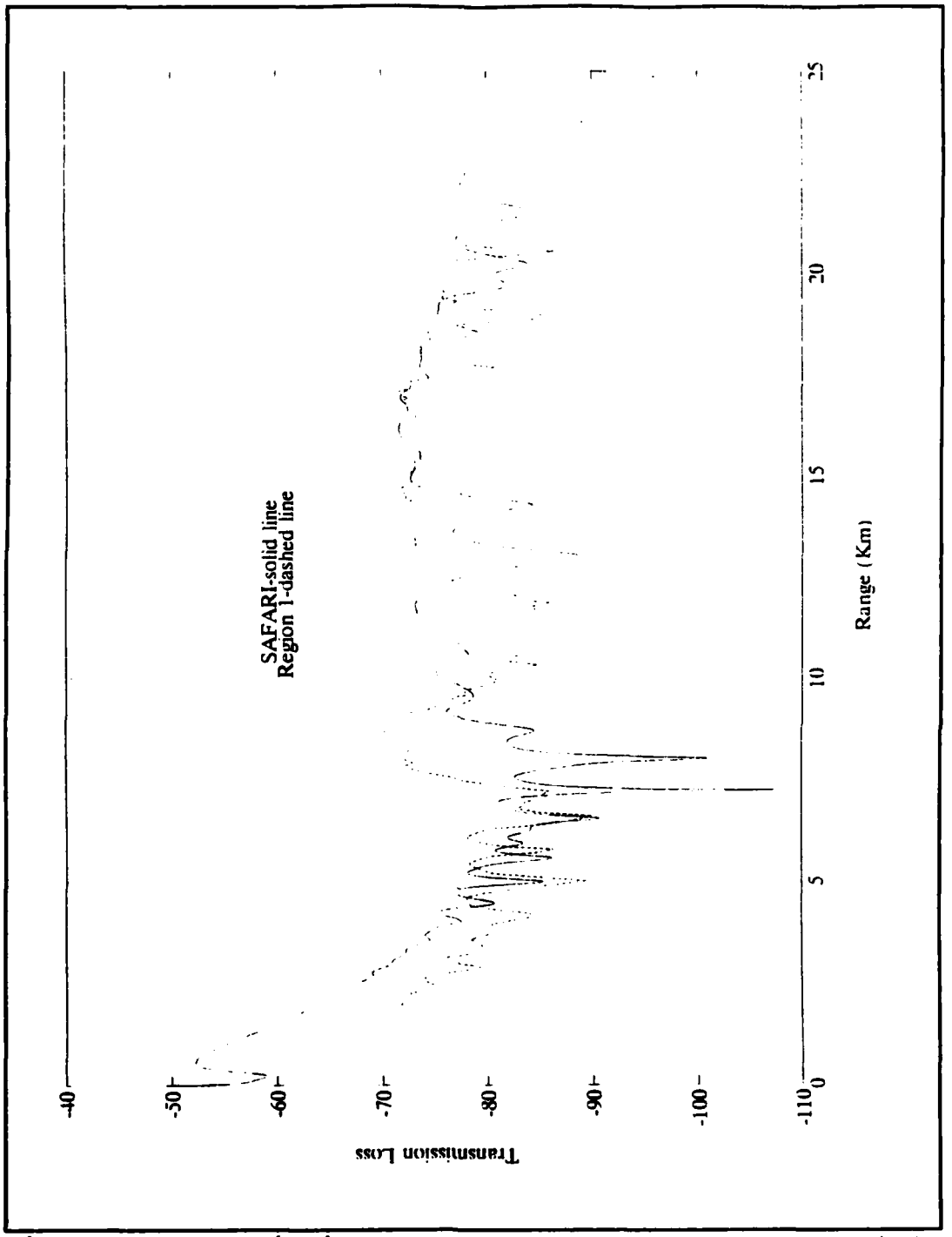

Figure 47 Transmission Loss, SAFARI vs NATIVE 1, Event 1, Float 0, Region 1 at 7 Hz

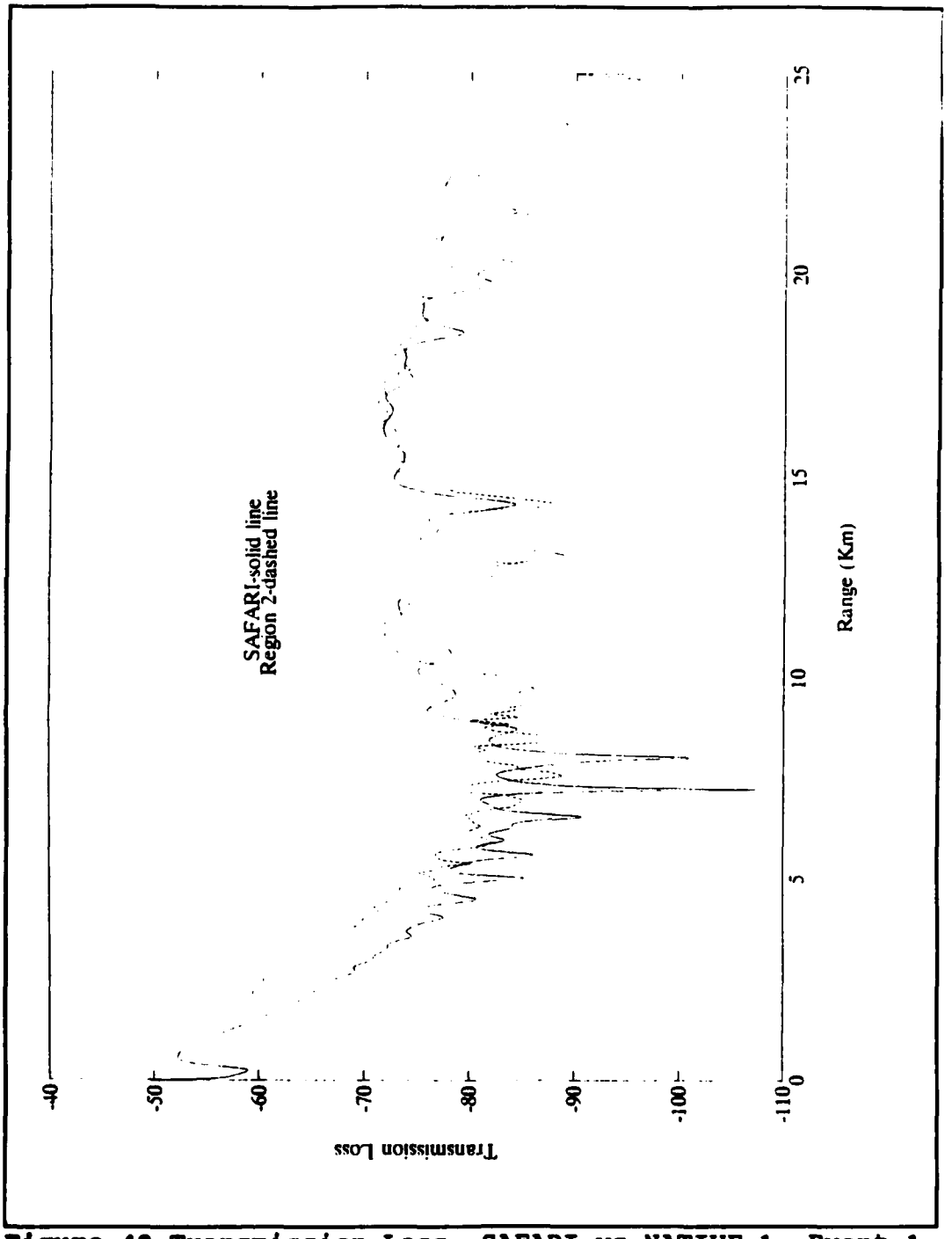

Figure 48 Transmission Loss, SAFARI vs NATIVE 1, Event 1, Float 0, Region 2 at 7 Hz

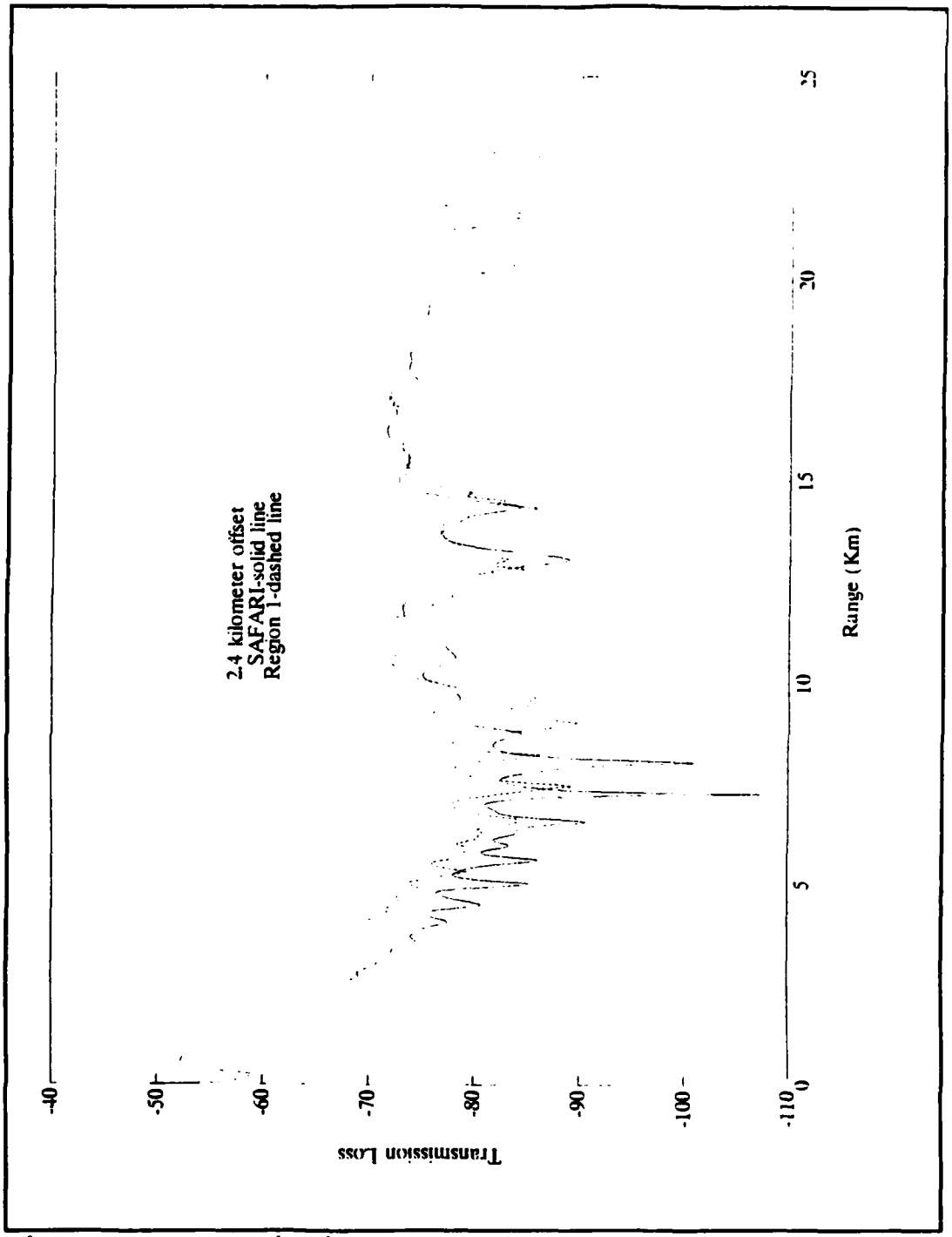

Figure 49 Transmission Loss, SAFARI vs NATIVE 1, Event 1, Float 0, Region 1 at 7 Hz, with 2.4 km Offset in Range

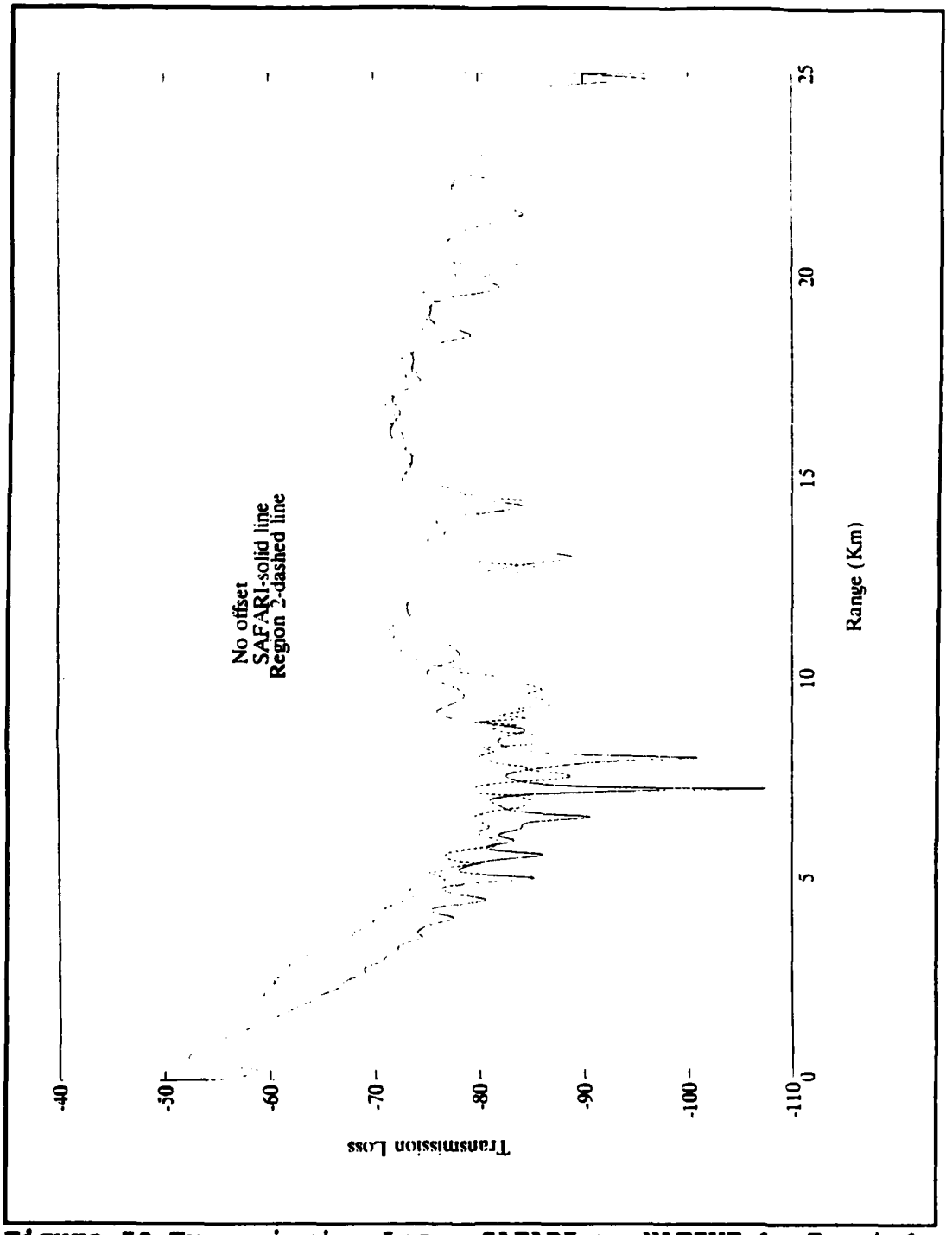

Figure 50 Transmission Loss, SAFARI vs NATIVE 1, Event 1, Float 0, Region 2 at 7 Hz, with No Offset in Range

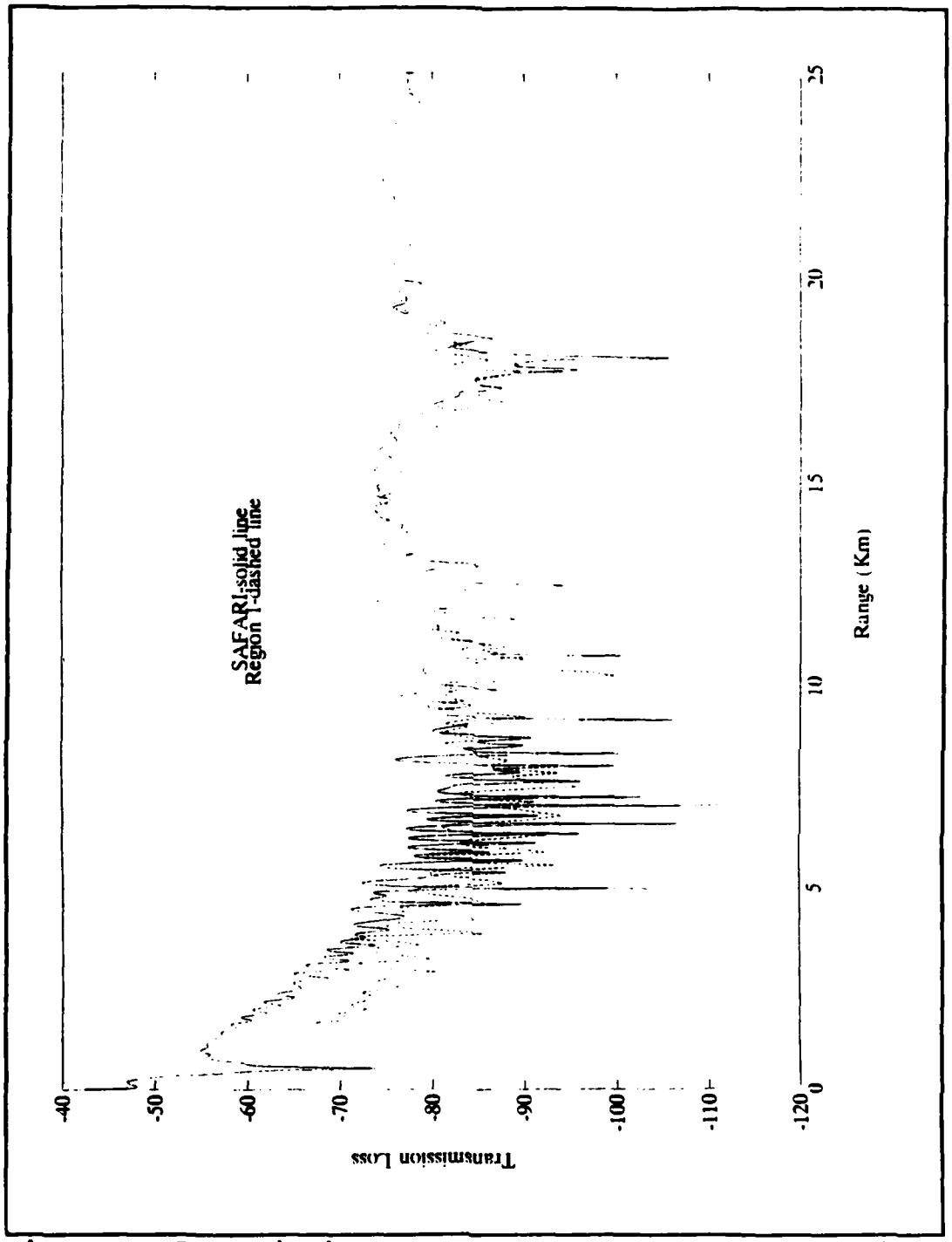

Figure 51 Transmission Loss, SAFARI vs NATIVE 1, Event 1, Float 0, Region 1 at 10 Hz

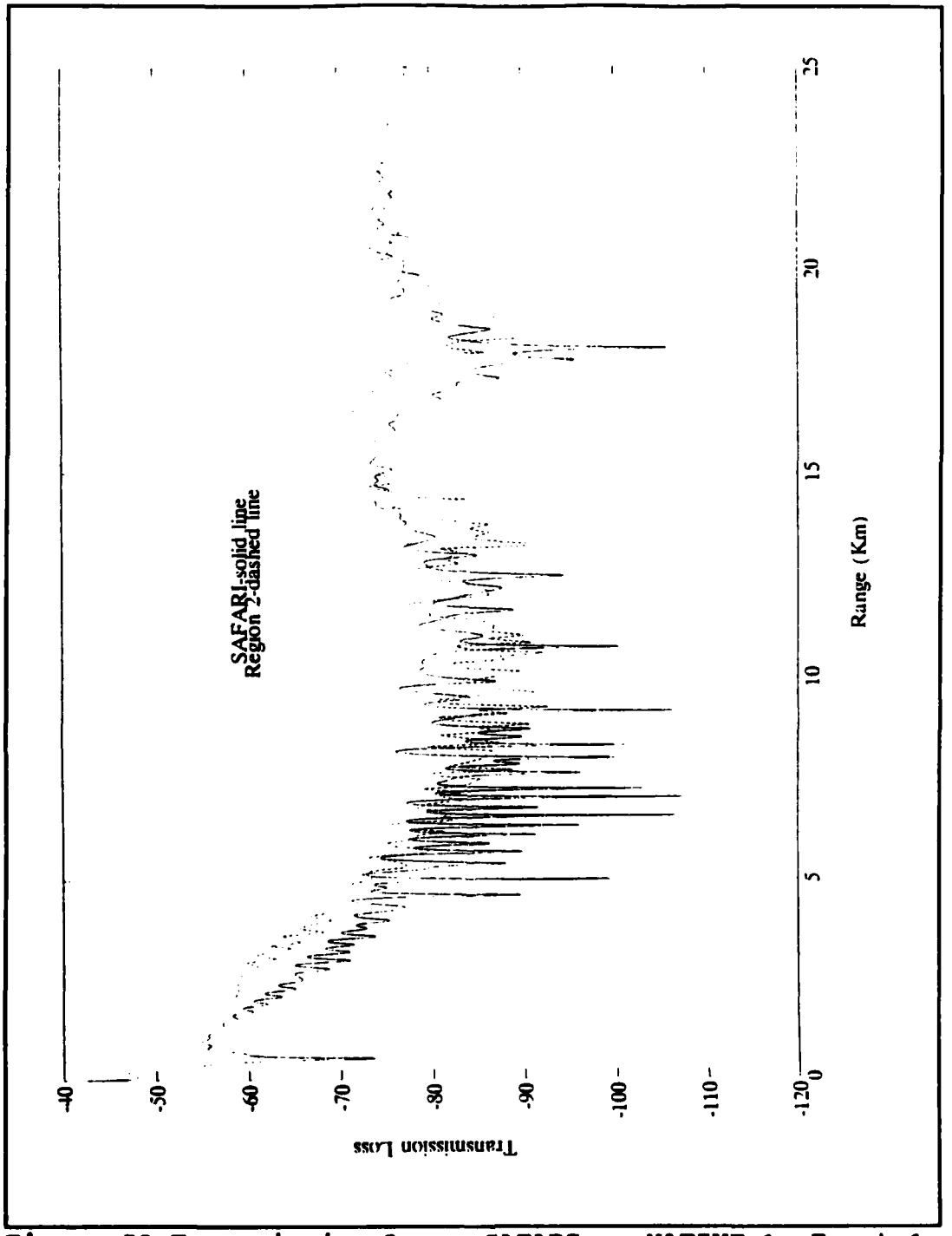

Figure 52 Transmission Loss, SAFARI vs NATIVE 1, Event 1, Float 0, Region 2 at 10 Hz

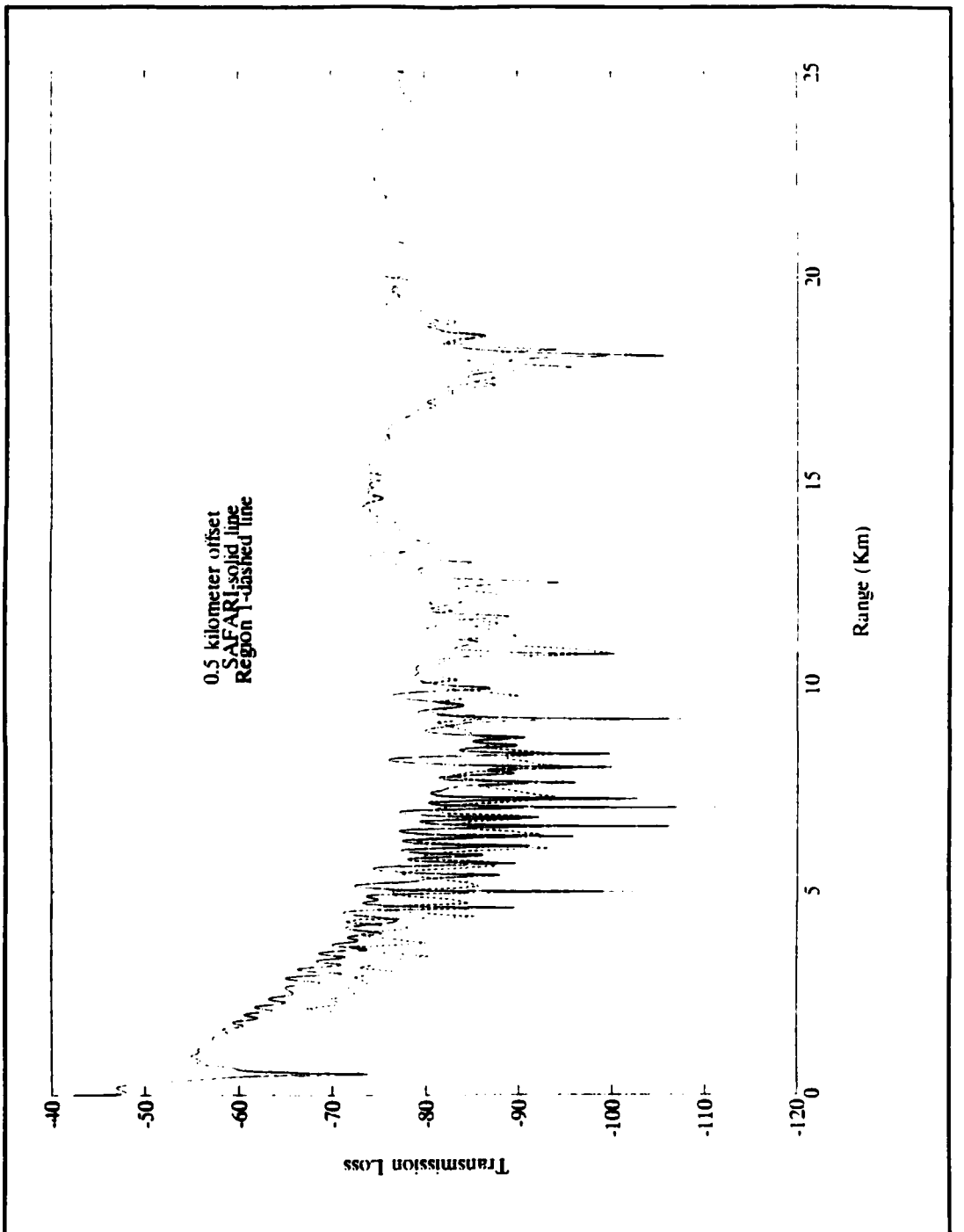

Figure 53 Transmission Loss, SAFARI vs NATIVE 1, Event 1, Float 0, Region 1 at 10 Hz, with 0.5 km Offset in Range

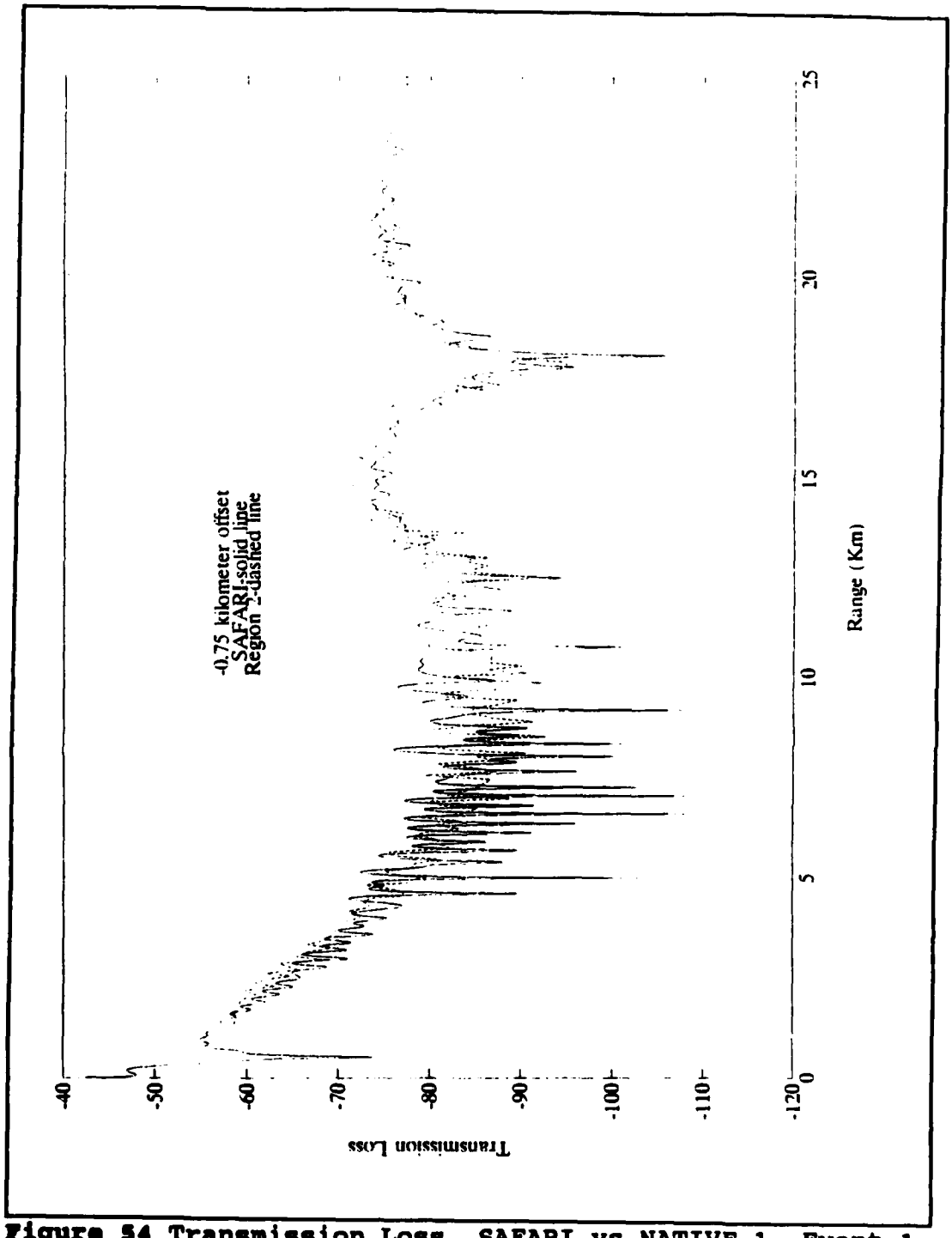

Figure 54 Transmission Loss, SAFARI vs NATIVE 1, Event 1, Float 0, Region 2 at 10 Hz, with -0.75 km Offset in Range

LIST OF REFERENCES

1. Naval Oceanographic and Atmospheric Research Laboratory, ID:021:222:91, *Noise and Transmission Loss in Environments (NATIVE 1) Environmental Report (Draft)*, by Bruce R. Gomes,Sheila McDonnell, and LT Mark Null (USN), May 1991

2. Marine Physical Laboratory, Technical Memorandum 426, Freely Drifting Swallow Float Array: August 1990 NATIVE 1 Experiment (First Deployment), by G.L. D'Spain, W.S. Hodgkiss, G.L. Edmonds, and M. Darling, February 1991

3. Naval Air Developement Center, Technical Memorandum No. 5044-101290, The Extremely Low Frequency (ELF) Projector Sopurce Level Reconstruction for the Native 1 Sea Test, August 1990, by Anthony Brescia, 10 December 1990

4. Bruce R. Gomes, Naval Oceanographic and Atmospheric Research Laboratory, Request for NATIVE 1 environment and source level for Event 1, 10 June 1991

5. Naval Oceanographic and Atmospheric Research Laboratory, unknown, unclassified excerpts *from* CONFIDENTIAL Exercise Plan for NATIVE 1 (U),unknown, p. B-24, 19 December 1989

6. G.L. D'Spain, W.S. Hodgkiss, and G.L. Edmonds,"The Simultaneous Measurement of Infrasonic Acoustic Particle Velocity and Acoustic Pressure in the Ocean by Freely Drifting Swallow Floats", unpublished, Marine Physical Laboratory, 30 October 1990

7. Supreme Allied Commander Atlantic Undersea Research Centre, SR-113, *SAFARI Seismo-Acoustic Fast field Algorithm for Range-Independent environments User's Guide*, by H. Schmidt, September 1988

8. Pekeris, C.L., "Theory of propagation of explosive sound in shallow water," *Memoirs, Geological Society of America*,27,1948

9. Zienkiewitz, O.C., *The Finite Element Method*, 3rd Edition, Maidenhead, McGraw-Hill,1977

10. DiNapoli, F.R. and Deavenport, R.L., "Theoretical and numerical Green's function solution in an plane layered medium.", Journal of the Acoustical Society of America,67,pp. 92-105, 1980

11. Marine Physical Laboratory electronic mail, Unclassified letter, Message ID 9108141608.AA08463@babylon, Subject: Research Data Files, received 14 August 1991

12. Strum, R.D., and Kirk, D.E., Discrete Systems and Digital Signal Processing, p.54, Addison Wesley Publishing Co., 1989

DISTRIBUTION LIST

1.	Defense Technical Information Center Cameron Station Alexandria, VA 22304-6145	2
2.	Library Code 52 Naval Postgraduate School Monterey, CA 93943-5000	2
3.	Superintendent Attn: Prof A.B. Coppens, Code PH/Cz Naval Postgraduate School Monterey, CA 93943-5000	1
4.	Superintendent Attn: Prof J.V. Sanders, Code PH/Sd Naval Postgraduate School Monterey, CA 93943-5000	1
5.	LCDR J.L. Cleveland Jr. 4279 S.E. Whiticar Way Stuart, FL 34997	2
6.	Commanding Officer Attn: Bruce Gomes, Code 222 Naval Oceanographic and Atmospheric Research Laboratory Stennis Space Center, MS 39529-5004	1
7.	Commanding Officer Attn: Shelby Sullivan, Code 40 Naval Ocean Systems Center San Diego, CA 92152-6400	1
8.	Marine Physical Laboratory Attn: W.S. Hodgkiss Naval Ocean Systems Center Bldg 106 Rm 144 Bayside San Diego, CA 92152-6400	1
9.	Massachusetts Institute of Technology Department of Ocean Engineering Attn: Prof H. Schmidt Cambridge, MA 02139	1